Synchrony Measurement and Connectivity Estimation of Parallel Spike Trains from in vitro Neuronal Networks

Messung der Synchronität und Abschätzung der Konnektivität von in-vitro Spike-Trains

Doctoral thesis

for a doctoral degree at the Graduate School of Life Sciences

Julius-Maximilians-Universität Würzburg

Section Neuroscience

submitted by

Manuel Ciba

from Erlenbach am Main, Germany

Würzburg 2020

Synchrony Measurement and Connectivity Estimation of Parallel Spike Trains from in vitro Neuronal Networks

Messung der Synchronität und Abschätzung der Konnektivität von in-vitro Spike-Trains

Doctoral thesis

for a doctoral degree at the Graduate School of Life Sciences

Julius-Maximilians-Universität Würzburg

Section Neuroscience

submitted by

Manuel Ciba

from Erlenbach am Main, Germany

Würzburg 2020

Submitted on: .....

(office stamp)

Members of the *Promotionskomitee*:

Chairperson:	Prof. Dr. Carmen Villmann
Primary Supervisor:	PD Dr. mult Andreas Bahmer
Supervisor (second):	Prof. Dr. Charlotte Förster
Supervisor (third):	Prof. Dr. Ing. Christiane Thielemann

Date of Public Defence: .....

Date of Receipt of Certificates: .....

However different the connections in our brain may be
we are all synchronized
by the need for love
and the fate of death

– N.N.

Contents

Summary

The goal of this doctoral thesis is to identify appropriate methods for the estimation of connectivity and for measuring synchrony between spike trains from in vitro neuronal networks. Special focus is set on the parameter optimization, the suitability for massively parallel spike trains, and the consideration of the characteristics of real recordings.

Two new methods were developed in the course of the optimization which outperformed other methods from the literature. The first method “Total spiking probability edges” (TSPE) estimates the effective connectivity of two spike trains, based on the cross-correlation and a subsequent analysis of the cross-correlogram. In addition to the estimation of the synaptic weight, a distinction between excitatory and inhibitory connections is possible. Compared to other methods, simulated neuronal networks could be estimated with higher accuracy, while being suitable for the analysis of massively parallel spike trains.

The second method “Spike-contrast” measures the synchrony of parallel spike trains with the advantage of automatically optimizing its time scale to the data. In contrast to other methods, which also adapt to the characteristics of the data, Spike-contrast is more robust to erroneous spike trains and significantly faster for large amounts of parallel spike trains. Moreover, a synchrony curve as a function of the time scale is generated by Spike-contrast. This optimization curve is a novel feature for the analysis of parallel spike trains.

Zusammenfassung

Ziel dieser Dissertation ist die Identifizierung geeigneter Methoden zur Schätzung der Konnektivität und zur Messung der Synchronität von in-vitro Spike-Trains. Besonderes Augenmerk wird dabei auf die Parameteroptimierung, die Eignung für große Mengen paralleler Spike-Trains und die Berücksichtigung der Charakteristik von realen Aufnahmen gelegt.

Im Zuge der Optimierung wurden zwei neue Methoden entwickelt, die anderen Methoden aus der Literatur überlegen waren. Die erste Methode “Total spiking probability edges” (TSPE) schätzt die effektive Konnektivität zwischen zwei Spike-Trains basierend auf der Berechnung einer Kreuzkorrelation und einer anschließenden Analyse des Kreuzkorrelograms. Neben der Schätzung der synaptischen Gewichtung ist eine Unterscheidung zwischen exzitatorischen und inhibitorischen Verbindungen möglich. Im Vergleich zu anderen Methoden, konnten simulierte neuronale Netzwerke mit einer höheren Genauigkeit geschätzt werden. Zudem ist TSPE aufgrund der hohen Rechengeschwindigkeit für große Datenmengen geeignet.

Die zweite Methode “Spike-contrast” misst die Synchronität paralleler Spike-Trains mit dem Vorteil, dass die Zeitskala automatisch an die Daten angepasst wird. Im Gegensatz zu anderen Methoden, welche sich ebenfalls an die Daten anpassen, ist Spike-contrast robuster gegenüber fehlerhaften Spike-Trains und schneller für große Datenmengen. Darüber hinaus berechnet Spike-Contrast eine Synchronitätskurve als Funktion der Zeitskala. Diese Kurve ist ein neuartiges Feature zur Analyse paralleler Spike-Trains.

Chapter 1

Introduction

1.1 Motivation

How does the brain work? Evidences for stone age cranial surgery around 7000 years ago (Alt et al., 1997) could indicate that this question has been of concern to mankind for a long time. Still, in the 21th century, there are many challenges in neuroscience (Markram, 2013) and the underlying mechanisms of basic brain functions are incompletely understood (Rees et al., 2002).

Understanding the brain is motivated by various areas that have a major impact on our daily lives: Gustavsson et al. (2011) estimated that at least a third of all people in the EU were affected by brain disorders in 2010, mostly anxietey disorders (12%), followed by migrain (10%), mood disorders such as depression (6%), addiction (3%), psychotic disorders such as schizophrenia (1%), dementia such as Alzheimer's disease (1%) and other disorders [1], which account for an estimated 25% of all direct health care costs. In developing countries, the proportion of the population with brain disorders such as depression and anxiety are rated even higher (WHO, 2017). Understanding the mechanisms of brain disorders will help to improve treatments such as deep brain stimulation (Mayberg et al., 2005), surgery (Téllez-Zenteno et al., 2005), treatment with psychopharmaca (Cooper et al., 2003) or psychedelics (Muttoni et al., 2019), meditation (Fox et al., 2014), and to understand neurotoxicological effects due to chemicals (Bondy and Campbell, 2005), to radiation (Dropcho, 2010), or stress (De Kloet et al., 2005). It can further improve knowledge of emerging brain properties such as human and social behavior (Dumas et al., 2011), or even address philosophical questions about the nature of consciousness (Schwartz et al., 2005; Dehaene, 2014).

Knowledge about the brain can be transferred to other areas: Bio-inspired computing such as artificial neural networks (Kar, 2016) or even new discoveries through curiosity-driven basic research can be expected (Botstein, 2012; Amon, 2015). Even in the field of astronomy, there is evidence that the network of cosmic galaxies is similar in structure and complexity to the neuronal networks in the human brain (Vazza and Feletti, 2017). The human brain consists of 10^{11} neurons (Williams and Herrup, 1988) and is one of the most complex systems.

[1] epilepsy (0.5%), stroke (0.3%), Parkinson's disease (0.2%), traumatic brain injury (0.2%), multiple sclerosis (0.1%), brain tumor (0.05%),

1.2 Connectivity and synchrony

What is the current understanding of how the brain works? Current theories and research on brain function differ in their perspectives on certain characteristics of the brain. Among others, different spatial and temporal scales are considered (Amunts et al., 2016). It is assumed that brain functions can be understood by recording every action potential from every neuron in the brain, which allows to draw conclusions about brain connectivity (Alivisatos et al., 2012). Such connections are called "functional connectivity" because they are defined by their function, which is the transmitted signal. Functional connectivity is a subset of the physical connectivity of neurons, also known as "structural connectivity". More precisely, functional connectivity is defined as the statistical correlation between signals generated by two neurons and also can contain the information about the direction of signal propagation. If the functional connectivity contains information about the direction and also allows a distinction between excitatory or inhibitory connections, it is called "effective connectivity" or "causal connectivity" (Yu et al., 2017). In a broader sense, effective connectivity is based on a coupling model and refers to the influence between two neuronal systems, either at the synaptic level or at the population level (Friston, 2011).

Self-organization is a fundamental brain operation in brain dynamic. The perturbation of spontaneous brain activity causes the brain to adjust to its environment (Buzsáki et al., 2013) by changing its effective connectivity. Many brain theories regard this adaptation as a process of optimizing the brain to understand its outside world. One of these theories is the free-energy principle by Friston (2010), which possibly unifies all optimization-based theories (e.g. the Bayesian brain hypothesis, the principle of efficient coding, and the cell assembly theory by Hebb). Common to all these theories is that a change in network connections is necessary for the brain to adapt to its environment. The investigation of functional or effective connections is therefore an important task in neuroscience (Friston, 1994b, 2011; Poli et al., 2015b; Yu et al., 2017).

Depending on the functional or effective connectivity, neuronal firing within a network can synchronize (Yu et al., 2017). Synchronization is an emergent property of coupled oscillators (Dörfler et al., 2013) and can generally be defined as a process of adjustment of rhythms between interacting self-sustained oscillators (Pikovsky et al., 2003). Neurons can be regarded as oscillators such as the so-called "pacemaker neurons" generating rhythmic burst activity (Ramirez et al., 2004). The similar terms "synchrony" and "synchronicity" should not be confused as they are used in different contexts. The term "synchrony" means "the state of two or more events occurring at the same time", whereas "synchronicity" is used for a concept in psychology[2]. Whether two events can be considered synchronous depends on how "at the same time" is defined. In neural networks, the time window in which two events are considered synchronous can be defined differently. The time window can either be absolute

[2]The term "synchronicity" is a concept introduced by Carl Jung that describes a "meaningful coincidence of two or more events where something other than the probability of chance is involved" and is usually used in the context of paranormal phenomena (Jung, 1997; Cambray, 2002).

due to latencies or synaptic delays (Jeffress, 1948; Bahmer and Langner, 2006) or it can be relative to the oscillation rhythms. For instance, oscillations in the brain vary between milliseconds and slower time scales, such as the 24-h period of the circadian rhythm (Buzsaki, 2006).

Synchrony in complex neuronal networks is thought to play a key role in neuroscience as it is related to cognitive processes (Ward, 2003), sensory awareness (Engel and Singer, 2001), pathological states such as epilepsy (Fisher et al., 2005), and tremors caused by Parkinson's disease (Pare et al., 1990; Arnulfo et al., 2015). The reason why synchrony is fundamental to the neurosciences is well illustrated by the example of the electroencephalography (EEG). The higher the number of neurons which fire synchronously, the higher is the EEG power in the correspondig frequency band (Klimesch, 1999; Buzsáki et al., 2012). In epilepsy, the synchrony over large brain areas or certain networks is increased (Schevon et al., 2007). In the context of higher brain functions, synchrony has been suggested as a possible – albeit controversial (Shadlen and Movshon, 1999) – solution to the "binding problem" (Singer, 1999). The binding problem describes the problem of how different sensory stimuli are segregated or combined by the brain. For example, different locations of the visual brain are functionally specialized to analyze different features such as shapes and colors (Zeki, 1978). The question of the binding problem is: How does the brain combine or segregate them correctly? Synchrony may "tag" the features together. There is also evidence that spike synchrony is used to carry information complementary to a firing rate code. For example, Kilavik et al. (2009) showed that intensive practice of a particular task leads to increased spike synchrony and a reduced spike rate in the motor cortex. Furthermore, it is suggested that synchronized cell assemblies are involved in non-linear computations (Tetzlaff et al., 2015). Synchronized activity is also the fundamental feature in the "synfire chain" model proposed by Abeles (2012) to explain reliable signal transmission over the network. A synfire chain is a feed-forward network of excitatory neurons organized in different layers. A neuron of a layer is connected to all neurons of the next layer. Network activity propagates synchronously or asynchronously. In addition to synchrony within the brain, there is also synchronization between interacting brains. For example, a listener's brain activity synchronizes with the speaker's brain activity (Dumas et al., 2011) or brain activities synchronizes between musicians playing in unison (Washburn et al., 2019).

1.3 Connectivity estimators and synchrony measures

The study of network dynamics defined by connectivity and their emergent properties such as synchrony plays a central role in neuroscience. To investigate such networks, the network activities have to be recorded. With methods that use microelectrode arrays (MEAs), extracellular and, depending on the technology, even intracellular neuronal activity can be recorded over time from a neuronal network at different spatial positions (Spira and Hai, 2013). Since it is assumed that the

information is mainly encoded by the temporal occurrence of action potentials[3] (Rieke, 1999), the recorded neuronal activity is reduced to spike time series using a spike-detection method (Wilson and Emerson, 2002; Lieb et al., 2017). Such a sequence of spike times is called a "spike train".

By comparing the spike trains of two neurons, the functional or effective connectivity of these neurons can be estimated using functional or effective "connectivity estimation" methods (e.g. see Garofalo et al. (2009b)). If the functional or effective connectivity of all neuron pairs is estimated, a network graph can be constructed. The network topology can be further characterized using complex measuers from graph theory such as the network centrality (Rodrigues, 2019) or small worldness (Poli et al., 2015b). Connectivity estimation in combination with complex measures from graph theory therefore enables the analysis of spike trains and the investigation of neural networks.
Another way to analyze spike trains is to measure the synchrony between two or more spike trains using "synchrony measure" methods (e.g. see Eisenman et al. (2015)). Such methods usually provide a single value that quantifies the synchrony level of the entire recording.
Studying methods from the class of functional or effective connectivity estimators and methods from the class of synchrony measures can be confusing because network connectivity and synchrony are related as discussed in section 1.2. For example, methods for estimating functional connections apply synchrony measures to estimate the strength of the connection (e.g. cross-correlation (Garofalo et al., 2009b)). Further confusion can arise because some analysis methods focus on finding the temporal position of significant synchronous events (Grün et al., 2002), estimating signal propagation (Kreuz et al., 2017), or identifying neural subpopulations within a network (Gerstein, 2010; Satuvuori et al., 2018). Other measures quantify the synchrony level of the entire spike train (Eisenman et al., 2015) which is the focus of this work. It should be noted that a spike train is not a continuous signal but a sequence of discrete events. Synchrony measures and connectivity estimators for continuous signals – such as for EEG signals (Dauwels et al., 2010; Haufe et al., 2013) – are not considered here. Likewise, synchrony measures between spikes and local field potentials are described elsewhere, e.g. in Li et al. (2019).
Another reason for confusion is the different terms used in the literature regarding synchrony measures. Terms such as spike train "measure" (Paiva et al., 2010), "synchrony" (Eisenman et al., 2015), "(dis)similarity" (Schreiber et al., 2003; DeMarse et al., 2016), "correlation" (Cutts and Eglen, 2014), or "distance[4]" (Victor and Purpura, 1996; Quian Quiroga et al., 2002) are used depending on the research question. In this work, the term "synchrony" is used.

Many methods have been proposed in the literature for estimating connectivity (Gourévitch and Eggermont, 2007c; Garofalo et al., 2009b; Isomura et al., 2014b; Poli et al., 2016b) and measuring synchrony (Selinger et al., 2004; Paiva et al., 2010;

[3] It should be noted, that the *Holonomic Brain Theory* considers also sub-threshold oscillations within fine dendritic patches of a neuronal network as a carrier of Fourier-transformed information according to the principles in holography (Pribram and Carlton, 1986). In this case, spikes are only a subset of the whole information.
[4] If a distance measure is inverted, it can be used as a synchrony measure or vice versa.

Cutts and Eglen, 2014; Eisenman et al., 2015; Satuvuori et al., 2017). However, there is currently no gold standard, which means that a variety of methods are used, making it difficult to compare research. Furthermore, some of these methods depend heavily on parameters that have to be selected by the user. If different parameters are chosen, even identical methods are no longer comparable. In addition, there is a risk of selecting parameter values that are not suitable, especially if the data contains several time scales (Chicharro et al., 2011). In the worst case, an inappropriate choice of parameter leads to misinterpretations, as in the case of the correlation index when choosing a time scale parameter that is too large (Tchumatchenko et al., 2011).

Example applications where spike trains have to be analyzed are *in vivo* recordings in the context of basic research (Kilavik et al., 2009) or pharmacological (Chiappalone et al., 2003) or toxicological (Johnstone et al., 2010) studies using *in vitro* neuronal networks on MEAs. Recently, standard MEAs with 60 electrodes are more and more replaced by CMOS-based high density microelectrode arrays (HDMEAs) with between 500 and 20.000 electrodes (Litke et al., 2004; Berdondini et al., 2009b; Dragas et al., 2017; Yuan et al., 2020) due to improved statistical significance of the network activity (Maccione et al., 2010) and for the investigation of effects down to the single cell level (Yuan et al., 2020). Such experiments generate massively parallel spike trains, which challenges the analysis methods with regard to the calculation speed.
Since the beginning of experiments with neuronal networks on MEAs, mainly neurons from animals have been used (Pine, 2006). Recently, however, stem cell-derived human neurons are increasingly being used to examine the possibility of replacing animal models (Amin et al., 2016). Especially in the early stages of development, these neurons generate signals with low signal to noise ratio (SNR) (Amin et al., 2016). This increases the likelihood of erroneous spike trains due to spike detection errors (Lieb et al., 2017). It is desirable that connectivity estimators and synchrony measures are as robust as possible to such errors and at the same time as sensitive as possible to the effect examined.

Previous comparisons of connectivity estimators (Garofalo et al., 2009b; Poli et al., 2015b) as well as comparisons of synchrony measures (Kreuz et al., 2007b; Paiva et al., 2010; Cutts and Eglen, 2014; Eisenman et al., 2015) did neither consider the usability for massively parallel spike trains from HDMEAs recordings, nor the robustness against erroneous spike trains. Furthermore, there is no established procedure to compare and benchmark connectivity estimators or synchrony measures with respect to signals of *in vitro* neuronal networks. In comparisons of connectivity estimators, only simulated neuronal networks with about 100 neurons were considered, which did not take into account the complexity of experimental data (Garofalo et al., 2009b; Poli et al., 2015b). *In vitro* neuronal networks usually contain between 50,000 to 300,000 neurons (Novellino et al., 2011). Neuronal signals show a wide diversity in signal characteristics depending on the size, density, and topology of the network as well as the neuron type (Reimer et al., 2012). This diversity is difficult to address in simulated data. Eisenman et al. (2015) therefore used experimental data of *in vitro* neuronal networks on MEAs to compare different synchrony measures.

In this study, however, only a small part of the available synchrony measures was considered. Furthermore, the data are not publicly available, which prevents the inclusion of new synchrony measures in the study, such as the recently developed measures of Satuvuori et al. (2017). The present work aims at filling these open issues.

1.4 Aims of the work

The following research question arises from the discussion in the previous section. What are the most appropriate connectivity estimators and synchrony measures for spike train signals from *in vitro* neuronal networks considering

(a) the choice of appropriate parameter values,

(b) the suitability for massively parallel spike trains such as from HDMEAs, and

(c) the characteristics of experimental data such as different time scales or erroneous spike trains?

In order to answer this question, evaluation methods have to be developed that include the characteristics of experimental data. The developed evaluation methods should be publicly available in order to help the research community to establish a uniform benchmarking.

The structure of this work is as follows. Chapter 2 contains the publication *Total spiking probability edges: A cross-correlation based method for effective connectivity estimation of cortical spiking neurons* by De Blasi et al. (2019) which compares functional connectivity estimators and introduces a novel method called “total spiking probability edges (TSPE)” to estimate the effective connectivity. Chapter 3 contains the publication *Spike-contrast: A novel time scale independent and multivariate measure of spike train synchrony* by Ciba et al. (2018) which introduces a novel method called “Spike-contrast” to measure spike train synchrony. Chapter 4 contains the publication *Comparison of different spike train synchrony measures regarding their robustness to erroneous data from bicuculline-induced epileptiform activity* by Ciba et al. (2020) which compares and evaluates different spike train synchrony measures. The general discussion is provided in chapter 5.

Chapter 2

Total spiking probability edges: A cross-correlation based method for effective connectivity estimation of cortical spiking neurons

Stefano De Blasi[1,], Manuel Ciba[1], Andreas Bahmer[2], Christiane Thielemann[1]*

1 Biomems lab, University of Applied Sciences Aschaffenburg, 63743 Aschaffenburg, Germany.
2 University ENT-Clinic Würzburg, Theoretical and Experimental Neurophysiology, 97080 Würzburg, Germany.
***** Corresponding author, biomems@th-ab.de

Published in *Journal of Neuroscience Methods*
Volume 312, 15 January 2019, Pages 169-181

Abstract

Background:
Connectivity is a relevant parameter for the information flow within neuronal networks. Network connectivity can be reconstructed from recorded spike train data. Various methods have been developed to estimate connectivity from spike trains.

New method:
In this work, a novel effective connectivity estimation algorithm called *Total Spiking Probability Edges* (TSPE) is proposed and evaluated. First, a cross-correlation between pairs of spike trains is calculated. Second, to distinguish between excitatory and inhibitory connections, edge filters are applied on the resulting cross-correlogram.

Results:
TSPE was evaluated with large scale *in silico* networks and enables almost perfect reconstructions (true positive rate of approx. 99% at a false positive rate of 1% for low density random networks) depending on the network topology and the spike train duration. A distinction between excitatory and inhibitory connections was possible. TSPE is computational effective and takes less than three minutes on a high-performance computer to estimate the connectivity of an one hour dataset of 1000 spike trains.

Comparison of existing methods:
TSPE was compared with connectivity estimation algorithms like Transfer Entropy based methods, Filtered and Normalized Cross-Correlation Histogram and Normalized Cross-Correlation. In all test cases, TSPE outperformed the compared methods in the connectivity reconstruction accuracy.

Conclusions:
The results show that the accuracy of functional connectivity estimation of large scale neuronal networks has been enhanced by TSPE compared to state of the art methods. Furthermore, TSPE enables the classification of excitatory and inhibitory synaptic effects.

2.1 Introduction

The human brain consists of billions of neurons and one of the current scientific challenges is to understand the information processing within the brain. For this purpose, it is desirable to analyze and maybe one day even comprehend the neuronal information flow based on sequences of action potentials.

The brain is a huge network formed of neuronal populations connected to each other via synapses, axons and dendrites. Understanding of basic concepts of the connectivity within our nervous system will be crucial for elucidating how neurons and neural networks process information. Definition of connectivity is generally made at three different levels: structural, functional, and effective Friston (1994a); Poli et al. (2015a). Structural connectivity describes the anatomic and mostly static connections within a physical network containing synapses and neurons. Functional connectivity is a statistical concept that defines the correlation between all network neuron activities, depending on which physical connections transmitted action potentials. Effective connectivity focuses on the causality in a network Poli et al. (2015a) including directed connections addressing the question which neuron is source and which is target. By means of the effective connectivity it is possible to discriminate between inhibitory or excitatory synaptic effects and to determine synaptic strength.

Functional relation within *in vitro* neuronal networks can be analyzed by the temporal correlation between recorded spike trains. Existing methods for the estimation of functional or effective connectivity calculate relations between the activities of different neurons, e.g. incoming synaptic action potentials influence the behavior of the receiving neuron. Functional or effective connectivity estimation algorithms applied on spike trains estimate connections strengths between network nodes. These connection strengths can be displayed for illustration in a connectivity matrix (CM). CM values strongly depend on the applied algorithm in contrast to synaptic weight matrix (SWM) which contains synaptic parameters depending on the neuron model. To estimate the functional or effective connectivity different methods based on information theory Gourévitch and Eggermont (2007a); Garofalo et al. (2009a), pattern recognition Perkel et al. (1967); Masud et al. (2017), model fitting Isomura et al. (2014a); Friston et al. (2011) or data mining Diekman et al. (2014) have been developed and applied. The quality of the results is strongly dependent on data sets gained from *in vivo* or *in vitro* neural networks.

Some methods are not developed for large and complex networks, for example estimating the connectivity by modeling *in silico* neuronal networks Isomura et al. (2014a, 2015); Friston et al. (2011) or by using data mining methods Diekman et al. (2014). Another method is Partial Correlation, which is able to distinguish between direct and indirect connections by considering linear contributions. Partial Correlation estimates connectivity precisely for *in silico* with a small amount of neurons, e.g. 130 neurons Kadirvelu et al. (2017). However, Partial Correlation is inaccurate for large scale network models Poli et al. (2016a) because of the complex amount of possibilities for considered indirect contributions. Therefore, in this work we focus on a scenario measuring signals of a small subset of a large scale neuronal network, which is more realistic for most *in vitro* and *in vivo* applications.

As the number of electrodes in electrophysiological recordings have increased up to several thousands accompanied with huge data sets, used algorithms for connectiv-

ity analysis have to be highly computationally effective.

For this purpose, a novel connectivity estimation method, called *Total Spiking Probability Edges* (TSPE), based on cross-correlation and edge filtering at different time scales is proposed and the theoretical framework is outlined in this work. TSPE enables the classification between inhibitory and excitatory connections, which is a feature of effective connectivity estimation.

By means of simulated data sets encompassing various topologies (*random* and *scale-free*) results of TSPE are compared to a wide range of state-of-art connectivity estimation algorithms, including filtered and normalized cross-correlation histogram (FNCCH) Pastore et al. (2018b), delayed transfer entropy (DTE), delayed higher order transfer entropy (DHOTE), delayed transfer entropy coincidence index (DTECI), delayed higher order transfer entropy coincidence index (DHOTECI) Stetter et al. (2012); Ito et al. (2011), normalized cross-correlation (NCC) Bedenbaugh and Gerstein (1997), normalized cross-correlation coincidence index (NCCCI) and combined high order transfer entropy (CDHOTE). Each of these algorithms is adapted to connectivity estimation for large scale networks and described in the attachment. Evaluated algorithms are applied on every combination of a possible source neuron X and target neuron Y in the network to be explored. For each neuron pair, dependency in both directions are studied. The knowledge about causal relationships between neurons is another feature of effective connectivity estimation.

The TSPE algorithm and evaluation framework is implemented in *MATLAB* and available on `https://github.com/biomemsLAB/TSPE`.

2.2 Methods

2.2.1 Connectivity estimation algorithm TSPE

The proposed effective connectivity estimation method TSPE is based on the following assumptions:

- If the spike rate of a neuron increases after it has received an input signal, the connection is considered excitatory. Due to refractory times of the receiving neuron, the spike rate drops again after the excitatory input signal. The resulting cross-correlogram of emitting and receiving spike train shows a maximum (excitatory input) followed by low values (refractory time).

- If the spike rate of a neuron decreases after receiving an incoming action potential, the connection is considered inhibitory. The resulting cross-correlogram of emitting and receiving spike train shows a minimum (inhibitory input) surrounded by high values (activity before and after the inhibitory input). In this way inhibitory stimulation can only be identified if the receiving neuron is active before the stimulation.

In order to capture these local maxima and minima of the cross-correlogram, we apply an edge filter to the cross-correlogram. More precisely, the cross-correlation between spike train X and spike train Y (see Fig. 2.1.(c)) is calculated (see NCC in the attachment) to obtain the cross-correlogram $NCC_{XY(d)}$, where d is the temporal displacement (see Fig. 2.1.(d)). Next, the filter is applied by convolving $NCC_{XY(d)}$ with 1D edge filter $g_{(i)}$ (Fig. 2.1), resulting in spiking probability edges (SPE)

$$SPE_{X \to Y(d)} = NCC_{XY(d)} * g_{(i)}. \tag{2.1}$$

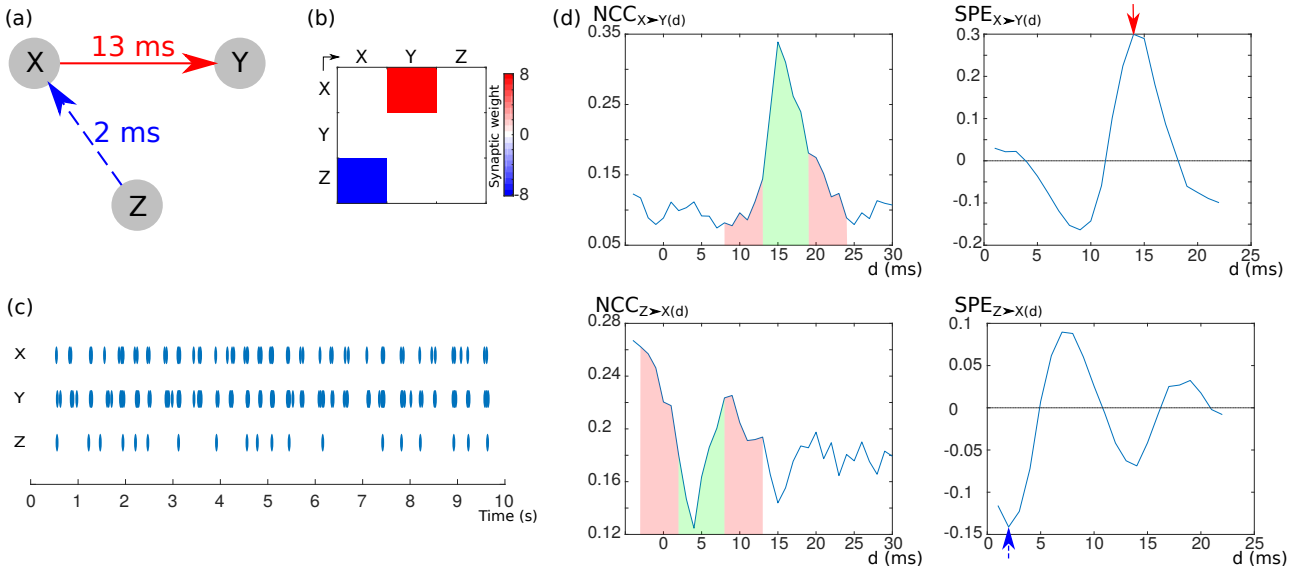

Figure 2.1: **Principle of SPE**: An exemplary network of three neurons (a) with a synaptic weight matrix (SWM) (b). Neuron X has an excitatory impact on Y with a latency of 13 ms after activation, while X is influenced by an inhibitory input of Z with a latency of 2 ms. (c) Spike trains of the three neurons X, Y and Z. (d) NCC of neuron pair $X \to Y$ and $Z \to X$ (left column). The convolution of the NCC with an edge filter $g_{(i)}$ results in the respective SPE (right). Global maxima (excitatory) and minima (inhibitory) are indicated by red and blue arrows, respectively. The latency can be seen on the abscissa. Areas in the left column show the corresponding areas for the calculation of the maximum and minimum (green: addition, red: subtraction).

We define the edge filters as a function $g_{(i)}$ with window size parameters a, b, c (in sampling periods, see

Fig. 2.2 (a)).

$$g_{(i)} = \begin{cases} -\frac{1}{a} & \text{if } 0 < i \leq a \\ \frac{2}{b} & \text{if } a + c < i \leq a + b + c \\ -\frac{1}{a} & \text{if } a + b + 2c < i \leq 2a + b + 2c \\ 0 & \text{else.} \end{cases} \tag{2.2}$$

a is the window size for the surrounding area of the point of interest which is used to calculate the local spiking probability average. b is the window size of the observed area. Small values for b increase the sensitivity for single outliers at the cross-correlogram. To avoid the including of overlapped spiking probabilities of interest with the local spiking probability average a soft crossover parameter c can be used. For an *in silico* evaluation with constant transmission times and a simple neuron model the usage of c is not necessary. Note that without using c the spiking probability edges of complex networks (*in vitro* or *in vivo*) can be smoothed, which is disadvantageous for an edge detection.

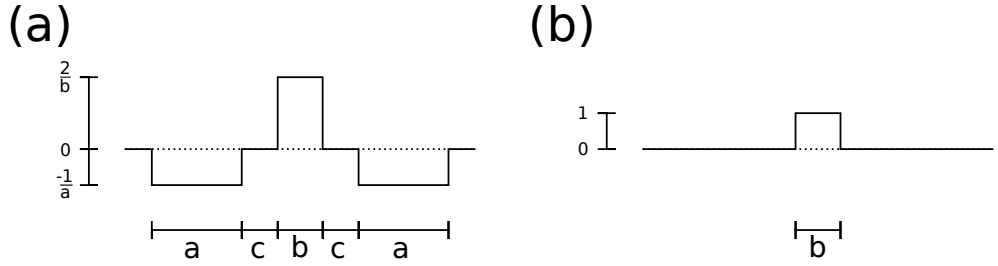

Figure 2.2: **Design of edge filter $g_{(i)}$ and running total filter $h_{(i)}$**: (a) The designed edge filters have an arithmetic mean of zero and are applied to the cross-correlogram. (b) The running total filters are designed by the same parameter b of the corresponding edge filter.

If the mean of function $g_{(i)}$ is zero, the calculation results in an arithmetic mean of zero for $SPE_{(d)}$, which prevents an offset for the resulting value range of $SPE_{(d)}$. If $NCC_{X \to Y(d)}$ shows a local maximum, $SPE_{X \to Y(d)}$ leads to a positive peak, while a local minimum for $NCC_{X \to Y(d)}$ results in a negative peak, see Fig 2.1.(d). Thus, negative peaks of $SPE_{X \to Y(d)}$ indicate an inhibitory effect of neuron X to neuron Y while positive peaks correspond to excitatory effects. By considering the highest absolute value of $SPE_{X \to Y(d)}$, the synaptic relation $X \to Y$ is obtained.

Since the network activity is significantly higher at periods of network bursts, this leads to a local offset of $SPE_{X \to Y(d)}$ and distort the calculation by overestimating the influences on receiving neurons. Normalization can reduce this unwanted impact. For this purpose, each $SPE_{(d)}$ is divided by the sum over all neuron pair results for the delay d,

$$SPE'_{X \to Y(d)} = \frac{SPE_{X \to Y(d)}}{\sum_{X=1}^{X=N} \sum_{Y=1}^{Y=N} SPE_{X \to Y(d)}}. \tag{2.3}$$

Parameter values $a = 5$, $b = 4$, and $c = 0$ (no smoothing) provided the best results to our simulated data. Thus, this combination captures the time constant of the used neural model. For more realistic applications different time scales should be considered because neurons are able to emit action potentials in several firing patterns. To cover multiple spiking behaviors of neurons $SPE'_{X \to Y(d)}$ is extended by the integration of many combinations of filter parameters we chose $a = [3, 4, 5, 6, 7, 8]$, $b = [2, 3, 4, 5, 6]$, $c = [0, 1]$ with vector length N_a, N_b, N_c. We found that low values of a and b increase the sensitivity to noise whereas high values do not affect results. Further $N_a \cdot N_b \cdot N_c$ combinations were taken into account. This introduces different lengths of convolution results $SPE'^{(n)}_{X \to Y(d)}$ (n is the index of the used edge filter). To obtain result vectors with same length 1D running total filters $h^{(n)}_{(i)}$ (see Fig. 2.2.(b)) are applied to $SPE'^{(n)}_{X \to Y(d)}$. For each edge filter $g^{(n)}_{(i)}$ a corresponding

running total filter is designed (2.4) by using the same parameter b from (2.2).

$$h_{(i)} = \begin{cases} 1 & \text{if } 0 < i \leq b \\ 0 & \text{else.} \end{cases} \tag{2.4}$$

As all $SPE'^{(n)}_{X\to Y(d)}$ have the same length, a matrix is obtained by introducing a row for each calculated $SPE'^{(n)}_{X\to Y(d)}$ (see Fig. 2.3.(d)). An vertically addition of this matrix enables the consideration of different time scales.

$$TSPE_{X\to Y(d)} = \sum_{n=1}^{N_a \cdot N_b \cdot N_c} SPE'^{(n)}_{X\to Y(d)} * h^{(n)}_{(i)} \tag{2.5}$$

The resulting $TSPE_{X\to Y(d)}$ values are interpreted as described before for $SPE'_{X\to Y(d)}$. The sign of $TSPE_{X\to Y(d)}$ with d at the absolute extreme value allows a discrimination between inhibitory from excitatory effects.

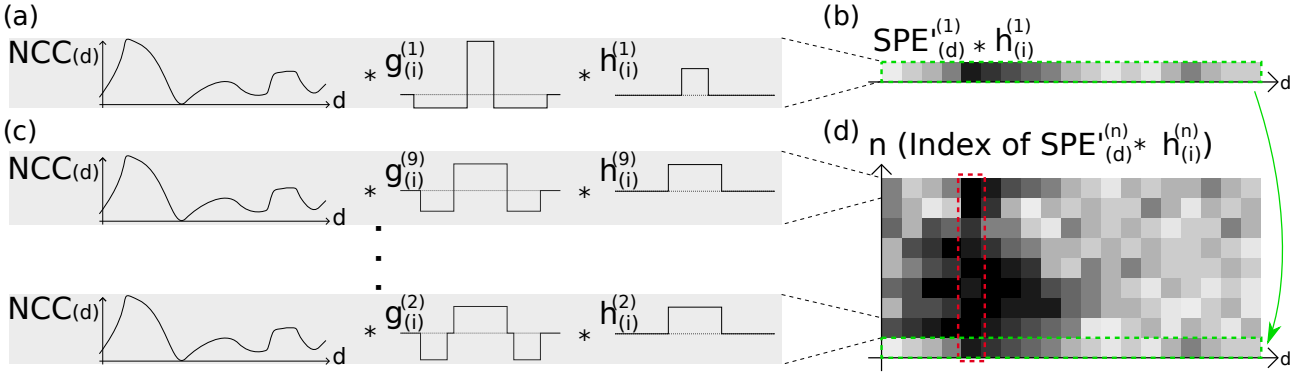

Figure 2.3: **Principle of TSPE**: (a) After the $SPE_{(d)}$ is calculated by a convolution of $NCC_{(d)}$ with an edge filter $g^{(1)}_{(i)}$ (see Fig. 2.1), a second convolution with a 1D running total filter $h^{(1)}_{(i)}$ is performed. (b) The result of the second convolution $SPE'^{(1)}_{(d)} * h^{(1)}_{(i)}$ is plotted with a gray scale plot. Dark color indicates a high value at a certain delay time d. (c) In order to capture the variance of time constants of the neurons, n edge filters $g_{(i)}$ are calculated for different window parameters. By $n = 9$ filtering operations, a three dimensional representation is obtained (d). The abscissa is the delay time and the ordinate is the index of calculated $SPE'_{(d)} * h_{(i)}$, while the gray scale indicates the resulting value. The green marked convolution (b) can be found in function (d) as first row, which is also marked green. The resulting $TSPE_{(d)}$ can be obtained by adding the values vertically. The absolute maximum is the most likely point of effect, which is marked red.

2.2.2 Implementations

For DTE, DHOTE, DTECI and DHOTECI we used the toolbox described in Ito et al. (2011), which is a MATLAB executable (MEX) application. CDHOTE is based on the calculations of DTECI and DHOTECI. The implementation of NCC, NCCCI, FNCCH and TSPE are realized with sparse matrices multiplications (unbinned simulation data, approx. 0.2% filled). All spike trains are stored in a common sparse matrix with the length that equals the sampling number. This matrix is multiplied with the transposed and time shifted matrix. The normalization matrix is calculated by multiplying the standard deviation (SD) vector with the its transposed version. For a faster calculation of TSPE the mean values of spike trains (0.005 to 0.04 at bin size of 1 ms) were omitted, because they did not affect the accuracy.

2.2.3 Evaluation methods

Simulation

For the evaluation of connectivity estimation algorithms, neuronal network behavior was simulated with the Izhikevich model, which is designed for large scale simulations Izhikevich (2003). The change over time of the membrane potential v in mV is

$$\dot{v} = 0.04 \cdot v^2 + 5 \cdot v + 140 - u + I \tag{2.6}$$

and the recovery variable u is

$$\dot{u} = a_{\mathrm{IZ}} \cdot (b_{\mathrm{IZ}} \cdot v - u), \tag{2.7}$$

which takes the inactivation of sodium Na^+ and activation of potassium K^+ channels into account. Variable I is the synaptic current and a_{IZ} is the time scale parameter for u, while b_{IZ} describes the sensitivity of u to the sub-threshold fluctuations of v.
By reaching the threshold of $v \geq 30\,\mathrm{mV}$, the neuron emits an action potential and the refractory period is activated. In that case variables v and u are changed obeying the rule (2.8). c_{IZ} is the reset potential and parameter d_{IZ} describes the reset value of the recovery variable u after each spike,

$$\text{if } v \geq 30\,\mathrm{mV}, \text{then} \begin{cases} v = c_{\mathrm{IZ}} \\ u = u + d_{\mathrm{IZ}} \end{cases} . \tag{2.8}$$

Parameters are for regular spiking (RS) excitatory neurons $a_{\mathrm{IZ}} = 0.02; b_{\mathrm{IZ}} = 0.2; c_{\mathrm{IZ}} = -65; d_{\mathrm{IZ}} = 8$. Parameters for fast spiking (FS) inhibitory neurons are $a_{\mathrm{IZ}} = 0.02; b_{\mathrm{IZ}} = 0.2; c_{\mathrm{IZ}} = -65; d_{\mathrm{IZ}} = 2$. The sampling rate of simulation is 1 kHz, which is enough to separate action potentials and a standard Izhikevich (2003). Synaptic transmission times are between 1 and 20 ms, which is realistic for monosynaptic delay times in cortex Mason et al. (1991); Swadlow (1994). The distribution of delay times was chosen uniformly.
Each simulated network contains 1000 neurons, which is a standard for large scale *in silico* models Izhikevich (2003). Electrophysiological recording methods can only measure a subset of the signals of a neuronal network. In order to take this into account only a subset of the simulated network is used for the connectivity estimation evaluation. Each subset contains 100 spike trains from randomly chosen 80 excitatory and 20 inhibitory neurons. This ratio of 4 to 1 reflects the observations in cortex and is also used in the large scale network. A square symmetric SWM with size of the number of neurons stores the synaptic properties of the network. The evaluation includes various network types and complexities:

- *Random networks* Erdös and Rényi (1959) with connection probability $p = 0.05$, $p = 0.1$ and $p = 0.15$
- Watts-Strogatz (WS) *small-world networks* Watts and Strogatz (1998) with a mean degree of 100 and a rewiring probability of 0.5
- implementation of Catanzaro (IC) *scale-free networks* Catanzaro et al. (2005) with a minimum degree of 10 and $\gamma = 2.0$
- Barabasi–Albert (BA) *scale-free networks* Barabási and Bonabeau (2003) with step wise growing of 24 connections (12 input- and 12 output-synapses)

Since *random networks* are used for the evaluation of many connectivity estimation algorithm evaluations Garofalo et al. (2009a); Ito et al. (2011); Pastore et al. (2018a), the Erdos–Renyi (ER) random network topology Erdös and Rényi (1959) was implemented using different connection probabilities p, following a Poisson distribution for input- and output-degrees. The mean degree of the *random network* in Figure 2.4 for example is five, see degree distribution in Figure 2.4. By setting a connection probability p, a *random network* with N

neurons has a mean degree of $N \cdot p$. *Random networks* with different connection probabilities are simulated to study effects of increasing network complexity on the algorithm accuracy.

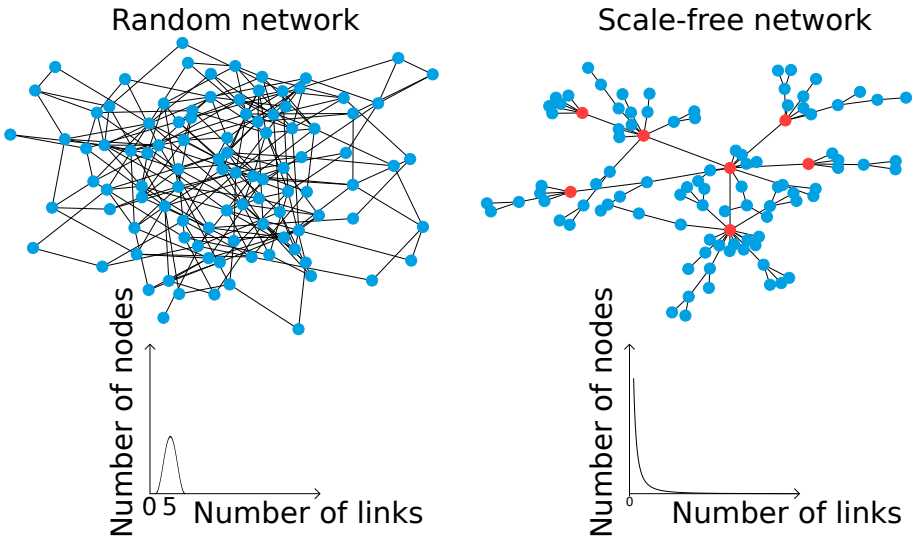

Figure 2.4: **Topologies of random and scale-free networks:** A *random network* is constructed choosing a constant connection probability. All nodes have approximately the same degree. The degree distribution for *random networks* is bell shaped. Most nodes of the network have five synapses. The construction of a *scale-free network* differs. Hub nodes are marked red and have a larger number of connections than the average of the *scale-free network*. Its distribution of node linkages is formed like a power law function. Thus, there are many nodes which are sparsely connected while some hubs are able to have lots of links.

Furthermore, a *small-world* topology is applied for evaluation because some studies Humphries et al. (2006) suggest that the neuronal network has *small-world* features. However, it is still controversial which network type it is exactly Muldoon et al. (2016). For a realistic simulation of *in vitro* spike trains, a log normal distribution for intracortical spontaneous mean firing rates (MFRs) Song and Wang (2005) is desired. One way to ensure more realistic MFRs is to model so called *scale-free* topologies for large scale neural network simulations De Blasi (2018a). Hub nodes have an immense number of connections with other nodes Barabási and Bonabeau (2003), which was also detected for neurons in regions of the brain Sporns et al. (2007); Bonifazi et al. (2009). In Figure 2.4 a *scale-free network* is illustrated with seven red marked hub neurons, resulting in a log normal distribution of node degrees. Since there are several forms of *scale-free* networks, exemplary two network generations were used: The IC Catanzaro et al. (2005) for uncorrelated *scale-free networks* and the BA Barabási and Bonabeau (2003) *scale-free network*.

Our simulated networks can contain antiparallel synapses whereas no self-connections and parallel synapses were implemented. In contrast to some *in silico* models Izhikevich (2003); Ito et al. (2011); Pastore et al. (2018a), our networks can contain connections between inhibitory neurons. The respective SWMs were constructed by modified implementations of the Python complex network package *NetworkX* Hagberg et al. (2008). For each simulation the mean of the log-normal distributed synaptic weights were set for potential network bursts. A higher density of connections requires a lower average synaptic weight for regular network bursts. For each simulated millisecond the network receives five external inputs at random nodes.

All simulations were performed in *2017a MATLAB*, MathWorks, with a modified version of the published code described in Izhikevich (2006). Each network type was generated and simulated ten times with different seed values for the random number generator of our simulation. Calculated mean values and standard deviations are used for the connectivity estimation evaluation. The *in silico* networks were designed according the guide described in De Blasi (2018a) for evaluation applications in neuroscience. The spike train subset of 100 neurons was recorded for 60 minutes, while studies were performed also for shorter time frames to analyze the impact of this parameter. It was demonstrated that long recording times improve the estimation results Ito

et al. (2011).

ROC Curve and AUC

The accuracy of a connectivity estimation algorithm is evaluated by comparing the results with the properties of the simulated network, described in the SWM. Since value ranges of CM are strongly dependent on the measured signal, these values are not directly comparable. In the best case, values of CM should be proportional to real synaptic weights of SWM. A threshold to distinguish between a 'real connection' and a 'statistical correlation' is used to calculate the thresholded connectivity matrix (TCM). This binary pattern of connection or non-connection will be used for the comparison with the SWM. The matches and mismatches between TCM and SWM are stored in four groups. Matches of connections are true positive (TP), mismatches are false positive (FP), matches for non existing synapses are true negative (TN), and mismatches are FP. A standard method to evaluate the performance of classifiers is the receiver operating characteristic (ROC) curve, which is a plot of true positive rate (TPR)

$$TPR = \frac{TP}{TP + FN} \tag{2.9}$$

depending on the false positive rate (FPR)

$$FPR = \frac{FP}{FP + TN}. \tag{2.10}$$

A perfect reconstruction of the SWM is indicated by a TPR of 1 and a FPR of 0. In case of equality of both rates classification is a random guess. Because of the sparse SWM a low FPR means a larger amount of wrong estimated connections than correctly estimated connections even with large TPRs. To prevent this misleading impression, the evaluation focuses on the TPR values at 1% FPR.
Another possibility to reduce the ROC to a single value of estimation accuracy is the area under the curve (AUC) Bradley (1997). While a AUC of 0.5 is a random guess, 1 means a perfect estimation.

Confusion matrix

A widely used visualization tool for the classification performance is the confusion matrix, or error matrix. It is a specific table layout that allows visualization of the performance of an algorithm. Each column of the matrix represents the labels while each row represents the predicted class. This visualization allows to see easily which classes are classified with high or low accuracy and which classes are often confused. In this study, inhibitory, excitatory, and no connection were used as class labels. The columns of a 2D confusion matrix are real labels obtained by the SWM. The rows contain the predicted classes of the classification algorithm. On the very right column the percentage of correctly classified connections of the output class is shown, at the bottom the percentage of correctly classified connections of the target classes is displayed. The general classification accuracy can be found in the lower right box. The classification ability of TSPE for distinguishing inhibitory from excitatory synapses is evaluated at a 1% FPR level.

2.3 Results

2.3.1 Accuracy of functional connectivity estimation

Generally, spike raster plots of all simulated topologies show spikes and network bursts with varying rate (see Fig. 2.5 left). For *random networks* the spike density within network bursts increases with connection probability p. For *scale-free networks*, spike density within network bursts is lower for the IC version than for the BA version.

The accuracy of the connectivity estimation methods NCC, NCCCI, FNCCH, DHOTE, DHOTECI, DTE, DTECI and CDHOTE was calculated for signals generated with *random* and *scale-free networks* and compared to the results of our TSPE algorithm. The results of all tested algorithms are depicted in Fig. 2.5 and better than random guessing (grey dashed line). The accuracy strongly depends on network topologies. For spike raster plots generated with *random networks*, the performances of the tested algorithms deteriorates with higher connection probability p. Methods based on a coincidence index (NCCCI, DHOTECI, DTECI) perform significantly better than their corresponding basic algorithms (NCC, DHOTE, DTE). This is particularly evident in the AUC values (right column in Fig. 2.5). The results of the TSPE algorithm show a ROC curve with a TPR up to 99.5% for $p = 0.05$ and $p = 0.1$. For $p = 0.15$ the performance accuracy decreased to 92%. The results of the FNCCH algorithm were similar to the results of TSPE for random networks with $p = 0.05$. However, the accuracy decrease for increased complexity ($p = 0.1$ and $p = 0.15$) was larger. The CDHOTE algorithm was inferior to NCCCI, DHOTECI, and DTECI for *random* and *small-world networks*. In contrast, for *scale-free network* topologies CDHOTE was superior.

All algorithms estimate the connectivity of *small-world networks* more accurately than that of complex *random networks* with $p = 0.15$. The SD of the results varied depending on topology. For *random* and *small-world networks*, the SD was lower than for *scale-free networks*. Especially for NCCCI, DTECI and DHOTECI large SDs are visible at the AUC values. At a FPR of 1% TSPE estimated the connectivity more precisely than any other tested algorithms. For both *scale-free networks* the accuracy of TSPE is inferior to the performance for *random* and *small-world networks*.

To study the performance dependency on the recording duration of spike train data, the TPR was measured at FPR of 1% for simulation durations of 1 min, 5 min, 10 min, 30 min and 60 min (see Fig. 2.6). The results show that accuracy increases with recording time. In case of *random networks* ($p = 0.05$ and $p = 0.1$) and *small-world networks*, TSPE is able to reach almost a TPR of 100% for a simulation duration of 60 min. Connectivity estimation saturates and therefore we assumed no accuracy increase for simulation durations longer than 60 minutes which is also true for *scale-free networks*.

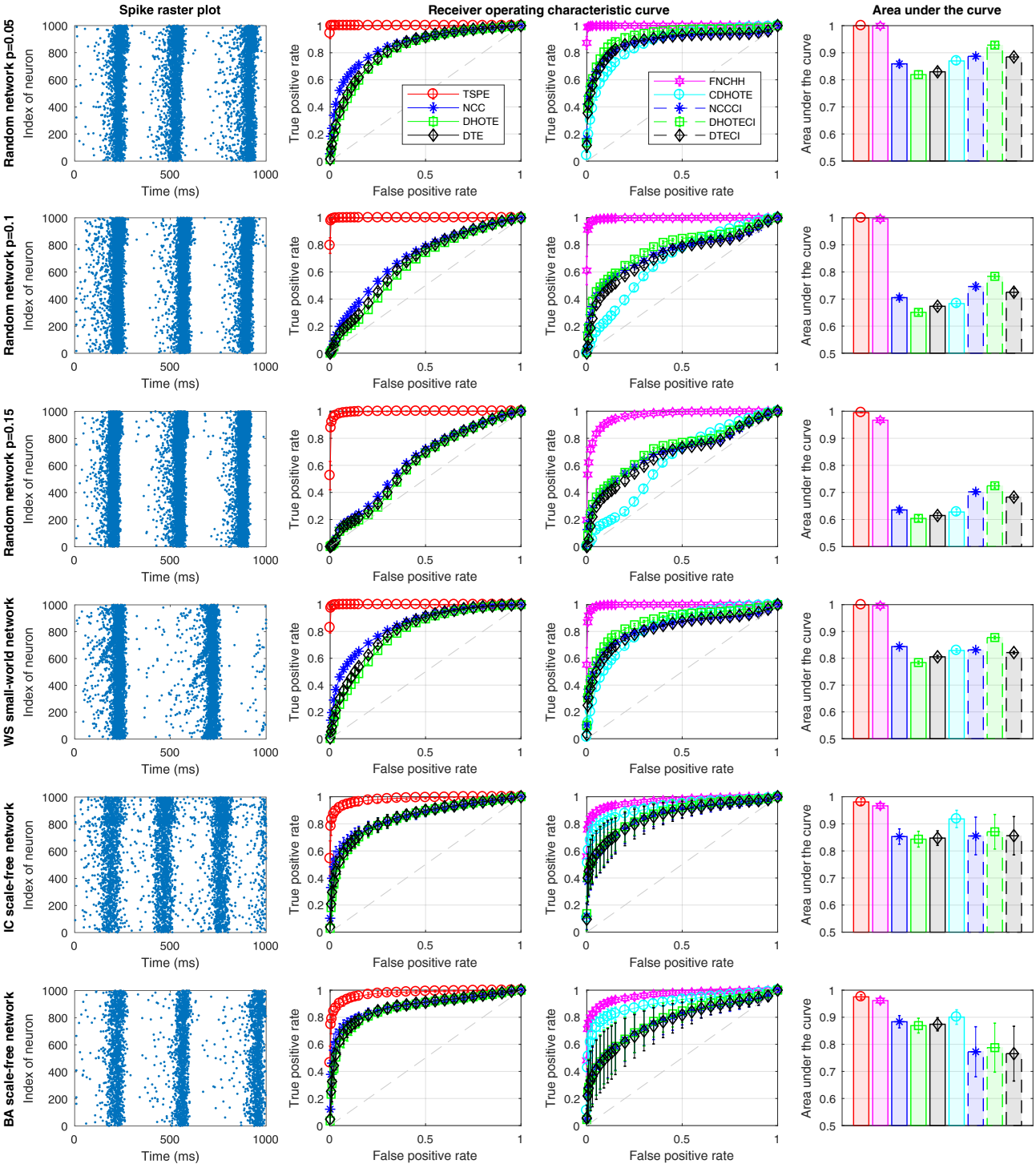

Figure 2.5: **Evaluation of connectivity estimation algorithms for different network topologies**: **Left column:** Spike trains of the simulated networks. For the evaluation a subset of only 100 spike trains with a simulation duration of 30 minutes were used. Network bursts appeared for all network topologies. **Middle columns:** ROC curves of all tested algorithms for $n = 10$ simulations per network topology. **Right column:** AUC values of all tested algorithms. With increased complexity of the *random networks* the accuracy of all algorithms decreased. Error-bars indicate standard deviation. TSPE outperformed all evaluated algorithms.

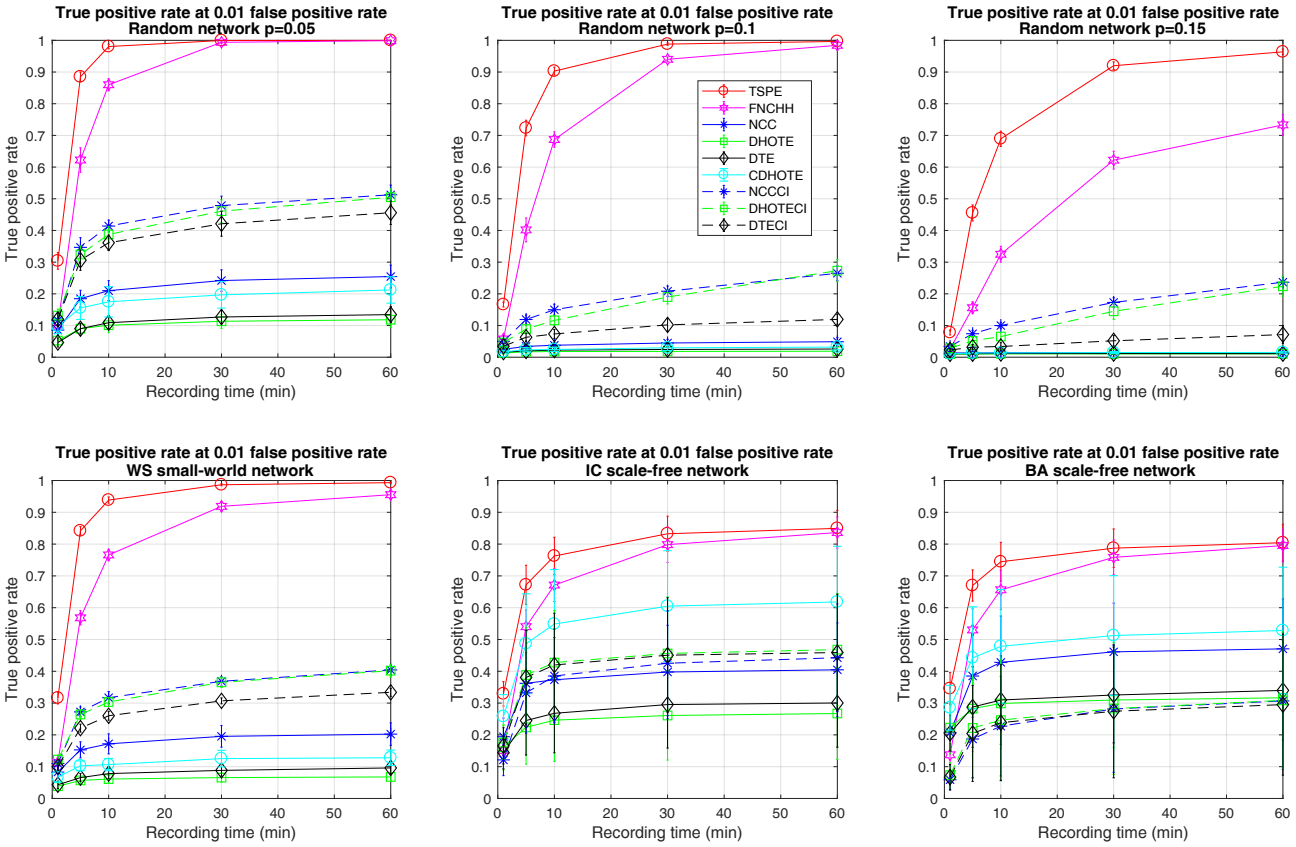

Figure 2.6: **Effects of the recording time on the accuracy of the connectivity estimation**. Accuracy estimation increases until a saturation is reached. Error-bars indicate standard deviation. Within the first ten minutes, the increase is strongest which is prominent for the TSPE algorithm.

2.3.2 Accuracy of effective connectivity estimation by TSPE

For effective connectivity not just connection strength but also information about causality and the synaptic effect is required. TSPE offers information about excitation and inhibition, which classification accuracy is studied in the following. In Fig. 2.7, the confusion matrices are plotted for TSPE at a FPR threshold level of 1%.

For *random networks* with $p = 0.05$, the total classification accuracy was 99.1%, which is practically the maximal achievable classification accuracy given that FPR is 1%. By increasing the complexity of *random networks* to $p = 0.1$, the total accuracy decreased by 0.3% (see blue boxes in Fig. 2.7). Further increase of complexity to $p = 0.15$ resulted in a large decrease of the classification performance and many effects were not detected instead of classified as a synaptic connection. For example, 32.3% of all inhibitory effects were not detected.

The classification of excitatory effects is more accurate for *small-world networks* than for *random networks* ($p = 0.1$ and $p = 0.15$). In contrast, for inhibitory effects the classification is more accurate for *random networks* ($p = 0.1$).

For both *scale-free network* types, the accuracy was 98.6 (92.3% and 88.7% for excitatory effects). However, 74% of all inhibitory effects were not classified correctly for the BA *scale-free* network (see Fig. 2.7 dark grey, bottom-center boxes).

To summarize, the classification accuracy for excitatory synapses was between 88.7 and 100%, for inhibitory effects it was between 26 and 96.6%.

Effective connectivity estimation also include the estimation of monosynaptic delay times. To evaluate the accuracy of this feature, the absolute difference of the estimated delay time to the respective morphological delay time was studied (see Fig. 2.8). The unrecognized connections are also included.

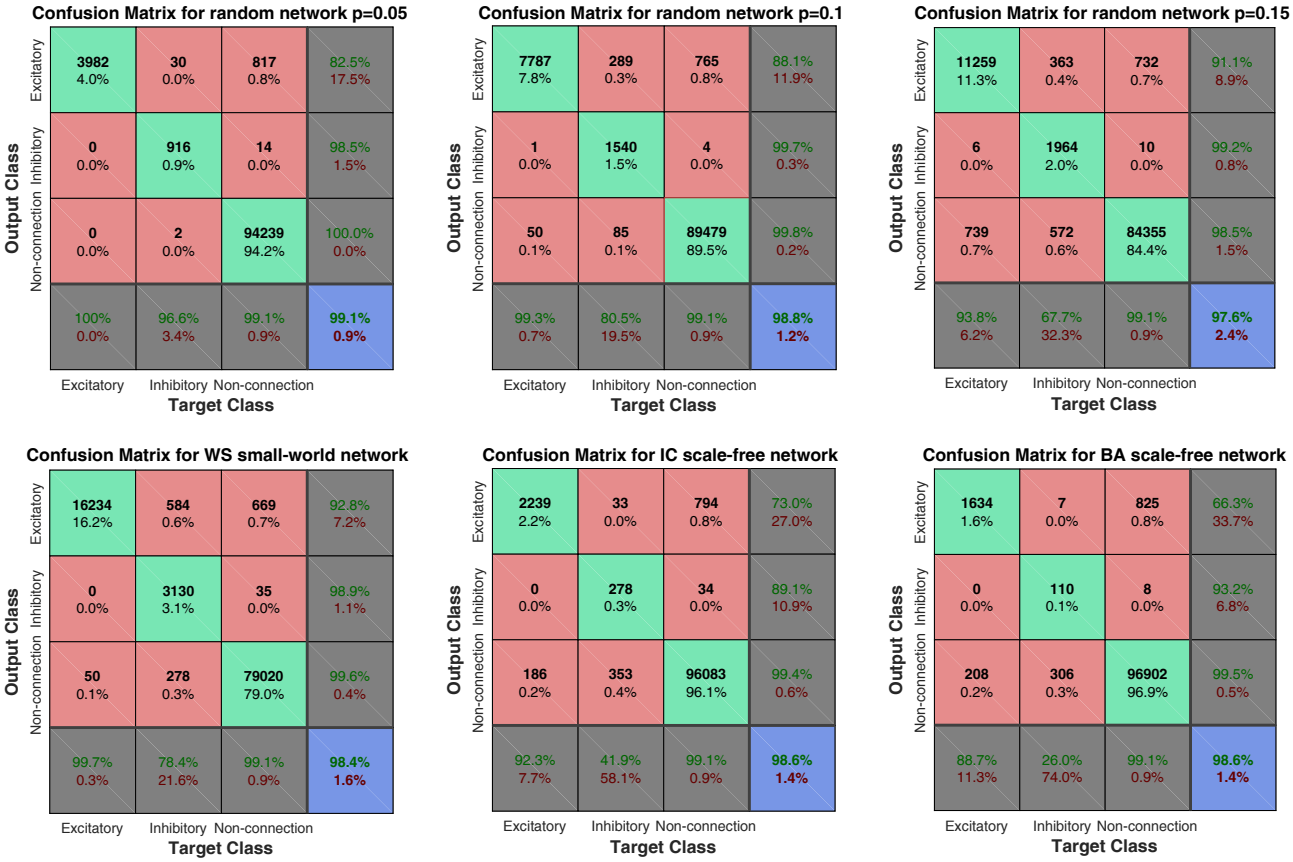

Figure 2.7: **Confusion matrices for connection types classified by TSPE for simulated network topologies**: Green (red) fields: correct (incorrect) classification (upper number: absolute, lower number: in percentage). Bottom row (grey): estimated connections to actual connections; Right column (grey): correctly estimated connections to all estimated connections. Blue field: total accuracy of classification. Grey and blue fields: green number percentage of correctness; red number percentage of incorrectness.

The delay times of excitatory effects were generally estimated more accurately. For the *random* and *small-world networks*, the majority of all estimated delay times matched or missed the actual delay time by only 1 ms. In general, the delay times of *scale-free networks* were more difficult to refer than with all other network topologies. Also for the delay estimation, inhibitory effects were more difficult to handle, resulting in up to 20% discrepancies of about 5 ms.

Since *random* and *scale-free networks* can be identified by their degree distribution, it is interesting whether this distribution can also be reconstructed. For this purpose, the actual degree distribution was compared with the estimated one (see Fig. 2.9).

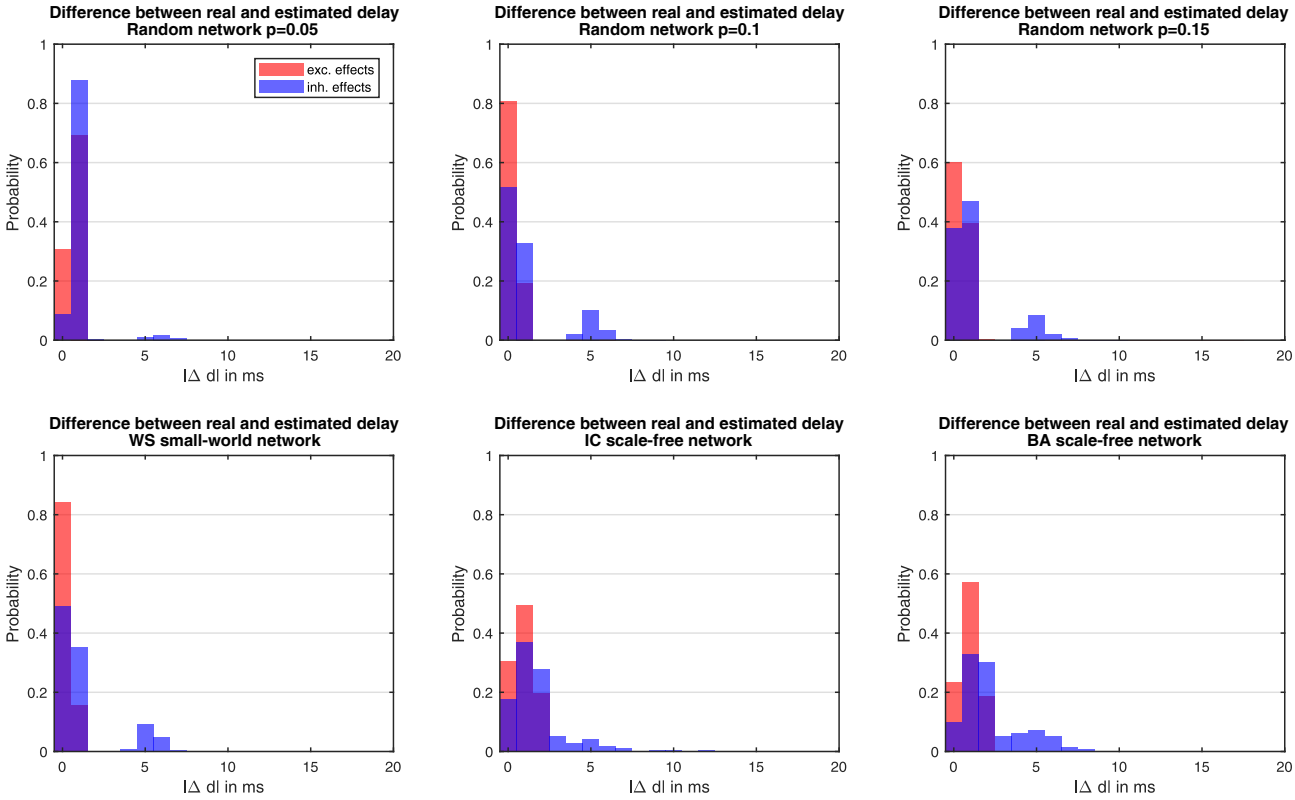

Figure 2.8: **Distribution of absolute estimation errors for delay times**. Estimated delay times of inhibitory effects are illustrated blue in front of the red illustrated excitatory effects. The delay times of inhibitory effects were generally estimated less accurately (especially for *scale-free networks*).

2.3.3 Calculation time

For a comparison of calculation efficiency, the processing time was measured for the calculation of connectivity estimation for IC *scale-free* networks with different number of spike trains (between 2 and 1000) and different simulation durations (between 1 and 60 minutes, see Fig. 2.10). Calculations were conducted using *MATLAB Distributed Computing Server* toolbox on a high-performance computer, which is equipped with 2 Intel Xeon 'Broadwell' E5-2680v4 processors, 8x32 GB DDR4 2400 MHz RAM, SSD and 4 SXM-2 P100 GPUs.
The results show that the calculation time increased linearly with recording time (indicated by blue dashed lines in Fig 2.10). Since the increase of recording time is also the increase of the amount of bins, the choice of a smaller bin size has the same influence on the calculation time. Due to the pairwise comparison of spike trains, the number of spike train comparisons increased exponentially (power of two) with the number of spike trains taken into account, which affected the computing time exponentially (indicated by green dashed lines in Fig 2.10). For large numbers of recorded spike trains, the calculation of transfer entropy (TE) based algorithms, like DTE or DHOTE, was longer than the calculation of cross-correlation (CC) based algorithms. NCC, TSPE and FNCCH were parallelized (matrix operation based algorithms). For example, the calculation time for a IC *scale-free* network with 1000 recorded spike trains and a simulation duration of 10 minutes was approx. 25 seconds for NCC, NCCCI or FNCCH, 45 seconds for TSPE, 16 minutes for DTE or DTECI, and 51 minutes for DHOTE or DHOTECI.

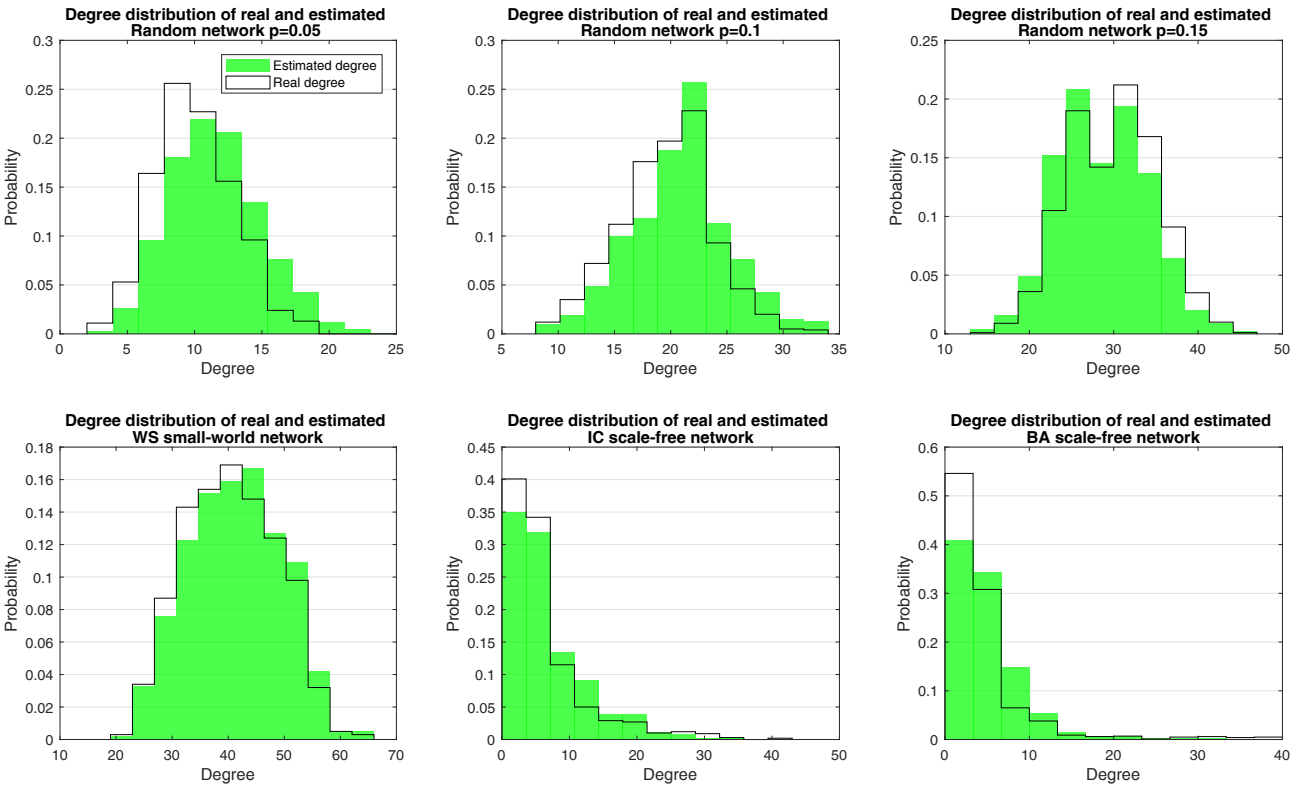

Figure 2.9: **Comparison of actual and estimated degree distributions**. The degree distribution used for the simulation is illustrated blank with edges and the estimated distribution is green. The low degree range is justified by the subset size of 100 neurons.

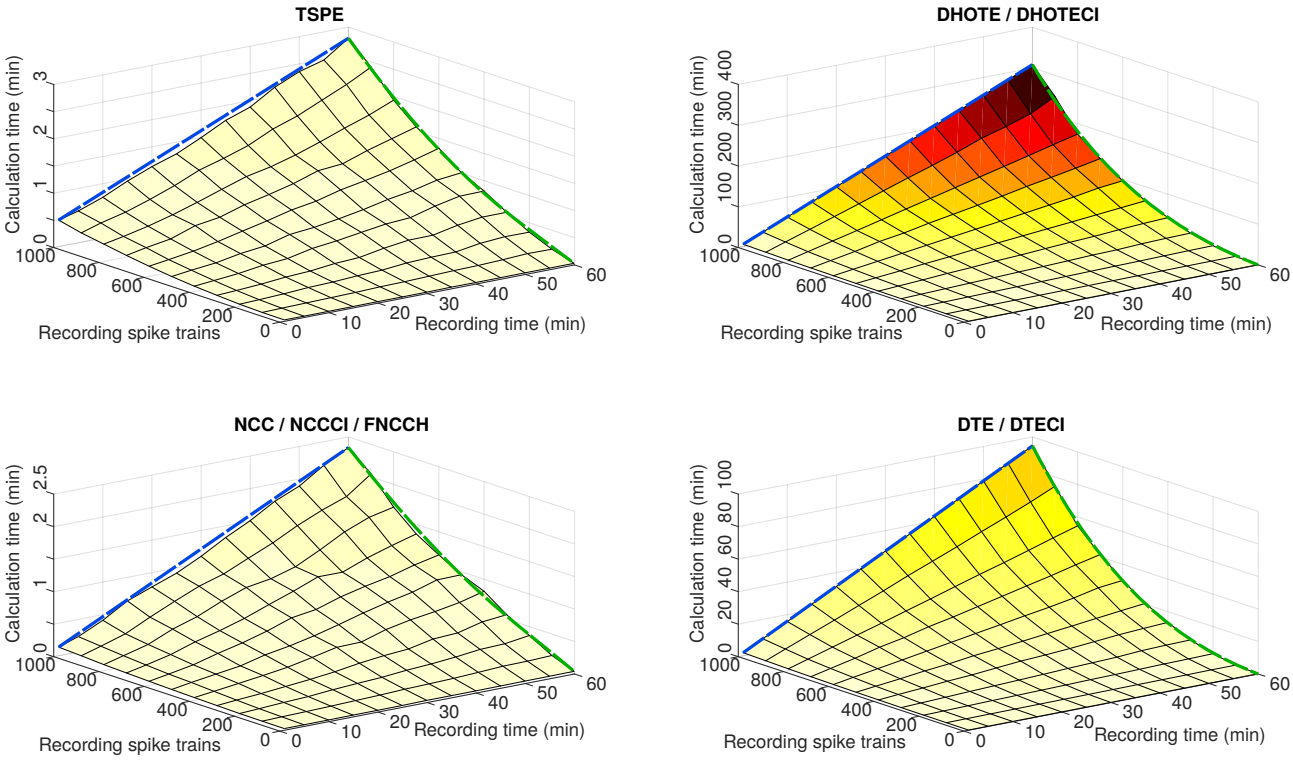

Figure 2.10: **Comparison of calculation times of tested algorithms**: The connectivity estimation algorithms were evaluated using data generated by IC *scale-free networks* for different lengths of recording and a variable number of spike trains. Red colored areas indicated long and light areas indicated small calculation times. Calculation time increased linearly with duration (indicated by blue dashed lines) but exponentially with number of spike trains (indicated by green dashed lines). Calculation time was in the following ascending order for algorithm groups: 1) NCC, NCCCI, FNCCH, TSPE 2) DTE, DTECI 3) DHOTE, DHOTECI.

2.4 Discussion and conclusion

In this work, a novel estimation algorithm for effective connectivity is proposed called *Total Spiking Probability Edges* (TSPE). The new algorithm is based on cross-correlation and detects correlation by edge filtering on different time scales of the cross-correlogram. A large framework of *in silico* networks with different topologies was used to benchmark the performance of the novel approach in comparison to FNCCH, NCC, NCCCI, DHOTE, DHOTECI, DTE, DTECI and CDHOTE. Influences of recording time on estimation accuracy and calculation time was analyzed. Furthermore, the classification ability in terms of inhibitory and excitatory effects of TSPE was evaluated.

The novel method is able to outperform the accuracy of other connectivity estimation algorithms when applied on simulated neuronal network data with different topologies. Especially for spike trains with a long recording duration like 30 minutes TSPE was outperforming. With TSPE, it was possible to discriminate between estimated excitatory and inhibitory connections, which is characteristic for effective connectivity. The total classification accuracy varied between 97.6 and 99.1%, depending on complexity of network topology. This estimation feature enables the characterization of the analyzed biological network.

Although these results are very promising, we also see critical aspects. TSPE is not able to detect effects of self-connections. Thus, the diagonal values of the CM have to be neglected or set to zero. Like for all other evaluated algorithms, the current implementation does not take multiple effects, e.g. driven by parallel connections, for a causal relation into account. Further, inhibition is more difficult to identify and to classify than excitation with estimation algorithms Ito et al. (2011); Masud et al. (2017); Pastore et al. (2018b) which is one aim of further improvements of TSPE.

TSPE is easy to implement and fast for large spike train datasets. Since new technologies of electrophysiological recording are able to record from thousands of electrodes, e.g. HDMEA chips with 4096 electrodes Berdondini et al. (2009a), it is crucial to minimize the computation time for large numbers of recorded spike trains. In our studies, TSPE, FNCCH, NCC and NCCCI were computed for 1000 spike trains (30 minutes duration) in less than 2 minutes, while Transfer Entropy based methods needed more than 45 minutes. Nevertheless, also the Transfer Entropy based methods take less than 3 minutes for 30 minutes of 60 channel recordings (standard MEA chip), which is considered acceptable for this application. The *in silico* model for evaluation was sampled at 1 kHz, which is enough to separate action potentials. We simulated the described model also for 10 kHz (data not shown) and found no difference in accuracy for the evaluated algorithms with the unbinned or binary binned (1 ms bin size) spike trains. We recommend a binning for preprocessing because of the linearly increasing computing time for evaluated connectivity estimation algorithms with smaller bin sizes. The gradient of computing time is smaller for cross correlation based connectivity estimation algorithms than for the TE based algorithms. Thus, long term experiments will benefit by applying TSPE or NCC.

For future research, the determination of an accurate threshold will be addressed. It is not possible to select a threshold at 1% FPR for real spike trains without knowing the connectivity of biological *in vitro* network, which is generally true for all reviewed algorithms. There are two common ways to select a threshold by means of signif-

icance test. First, a threshold can be obtained by calculating the 99% quantile of all possible connections for a generated surrogate spike train dataset Grün (2009), which theoretically estimates 1% wrong. This threshold should lead to 1% FPR for the real recorded dataset. Second, a threshold can be determined by calculating the mean value and a multiple of SDs of the resulting CM. One disadvantage of the first method is the multiplication of calculation time for the number of generated surrogate data, whereas the second method has a negligible calculation time.
Another problem for all evaluated methods is the activity dependent plasticity of connectivity, which should be considered for long term recordings of *in vitro* or *in vivo* neuronal networks. Since a long duration of recording improves the performance of connectivity estimation algorithms, a compromise between recording time and plasticity of connectivity has to be found. Our research will be continued with the development of innovative threshold selection methods for connectivity estimation and the application of SPE and TSPE for spike trains of *in vitro* experiments. The ability of TSPE to distinguish between excitatory and inhibitory effects could improve the meaningfulness of these experiments.
To summarize, the evaluation results show that the accuracy of connectivity estimation of large scale neuronal networks has been enhanced by the novel algorithm TSPE. This advantage combined with the ability to distinguish between excitatory and inhibitory effects will help to improve the accuracy of future experiments. To establish a standardized framework for comparison between connectivity estimation algorithms, the used simulation framework for large scale neural networks with different topologies is available for all as well as the *MATLAB* based TSPE toolbox, which has the potential of parallelization, `https://github.com/biomemsLAB/TSPE`.

Appendix

Comparison algorithms

Cross-Correlation

In 1967 CC has already been used to measure similarity between spike trains X and Y Perkel et al. (1967). By multiplying the time-shifted signal $x_{(i-d)}$ element-wise with another non-shifted signal $y_{(i)}$, temporal similarities are revealed as a function of time shift d. CC is defined as

$$CC_{X\to Y(d)} = \sum_{i=-\infty}^{\infty} y_{(i)} \cdot x_{(i-d)}. \tag{2.11}$$

Since the value range of the result of Eq (2.11) depends on the MFR, a normalization is needed. Using different types of normalization strongly affect the results of connectivity estimation. While some implementations are not able to detect inhibitory connections Masud et al. (2017), other methods of CC are even able to distinguish between inhibitory and excitatory connections Barthó et al. (2004). The most common method is normalized cross-correlation histogram (NCCH), which normalizes results with the geometric mean of total spiking times n_x and n_y of both spike trains Pasquale et al. (2008); Berdondini et al. (2009c); Maccione et al. (2012); Poli et al. (2015a); Pastore et al. (2016); Ito et al. (2011); Brosch and Schreiner (1999);

Kiemel and Cohen (1998); Eytan et al. (2004).

$$NCCH_{X\to Y(d)} = \frac{1}{\sqrt{n_x \cdot n_y}} \sum_{i=-\infty}^{\infty} y_{(i)} \cdot x_{(i-d)} \tag{2.12}$$

Another method of normalization is the usage of SD $\sigma_x \cdot \sigma_y$ and the number of bins N of the binned spike train. Additionally, the mean values $\bar{x}$ and $\bar{y}$ are subtracted of the respective spike moves before multiplication. This normalized version of CC is called NCC and is defined as Bedenbaugh and Gerstein (1997)

$$NCC_{X\to Y(d)} = \frac{1}{N} \sum_{i=-\infty}^{\infty} \frac{(y_{(i)} - \bar{y}) \cdot (x_{(i-d)} - \bar{x})}{\sigma_x \cdot \sigma_y}. \tag{2.13}$$

For sparse spike trains NCC and NCCH lead to similar results. However, the performance of NCC increases with increasing spike train length Ito et al. (2011). Thus, here only NCC is used for evaluation. Since the resulting matrix for the pairwise comparison of all combinations of spike trains is symmetric, the number of independent calculations for NCCs is $\frac{K^2-K}{2}$, where K is the number of spike trains.

Filtered and Normalized Cross-Correlation Histogram

Based on NCCH, the mean value of the cross-correlogram is calculated in a W window that is subtracted from the central value Pastore et al. (2018b). Positive values indicate excitatory effects and inhibitory effects for negative values. FNCCH is mathematical defined as

$$FNCCH_{X\to Y(d)} = NCCH_{X\to Y(d)} - \frac{1}{W} \sum_{v=-\frac{W}{2}}^{v=\frac{W}{2}} NCCH_{X\to Y(d)}. \tag{2.14}$$

Transfer Entropy

TE measures statistical dependence of three random processes, e.g. spike trains. The source spike train is considered the first random process, the target spike train the second process and the third process the future bin of the target spike train. Therefore, spike trains are usually delayed by one bin (Eq. 2.15). This form of TE is called delay one transfer entropy (D1TE) and known as the original definition Schreiber (2000).

$$TE_{X\to Y} = \sum_{x_i\in X} \sum_{y_i\in Y} \sum_{y_{i+1}\in Y} p(y_{i+1}, y_i, x_i) \cdot \log_2 \frac{p(y_{i+1}|y_i, x_i)}{p(y_{i+1}|y_i)} \tag{2.15}$$

TE is able to detect linear and nonlinear correlations Gourévitch and Eggermont (2007a); Garofalo et al. (2009a). The advantage of TE taking own history into account is tremendous for neuronal data because of refractory periods after spiking statements Ito et al. (2011). In contrast to Mutual Information, it is also possible to distinguish between source and target neuron

D1TE needs n^3 independent calculations for signals with base n (e.g. binary spike trains have the base two). If base two is used the results in CM are in bits. The higher the values, the stronger the information flow from source to target neuron.

D1TE showed good results for *in silico* evaluations Garofalo et al. (2009a); Pastore et al. (2016); Poli et al. (2016a). However, these models did not take variable delay times of axonal conductions into account, which is reason for an easy but unrealistic selection of optimal bin sizes (e.g. in their studies 1 ms). In reality, it is a problematic issue to choose a good value because it depends on each pair of spike trains.

Higher Order Transfer Entropy

Normally, TE is used with an order of one bin for both spike trains Lungarella and Sporns (2006); Garofalo et al. (2009a); Pastore et al. (2016); Poli et al. (2016a). However, D1TE can be extended to an higher order transfer entropy (HOTE) by increasing its temporal range Stetter et al. (2012); Ito et al. (2011), see Eq. 2.16.

$$HOTE_{X\to Y} = \sum_{x_i^{(l)}\in X}\sum_{y_i^{(k)}\in Y}\sum_{y_{i+1}\in Y} p(y_{i+1}, y_i^{(k)}, x_i^{(l)}) \cdot \log_2 \frac{p(y_{i+1}|y_i^{(k)}, x_i^{(l)})}{p(y_{i+1}|y_i^{(k)})} \quad (2.16)$$

Parameters k and l are the number (=order) of history bins of target and source spike train taken into account. For $k = 1$ and $l = 1$ HOTE would be equal to D1TE. The number of patterns is 2^{1+k+l} and rises exponentially with the chosen order. Thus, HOTE can be computationally intensive compared with D1TE.

Delayed Higher Order Transfer Entropy

Another modification of TE was introduced to neuroscience Ito et al. (2011), which was already used in other fields of research Overbey and Todd (2009). By shifting the source spike train with a delay d in the past, it is possible to consider effects in a variable time window. This shifting process is similar to CC. Therefore, the Eq. 2.16 of HOTE is further extended to Eq. 2.17.

$$DHOTE_{X\to Y(d)} = \sum_{x_i^{(l)}\in X}\sum_{y_i^{(k)}\in Y}\sum_{y_{i+1}\in Y} p(y_{i+1}, y_i^{(k)}, x_{i+1-d}^{(l)}) \cdot \log_2 \frac{p(y_{i+1}|y_i^{(k)}, x_{i+1-d}^{(l)})}{p(y_{i+1}|y_i^{(k)})} \quad (2.17)$$

DHOTE with $d = 1$ is equal to the normal HOTE. For various delay times (e.g. 1 to 25 ms in 1 ms steps) DHOTE is calculated while the maximum value is used for the CM value of the examined connection $X \to Y$.
Thus, in contrast to normal TE or HOTE, the information flow is observed for variable delay times of the event. Since it is no longer necessary to take as many influences as possible in one bin into account, the selection of a small bin size in combination of a wide shifting range should be able to process all relevant effects. Nevertheless, selecting the smallest possible bin size, which would be limited by the sampling frequency, leads to a longer computing time because of the increasing signal length for probability calculations. We chose $l = 2$, $k = 3$ for DHOTE and $l = 1$, $k = 1$ for DTE.

Coincidence Index

A delay-dependent function $M_{(d)}$, like $NCC_{XY(d)}$ for example, is normally analyzed by chosing its peak value. In order to further improve the results of the analysis quali-

tatively, a widely used tool is introduced: The coincidence index (CI), see Eq. 2.18 Ito et al. (2011); Chiappalone et al. (2006a); Juergens and Eckhorn (1997); Jimbo et al. (1999).

$$CI = \frac{\sum_{d=d_\mathrm{p}-\frac{\tau}{2}}^{d_\mathrm{p}+\frac{\tau}{2}} M_{(d)}}{\sum_{d=d_\mathrm{min}}^{d_\mathrm{max}} M_{(d)}} \tag{2.18}$$

The CI algorithm integrates values in a range of τ around the maximum value and normalizes the integral. For $M_{(d)}$ we chose the absolute values of $NCC_{XY(d)}$. For reasons of overview, suffix -CI will indicate the use of CI, e.g. NCCCI for the CI of NCC. Furthermore, DTECI and DHOTECI are introduced as well.

Combined High Order Transfer Entropy

By combining the results of connectivity estimation algorithms, it is possible to get a different accuracy. Based on the idea of identifying significant connections by combining DHOTECI and DHOTE results Shimono and Beggs (2015), a geometric combination method is developed. CDHOTE is implemented by plotting DHOTECI values against DHOTE values. In this plot the value point M (max(DHOTE); max(DHOTECI)) is assumed to be the place with highest possibility for a connection. For the two-dimensional space, the Euclidean distance between any points P and Q is calculated following Eq. 2.20.

$$d(P,Q) = \sqrt{(P_1 - Q_1)^2 + (P_2 - Q_2)^2} \tag{2.19}$$

Calculating the Euclidean distance from the point of interest M to each value pair V with coordinates (DHOTE; DHOTECI), a new CM can be formed. Low values (distances) are more likely to indicate connections and the threshold is the Euclidean distance starting from 0.

$$CDHOTE_{X\to Y} = d(V_{X\to Y}, M) \tag{2.20}$$

Author contribution

Development of the algorithm: SDB. Performed the experiments: SDB. Analyzed the data: SDB, MC. Wrote the paper: SDB, MC, AB, and CT.

Chapter 3

Spike-contrast: A novel time scale independent and multivariate measure of spike train synchrony

Manuel Ciba[1,*], Takuya Isomura[2], Yasuhiko Jimbo[3], Andreas Bahmer[4], Christiane Thielemann[1]

1 Biomems lab, University of Applied Sciences Aschaffenburg, 63743 Aschaffenburg, Germany.
2 Department of Human and Engineered Environmental Studies, Graduate School of Frontier Sciences, The University of Tokyo, Bunkyo-ku, Tokyo 113-8656, Japan.
3 Department of Precision Engineering, School of Engineering, University of Tokyo, Bunkyo-ku, Tokyo 113-8656, Japan.
4 University ENT-Clinic Würzburg, Theoretical and Experimental Neurophysiology, 97080 Würzburg, Germany.
***** Corresponding author, manuel.ciba@th-ab.de

Published in *Journal of Neuroscience Methods*
Volume 293, 1 January 2018, Pages 136-143

Abstract

Background:
Synchrony within neuronal networks is thought to be a fundamental feature of neuronal networks. In order to quantify synchrony between spike trains, various synchrony measures were developed. Most of them are time scale dependent and thus require the setting of an appropriate time scale. Recently, alternative methods have been developed, such as the time scale independent *SPIKE-distance* by Kreuz et al..

New Method:
In this study, a novel time-scale independent spike train synchrony measure called *Spike-contrast* is proposed. The algorithm is based on the temporal "contrast" (activity vs. non-activity in certain temporal bins) and not only provides a single synchrony value, but also a synchrony curve as a function of the bin size.

Results:
For most test data sets synchrony values obtained with *Spike-contrast* are highly correlated with those of the *SPIKE-distance* (Spearman correlation value of 0.99). Correlation was lower for data containing multiple time scales (Spearman correlation value of 0.89). When analyzing large sets of data, *Spike-contrast* performed faster.

Comparison of existing Method:
Spike-contrast is compared to the *SPIKE-distance* algorithm. The test data consisted of artificial spike trains with various levels of synchrony, including Poisson spike trains and bursts, spike trains from simulated neuronal Izhikevich networks, and bursts made of smaller bursts (sub-bursts).

Conclusions:
The high correlation of *Spike-contrast* with the established *SPIKE-distance* for most test data, suggests the suitability of the proposed measure. Both measures are complementary as *SPIKE-distance* provides a synchrony profile over time, whereas *Spike-contrast* provides a synchrony curve over bin size.

3.1 Introduction

Synchrony within neuronal networks is thought to play an important role since it is related to e. g. cognitive processes (Ward, 2003), sensory awareness (Engel et al., 2001) as well as pathological states such as epilepsy (Fisher et al., 2005; Truccolo et al., 2014), and Parkinson's disease (Pare et al., 1990; Arnulfo et al., 2015). Recorded neuronal signals are often reduced to spike time series to conduct further analyses as it is assumed that information is mostly coded in the time of occurrence (Rieke, 1999). Such a sequence of spike times is called a spike train. The level of synchrony among two or more spike trains can be used to e. g. evaluate theoretical neuronal models (Jolivet et al., 2008), test stimulus response reliability of neurons (Mainen and Sejnowski, 1995), or quantify the effect of drugs in *in vitro* biosensor applications (Selinger et al., 2004; Flachs and Ciba, 2016).
In general, synchrony means "the state of two or more events occurring at the same time". Whether two events can be considered synchronous depends on how "at the same time" is specified. In neuronal networks such a time can be absolute due to latencies or synaptic delays (Jeffress, 1948; Bahmer and Langner, 2006), but also relative depending on the oscillatory rhythms. For instance, oscillations in the brain vary between milliseconds and slower time scales, such as the 24-hour period of the circadian rhythm (Buzsaki, 2006).

In order to quantify the level of synchrony, many different methods have been developed. When applied to spike train data, most of them are time scale dependent, requiring the user to define a relevant time scale (Victor and Purpura, 1996; van Rossum, 2001; Quian Quiroga et al., 2002; Schreiber et al., 2003; Selinger et al., 2004; Chiappalone et al., 2007b; Cutts and Eglen, 2014). Thereby, a risk exists of choosing suboptimal time scales, affecting the comparability or validity of results. In contrast, time scale independent measures are able to perform optimally without choosing the optimal time scale beforehand (Kreuz et al., 2007a). Recently, time scale independent measures have been developed, such as *ISI-distance* (Kreuz et al., 2007a, 2009), *SPIKE-distance* (Kreuz et al., 2013), and *SPIKE-synchronization* (Kreuz et al., 2015).

In this study, a novel spike train synchrony measure called *Spike-contrast* is proposed and evaluated. The general idea of the synchrony measure is based on an intuitive visual contrast when displaying spike trains as a raster plot. Synchronized spike trains can be observed as vertical bars whose visual contrast increases with increasing synchrony. Thus, by means of *Spike-contrast*, the synchrony between spike trains is calculated. To avoid the limitations of a fixed time window for which spikes are considered synchronous, the time window length is varied (this can be regarded as "zooming"). Synchrony is calculated as a function of the time scale, producing a synchrony curve whose maximum is defined as the overall synchrony value. If more than one maximum appears, this indicates that spike train data are synchronized at different time scales.
The mathematical description of the new measure is given in the method section 3.2.1. Implementation details are in method section 3.2.2 and 3.2.3. *Spike-contrast* is compared to the synchrony measure *SPIKE-distance* (Kreuz et al., 2013) as

SPIKE-distance has been successfully used in different applications, e. g. discrimination of the synchrony increase mediated by bicuculline and cyclothiazide in cultured hippocampal neurons (Eisenman et al., 2015), evaluation of a bioinspired locomotion system for a quadruped robot (Espinal et al., 2016), and correlating behavioral metrics and spike trains in an inverse neurocontroller (Dura-Bernal et al., 2016). For the comparison, both synchrony measures were applied to artificial spike train data featuring different levels of synchrony (section 3.2.4). The data include Poisson distributed spike trains and spike bursts, spike trains generated from simulated neuronal Izhikevich networks, and bursts that include shorter bursts (sub-bursts). Moreover, calculation speeds were compared.

3.2 Material and methods

3.2.1 Definition of *Spike-contrast*

The proposed synchrony measure *Spike-contrast* is based on the visual observation that synchronous spike trains form vertical bars when displayed as a raster plot. Fig. 3.1 shows three raster plots where each spike is represented as a black dot on a white background over time. If all spike trains are perfectly synchronized, the raster plot exhibits black vertical bars separated by white bars (Fig. 3.1 top). Here, the transition between black and white bars is referred to as "contrast". The higher the level of synchrony, the higher the gradient of the transition between black and white bars, and the higher the contrast. However, the contrast critically depends on the considered time scale. If only shorter and shorter parts of the spike trains are considered, spike trains appear less and less synchronized (Fig. 3.1 middle and bottom).

To eliminate the time scale dependence of the method, different time scales are considered by "zooming" into the signal. Finally, the maximum synchrony value found across the time scales is defined as the synchrony value S of the network. The zooming process is realized using various bin sizes to construct time histograms. The following steps are required (see also Fig. 3.2a), where N is the total number of spike trains, Δ is the bin size, and K is the total number of bins: 1) Creation of a time histogram counting the number of spikes per kth bin (Θ_k) across all spike trains. The histogram is used to calculate a first factor $Contrast$. 2) Creation of a second time histogram counting the number of spike trains showing at least one spike per kth bin (n_k). The histogram is used to calculate a second factor $ActiveST$. This factor is needed to compensate for unwanted high $Contrast$ values in cases where a single spike falls into a separate bin which is surrounded by empty bins. 3) Step one and two are repeated for different bin sizes Δ (for details see section 3.2.2) resulting in two curves $Contrast(\Delta)$ and $ActiveST(\Delta)$. 4) The product of $Contrast(\Delta)$ and $ActiveST(\Delta)$ yields the synchrony curve $s(\Delta)$. 5) The maximum of $s(\Delta)$ is defined as the final synchrony value S. More precisely, the synchrony measure is defined as

$$S = \max s(\Delta) \tag{3.1}$$

with

$$s(\Delta) = Contrast(\Delta) \cdot ActiveST(\Delta). \tag{3.2}$$

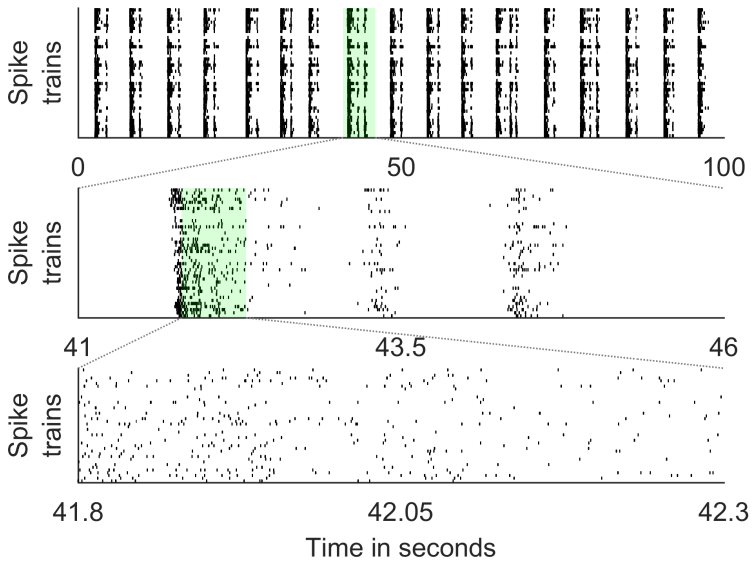

Figure 3.1: Raster plots of simultaneously recorded spike trains from an *in vitro* neuronal network cultured on a microelectrode array (MEA) chip with 64 recording sites. Considering a time period of 100 s (top) spike trains appear highly synchronized. When zooming into the signal, spike trains appear less and less synchronized (middle and bottom). This leads to the problem of having to choose an appropriate time scale to measure synchrony.

The first factor in Eq. 3.2, the spike train contrast, is defined as

$$Contrast(\Delta) = \frac{\sum_{k=1}^{K-1} |\Theta_k - \Theta_{k+1}|}{2 \sum_{k=1}^{K} \Theta_k}, \tag{3.3}$$

with Θ_k being the sum of all spikes of the kth bin over all spike trains, and K being the number of bins. For a signal length T and a bin size Δ with a bin overlap of $\Delta/2$, $K = 2 \cdot \lfloor T/\Delta \rfloor$. The second factor $ActiveST$ is defined as

$$ActiveST(\Delta) = \frac{1}{N-1} \left(\frac{\sum_{k=1}^{K-1} n_k \cdot \Theta_k}{\sum_{k=1}^{K} \Theta_k} - 1 \right) \tag{3.4}$$

with N being the number of spike trains, and n_k the number of spike trains containing at least one spike inside the kth bin. For a detailed explanation and derivation see appendix after section 3.4.2.

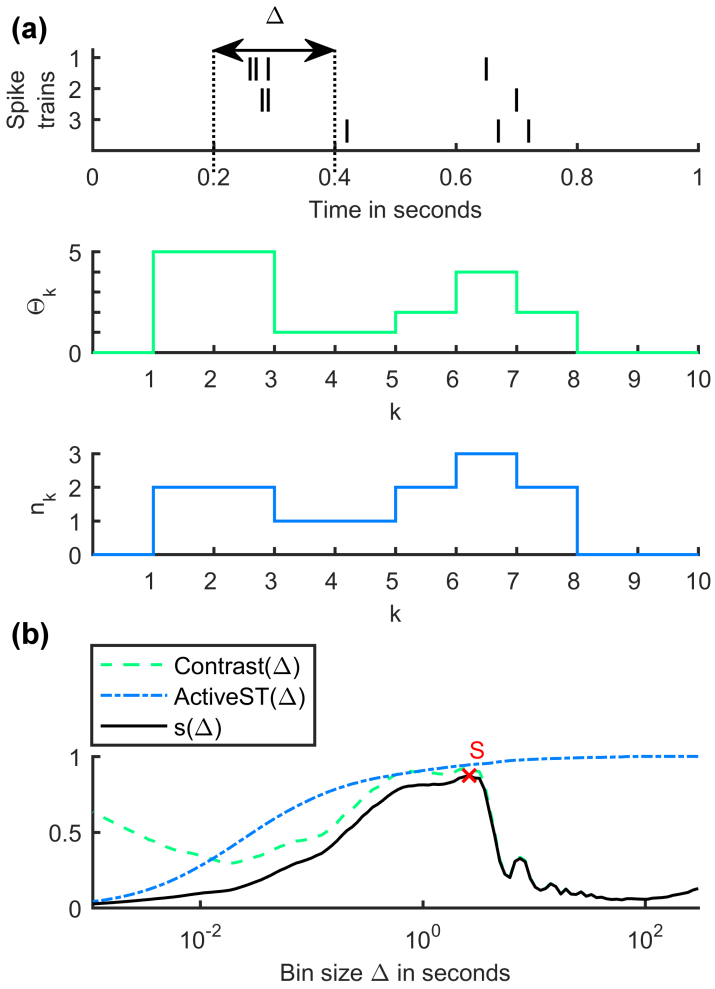

Figure 3.2: Visualization of factors and variables of *Spike-contrast* using example signals. (a) Raster plot of three artificial spike trains ($N = 3$). The number of spikes per bin Θ_k and the number of spike trains n_k containing at least one spike inside the kth bin are plotted as a histogram using a bin size Δ. Note that bins are overlapping by $\Delta/2$. (b) The synchrony curve $s(\Delta)$ is defined as the product of the two curves $Contrast(\Delta)$ and $ActiveST(\Delta)$. The final synchrony value S is defined as the maximum of $s(\Delta)$. The displayed curve resulted from an analysis of a 5-minute recording of a cortical neuronal network grown *in vitro* on an MEA chip.

3.2.2 Bin size selection

To obtain the synchrony function $s(\Delta)$, calculations for various bin sizes Δ are necessary. The choice of bin sizes not only influences the accuracy of the method, but also the calculation speed needed to obtain the final synchrony value. In order to compromise between calculation speed and accuracy, the following bin sizes were chosen in this study: The maximum bin size Δ_{max} is set to half of the signal length T. The minimum bin size Δ_{min} is set to half of the smallest inter-spike interval (ISI) or to a constant value L (whichever is greater):

$$\Delta_{max} = T/2 \tag{3.5}$$

$$\Delta_{min} = max(ISI_{min}/2,\, L) \tag{3.6}$$

The adaptive limit of $ISI_{min}/2$ is defined in order to ensure an empty bin besides every spike. This is a prerequisite for the calculation of the contrast. L is a minimum bin size limit, that can be used to limit the maximum calculation duration. For the analysis of neuronal signals from cortical networks, L could be set to $1\ \mathrm{ms}$, as the maximum oscillation frequency in cortical networks has been reported to be around 500 Hz (Buzsáki and Draguhn, 2004). If L is set to zero, Δ_{min} only depends on ISI_{min}. In this case, *Spike-contrast* is completely adaptive to the data. The calculation is started using the bin size Δ_{max}. For every further iteration the previous bin size is then multiplied by 0.9 until it underruns Δ_{min}. Especially, for large bin sizes the temporal structure of the spike train may be not represented well by the histogram (e. g. several spike bursts end up in one bin). In order to better preserve the signal characteristic, bins are overlapping by half of the bin size Δ.

3.2.3 Synchrony measure implementation

All calculations made in this work were conducted using MATLAB® (MATLAB 2016a, The MathWorks, Inc., Natick, Massachusetts, USA) on a regular personal computer (CPU: Intel® Core i5-2400 @ 3.10 GHz, RAM: 16 GB). The test data and the MATLAB and Python (Python Software Foundation, https://www.python.org/) source code of *Spike-contrast* is available online (https://github.com/biomemsLAB/Spike-Contrast). The source code of *SPIKE-distance* was downloaded along with the tool called *cSPIKE* (http://wwwold.fi.isc.cnr.it/users/thomas.kreuz/Source-Code/cSPIKE.html) with the time-critical components written in C and used in MATLAB as a MEX file. *SPIKE-distance* is defined in Kreuz et al. (2013). As the measure of *SPIKE-distance* yields zero for perfect synchrony, it is substracted from one for easier comparability with *Spike-contrast*.

3.2.4 Test data

In order to evaluate *Spike-contrast*, it was compared to *SPIKE-distance* by means of four spike train data sets with different synchrony levels (for example spike trains see Fig. 3.3, column one and two). Poisson processes were used as a simple model that allows to control synchrony in a defined manner. Moreover, the Izhikevich neuronal network model (Izhikevich et al., 2003) was used to get biologically plausible signals. Below, the synchrony levels of all test data correspond to the factor F, having values in the range of $[0, 1]$ ($F = 0$: highest synchrony level, $F = 1$: lowest synchrony level).

Test data 1: Poisson spike model The first set of data consisted of Poisson processes based on test data used in Cutts and Eglen (2014). Two spike trains were generated with a spike rate λ of 1.5 spikes per second and a signal length of $300\ \mathrm{s}$. Both spike trains shared a defined fraction of identical spikes. The shared spike train also came from a Poisson process with a rate of

$$\lambda_S = \lambda \cdot (1 - F) \tag{3.7}$$

with the factor F corresponding to different synchrony levels ($F = \{0, 0.05, 0.1, \ ... \ 1\}$). For each F, $n = 20$ spike train pairs were generated.

Test data 2: Poisson burst model The second set of data was composed of bursts of spikes (Cutts and Eglen, 2014). The temporal center of each burst was determined in the same way as for the spike times in test data 1 (Poisson spike model) with a shared fraction λ_S of burst centers. The value of λ from Eq. 3.7 was 0.05 bursts per second. Relative to the burst center, M spikes were randomly (uniform distribution) assigned in the range of $[-1, 1]$ seconds. The number of spikes, M, was drawn from a Poisson distribution with a mean value of 8. The relative spike times as well as M were assigned independently for each burst and spike train. For each F ($F = \{0, 0.05, 0.1, \ ... \ 1\}$), $n = 20$ spike train pairs were generated. Note that even for the most synchronous case ($F = 0$) both spike trains were not identical as only the burst center points of both spike trains were synchronized but not the spike times inside a burst (as they were assigned randomly).

Test data 3: Izhikevich network Simulated spike trains were generated with networks of Izhikevich neurons using the Matlab source code from Izhikevich et al. (2003). All parameters were set to the values used in the source code, resulting in a network of heterogeneous cortical neuron types. Each network consisted of 1000 neurons (800 excitatory, 200 inhibitory). In order to reduce the size of data, only 60 spike trains were randomly chosen for further use. The simulation time was 2.2 s, but the first 0.2 s were rejected as signals were not yet in a steady-state. To obtain different levels of synchrony, the inhibitory synaptic strengths of the networks were multiplied by the factor F. It resulted in an increasing level of synchrony with decreasing values of F. This approach was inspired by the effect of the $GABA_A$ receptor blocker bicuculline, which causes an increase in synchronized signals in neuronal networks (Scharfman, 1994). In total, 20 values of F in the range of $[0, 1]$ were used to obtain different levels of synchrony. Values of F were chosen to have a uniform distribution of synchrony levels. For each F, $n = 20$ networks were generated randomly.

Test data 4: Sub-bursts This data set contains bursts that consist of shorter bursts, which we call sub-bursts. This approach was chosen as burst patterns at several time scales can be observed in real data e. g. in *in vitro* recordings from cortex slices (Baker et al., 2006). The first step was to create a spike train ST_1 made of single spikes with equal ISIs of 2 s and a signal length of 300 s. Each spike of ST_1 was then replaced by a burst consisting of three spikes, resulting in spike train ST_2 (spike positions are used as the burst starting points in all replacement steps). The ISI of the spikes inside a burst was set to 10% of the original ISI of ST_1 (0.2 s). For the final spike train ST_3, the replacement step was repeated for ST_2. ST_3 contained sub-bursts made of spikes with ISIs of 0.02 s. Next, a second spike train was generated by copying ST_3, but with a random jitter applied to each spike. The amount of random jitter came from a uniform distribution in the range of $[0\,\mathrm{s}, 0.02\,\mathrm{s}] \cdot F$. For $F = 0$ no jitter was applied and spike trains were identical. For each F ($F = \{0, 0.05, 0.1, \ ... \ 1\}$), $n = 20$ spike train pairs were generated.

3.2.5 Comparison of calculation speed

To compare the calculation speed of *Spike-contrast* and *SPIKE-distance*, they were applied to test data consisting of Poisson spike trains. All spike trains had a constant length of $100\ \mathrm{s}$ so the first bin size of *Spike-contrast* was $50\ \mathrm{s}$. As the calculation speed of *Spike-contrast* depends on the minimal bin size Δ_{min}, Δ_{min} was set to a constant value of $1\ \mathrm{ms}$ to simulate a worst case scenario when analyzing neuronal data (assuming a maximum oscillation frequency of 500 Hz such as described in Section 3.2.2). Not only the number of total spikes was varied, but also the number of spike trains, as both measures handle multivariate data differently. The number of spikes per spike train was varied from 10 to $1,000$ and the number of spike trains was varied from 10 to $1,000$. So, the total number of spikes varied from 100 to $1,000,000$. Calculations were performed on a regular personal computer (CPU: Intel® Core i5-2400 @ 3.10 GHz, RAM: 16 GB).

3.3 Results

3.3.1 Correlation of the synchrony measures

Spike-contrast and *SPIKE-distance* were applied to four sets of simulated spike train data (Fig. 3.3a-d) with different levels of synchrony, denoted as factor F. An F-value of zero corresponds to a high level of synchrony and an F-value of one to a low level of synchrony. Both measures were able to detect a monotonic change in synchrony as a function of F with *SPIKE-distance* showing synchrony values from 0.7289 ± 0.0083 (mean $\pm$ standard deviation) and 0.9799 ± 0.0029, and *Spike-contrast* showing synchrony values from 0.1413 ± 0.0264 to 0.9869 ± 0.0034 for Izhikevich network generated data (Fig. 3.3 third column). The results of both measures showed a very high correlation for most test data (Fig. 3.3a-c), in the very right column). The Spearman correlation coefficient ρ was around one, indicating a monotonic relation. This means that if the synchrony value of *Spike-contrast* increased, the value of *SPIKE-distance* also increased and vice versa. In addition, the correlation is approximately linear as indicated by the regression line. However, when applied to the sub-burst test data set (Fig. 3.3d), the correlation between both measures was lower ($\rho = 0.89$). The synchrony values of *SPIKE-distance* gradually decreased with increasing jitter, while synchrony values of *Spike-contrast* remained almost constant.

3.3.2 Calculation speed

Fig. 3.4 shows the calculation speed as a function of spikes per spike train and number of spike trains. The calculation time of *SPIKE-distance* increased with increasing number of spike trains (Fig. 3.4 top), whereas the calculation time of *Spike-contrast* did not increased remarkably with increasing number of spike trains (Fig. 3.4 middle). *Spike-contrast* is faster than *SPIKE-distance* for large sets of data (e. g. containing more than 200 spike trains and 1000 spikes per spike train) but slower for smaller sets of data (Fig. 3.4 bottom). The largest set of data used in the calculation speed test consisted of 1000 spike trains and 1000 spikes per spike train ($1,000,000$ spikes in total). In this case, *Spike-contrast* was almost 10 times faster than *SPIKE-distance*.

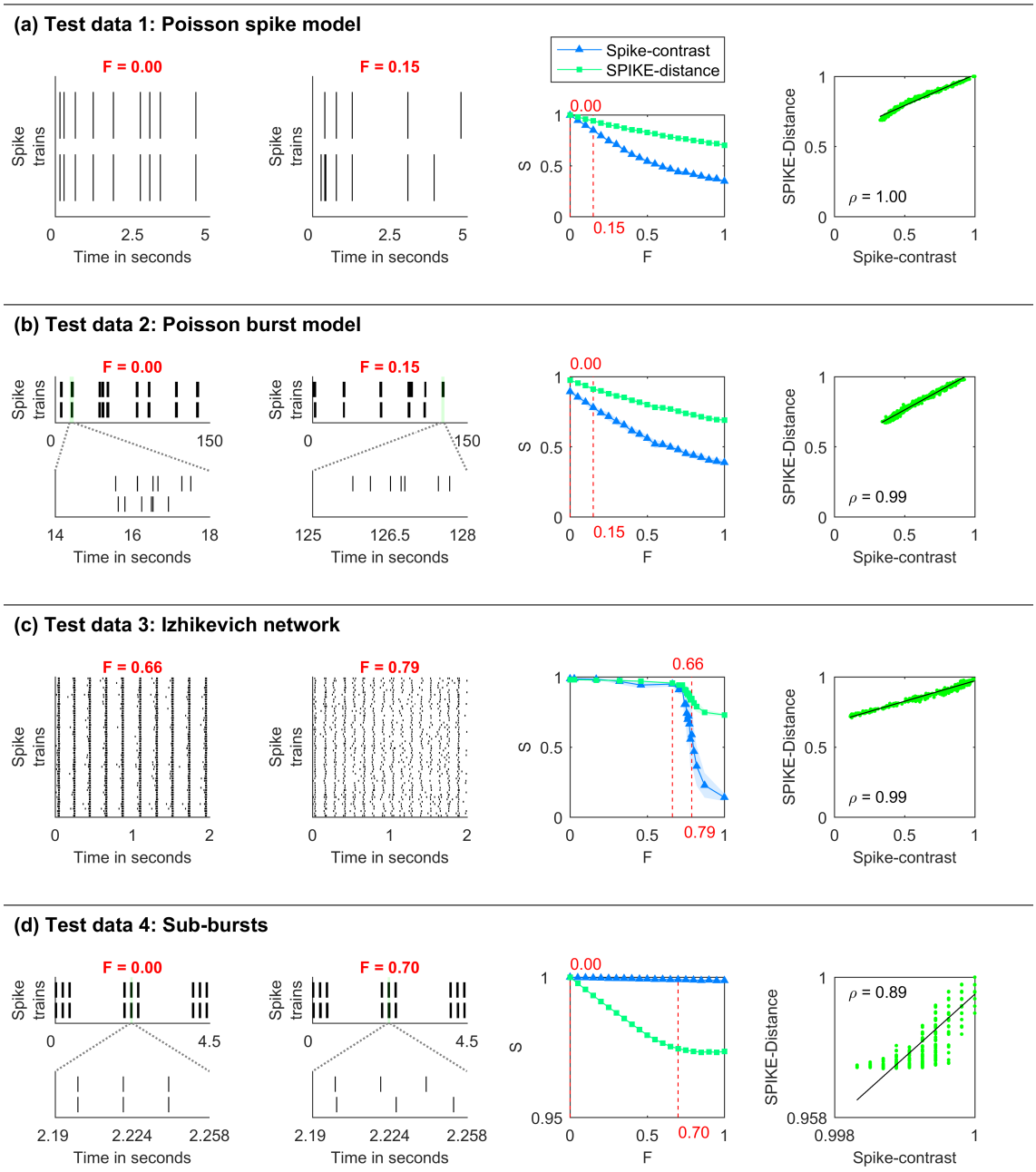

Figure 3.3: Comparison of *Spike-contrast* with *SPIKE-distance* using four different test data sets ((a) to (d)). **First two columns:** Test data sets with high ($F = 0$) and low ($F = 1$) synchrony. In (b) and (d) spike trains are magnified for visualization of single bursts. For each test data 20 synchrony levels $F = [0, 1]$ and for each F, $n = 20$ independent realizations were generated. **Third column:** Calculated synchrony values S from *Spike-contrast* and *SPIKE-distance*. Each data point represents the mean synchrony value. Shaded area: Standard deviation, only visible in (c). **Fourth column:** Synchrony values of *Spike-contrast* versus synchrony values of *SPIKE-distance* fitted with a linear regression line (ρ: Spearman correlation coefficient, in all cases correlation is significantly different from zero with $p << 0.01$ using large-sample approximation based on a t-statistic).

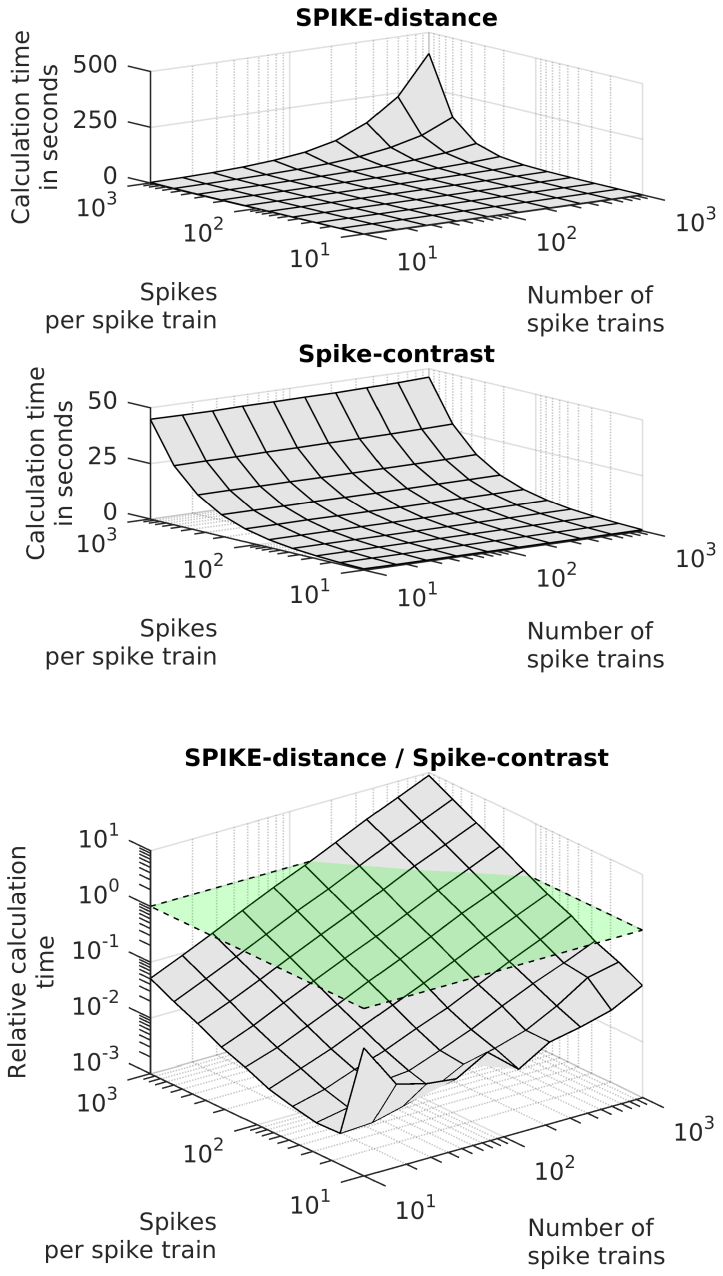

Figure 3.4: Calculation times for *SPIKE-distance* and *Spike-contrast*. **Top:** Absolute calculation times for *SPIKE-distance*. **Middle:** Absolute calculation times for *Spike-contrast*. **Bottom:** The ratio of the calculation times of *SPIKE-distance* to the calculation times of *Spike-contrast*. The green area outlined with dashed lines indicates equal calculation times. *Spike-contrast* is faster than *SPIKE-distance* if values are greater than the green area and vice versa.

3.4 Discussion

In this study, a novel spike train synchrony measure is proposed called *Spike-contrast*. It is compared to the spike train synchrony measure called *SPIKE-distance*

(Kreuz et al., 2013) by using artificially generated spike train data. Both measures are time scale independent, which means that their adapt themselves to the time scales found in the spike train data. Therefore, the user does not need to define synchrony by choosing e. g. a relevant time scale or a certain bin size. When applied to Poisson spike trains, Poisson burst trains, and spike trains from Izhikevich networks, synchrony values from *Spike-contrast* are highly correlated with synchrony values from *SPIKE-distance*. This suggests that similar synchrony values can be obtained from both measures for these cases. However, both measures differ in detecting synchrony in spike trains containing sub-bursts. In this specific test data, only spikes in these sub-bursts are desynchronized, while burst temporal positions remain fully synchronized. Synchrony value of *SPIKE-distance* decreases because of desynchronized spikes in sub-bursts. Conversely, *Spike-contrast* indicates no change in synchrony as burst positions are still synchronous. Whether the insensitivity of *Spike-contrast* can be considered a disadvantage depends on the scope of the analysis. Very recently, a new adaptive version of *SPIKE-distance* was developed, called *A-SPIKE-distance* (Satuvuori et al., 2017). It is motivated by the assumption that small time scales are typically less important when analyzing data containing multiple time scales (e. g. regular spiking and bursts). From that perspective, *Spike-Contrast* performs better than *SPIKE-distance* in the sub-bursts containing test data set. As *A-SPIKE-distance* neglects smaller time scales, we applied it to our test data as well. As expected, it is less sensitive to desynchronized spikes in sub-bursts compared to *SPIKE-distance*. However, *A-SPIKE-distance* is still more sensitive than *Spike-contrast* (results not shown).

3.4.1 Disadvantages

Compared to *SPIKE-distance*, *Spike-contrast* is not parameter-free, although it does not need a time scale parameter to be defined by the user. A bin shrink factor has to be determined (influencing the resolution of the synchrony curve $s(\Delta)$), the degree of bin-overlap (influencing the smoothness of the histogram), and optional, a minimum bin size limit L to avoid unnecessary calculations. We found that the parameter values used in this study presented a sufficient compromise between computational efficiency and accuracy because of the high correlation with *SPIKE-distance*. It should also be mentioned that in certain cases *Spike-contrast* may yield unexpected synchrony values. One extreme example would be a signal showing spikes during the first half and no spikes during the second half of the signal. In this case, *Spike-contrast* would yield a high synchrony value as there is a high contrast between the first and the second half of the signal (like considering all spikes in the first half as one burst). To avoid this limitation, spike trains could be tested for non-stationarity first (Gourévitch and Eggermont, 2007b). Another uncertainty is the question whether the bin placement relative to the spike train affects the calculated synchrony value. This question is hard to address, as simply shifting the spike train, e. g. by adding a time offset, also changes the entire signal characteristic affecting the spike train contrast (such an offset time can be considered as the quiescence time between bursts).

3.4.2 Advantages

Spike-contrast is faster than *SPIKE-distance* when calculating large data sets (e. g. almost 10 times faster for 1000 spike trains and 1000 spikes per spike train), although *Spike-contrast* is slower than *SPIKE-distance* when applied to smaller data sets (e. g. containing less than 200 spike trains and 1000 spikes per spike train). The calculation speed of *Spike-contrast* depends mainly on the number of spikes per spike train but is nearly independent of the number of spike trains. Therefore, it can be advantageous when analyzing large sets of data, like those recorded from high-density microelectrode array (MEA) chips providing 512 (Litke et al., 2004), 2048 (Dragas et al., 2017), or 4096 (Berdondini et al., 2009b) recording channels. If small time scales (e. g. order of milliseconds) are not relevant, the minimum bin size limit L (see section 3.2.2) may be set to a value greater than $0\ \mathrm{ms}$ to speed up calculation. For example, setting $L = 10\ \mathrm{ms}$ decreases the calculation times in the speed comparison (Fig. 3.4 middle) almost by a factor of 10. The reduced calculation time does not affect the final synchrony value S, as long as L is smaller than the location of the synchrony curve maximum. The calculation speed advantage of *Spike-contrast* is because of its multivariate nature. While bivariate measures calculate a synchrony value for each combination of spike trains and average across all synchrony values to get the final synchrony value, multivariate methods directly calculate one synchrony value from an arbitrary number of spike trains. Brown et al. (2004) accentuated the need for multivariate methods to analyze spike train data, so *Spike-contrast* complies with that request.

Even though *Spike-contrast* and *SPIKE-distance* are able to provide a single synchrony value, both measures differ in their additional output. *SPIKE-distance* provides a time-resolved synchrony profile, whereas *Spike-contrast* provides a synchrony curve as a function of bin size. Therefore, both measures can be considered complementary methods. The synchrony curve provides further information about temporal spike patterns. For example, more than one peak in the curve indicates synchrony at multiple time scales (e. g. synchronized networkbursts made of shorter synchronized bursts). To the best of our knowledge, this is a unique feature of *Spike-contrast*.

Acknowledgment

We thank Thomas Kreuz and Eero Satuvuori for many fruitful discussions and critically reading the manuscript. This work was supported by the Federal Ministry of Education and Research (BMBF03FH061PX3). The collaboration between the biomems lab and the Jimbo & Kotani lab was partially supported by the Germany's Free State of Bavaria within the framework of BayIntAn (HSAB_2016_93). We furthermore thank the Germany's Free State of Bavaria for financial support within the framework of ZeWiS.

Appendix

Derivation of the synchrony measure

Contrast For an observation period T, the histogram contains $K = T/\Delta$ bins (if bins are overlapped by $\Delta/2$, number of bins are $K = 2 \cdot \lfloor T/\Delta \rfloor$). The number of spikes falling into the kth bin is expressed as Θ_k. In order to obtain the contrast of the histogram, the differences between each neighboring pair of bin

$$\Theta_k - \Theta_{k+1} \tag{3.8}$$

are calculated. As the direction of the change does not matter, absolute values are used. Those values are reduced to one contrast value, by taking the sum

$$\sum_{k=1}^{K-1} |\Theta_k - \Theta_{k+1}|. \tag{3.9}$$

If all spike-containing bins are surrounded by empty bins, Eq. 3.9 reaches its highest possible value of

$$2 \sum_{k=1}^{K} \Theta_k, \tag{3.10}$$

therefore, this term is used for normalization between 0 and 1, giving the final definition of

$$Contrast(\Delta) = \frac{\sum_{k=1}^{K-1} |\Theta_k - \Theta_{k+1}|}{2 \sum_{k=1}^{K} \Theta_k} \tag{3.11}$$

for a given bin size Δ. For extreme examples, if $(\Theta_1, \Theta_2, \Theta_3, \Theta_4, \Theta_5, ...) = (0, 1, 0, 1, 0, ...)$, $Contrast(\Theta)$ is 1, while if $(\Theta_1, \Theta_2, \Theta_3, \Theta_4, \Theta_5, ...) = (1, 1, 1, 1, 1, ...)$, it is 0.

ActiveST Actually, the maximum of $Contrast(\Delta)$ could already be used to define the final synchrony value. If the bin size becomes very small compared to the inter-spike intervals, every spike may fall into a bin surrounded by empty bins, which also results in a maximum contrast value of 1. In order to compensate for this situation, a second factor $ActiveST$ is introduced, which becomes 0 if only one spike train contributes to the contrast value and 1 if all spike trains contribute to the contrast value. By calculating the product, a coefficient

$$s(\Delta) = Contrast(\Delta) \cdot ActiveST(\Delta) \tag{3.12}$$

is defined, which only reaches a high value if the contrast of the spike trains is high, and at the same time, if many spike trains contribute to the contrast.

Below, the definition of $ActiveST$ (quantity of "active spike trains") is given. Let us define n_k the number of spike trains that contribute to the sum of spikes Θ_k in the kth bin. If the observed set of data contains N spike trains, which are highly synchronized (all spike trains show spikes in the kth bin), then the number of active spike trains n_k equals N. If the kth bin does not contain any spikes, n_k is zero. To obtain a

value between 0 and 1 for each bin, n_k is normalized by N and averaged across all bins:

$$\frac{1}{K}\sum_{k=1}^{K}\frac{n_k}{N} = \frac{1}{K\cdot N}\sum_{k=1}^{K} n_k \tag{3.13}$$

Real recorded data, however, often show large periods of quiescence, resulting in most bins being empty. Empty bins would decrease the average, even if all spikes are perfectly synchronized. Therefore, the average is weighted by the number of spikes in each bin to ensure that only non-empty bins are considered:

$$\frac{\frac{1}{K\cdot N}\sum\limits_{k=1}^{K} n_k\cdot\Theta_k}{\frac{1}{K}\sum\limits_{k=1}^{K}\Theta_k} = \frac{\sum\limits_{k=1}^{K} n_k\cdot\Theta_k}{N\cdot\sum\limits_{k=1}^{K}\Theta_k} \tag{3.14}$$

The calculated value can be between $1/N$ (spike trains are not synchronized so n_k is not greater than 1 for every k) and 1 ($n_k = N$ for every k with $\Theta_k > 0$). In order to achieve a value of $ActiveST$ between 0 and 1, the term has to be normalized

$$ActiveST(\Delta) = \frac{\left(\frac{\sum\limits_{k=1}^{K} n_k\cdot\Theta_k}{N\cdot\sum\limits_{k=1}^{K}\Theta_k}\right) - \frac{1}{N}}{\frac{N-1}{N}} \tag{3.15}$$

leading to the final expression:

$$ActiveST(\Delta) = \frac{1}{N-1}\left(\frac{\sum\limits_{k=1}^{K-1} n_k\cdot\Theta_k}{\sum\limits_{k=1}^{K}\Theta_k} - 1\right) \tag{3.16}$$

Author contributions

Initiated the idea to find an intuitive synchrony measure: TI YJ. Development of the algorithm: MC. Conceived and designed the experiments: MC TI. Performed the experiments: MC. Analyzed the data: MC. Wrote the paper: MC TI YJ AB CT.

Chapter 4

Comparison of different spike train synchrony measures regarding their robustness to erroneous data from bicuculline-induced epileptiform activity

Manuel Ciba[1,*], Robert Bestel[1], Christoph Nick[1], Guilherme Ferraz de Arruda[2], Thomas Peron[3], Comin César Henrique[4], Luciano da Fontoura Costa[5], Francisco Aparecido Rodrigues[3], Christiane Thielemann[1]

1 Biomems lab, University of Applied Sciences Aschaffenburg, 63743 Aschaffenburg, Germany.
2 ISI Foundation, Via Chisola 5, 10126 Torino, Italy.
3 Institute of Mathematics and Computer Science, University of São Paulo - São Carlos, SP 13566-590, Brazil.
4 Department of Computer Science, Federal University of São Carlos - São Carlos, SP, Brazil.
5 Instituto de Física de São Carlos, Universidade de São Paulo, São Carlos, São Paulo, Brazil.
* Corresponding author, manuel.ciba@th-ab.de

Published in *Neural Computation*
Volume 32, Issue 5, May 2020, p.887-911

Abstract

As synchronized activity is associated with basic brain functions and pathological states, spike train synchrony has become an important measure to analyze experimental neuronal data. Many different measures of spike train synchrony have been proposed, but there is no gold standard allowing for comparison of results between different experiments. This work aims to provide guidance on which synchrony measure is best suitable to quantify the effect of epileptiform inducing substances (e.g. bicuculline (BIC)) in *in vitro* neuronal spike train data.
Spike train data from recordings are likely to suffer from erroneous spike detection, such as missed spikes (false negative) or noise (false positive). Therefore, different time-scale dependent (cross-correlation, mutual information, spike time tiling coefficient) and time-scale independent (Spike-contrast, phase synchronization, A-SPIKE-synchronization, A-ISI-distance, ARI-SPIKE-distance) synchrony measures were compared in terms of their robustness to erroneous spike trains.
For this purpose, erroneous spike trains were generated by randomly adding (=false positive) or deleting (=false negative) spikes (=*in silico* manipulated data) from experimental data. In addition, experimental data were analyzed using different spike detection threshold factors in order to confirm the robustness of the synchrony measures. All experimental data were recorded from cortical neuronal networks on MEA chips, which show epileptiform activity induced by the substance BIC.
As a result of the *in silico* manipulated data, Spike-contrast was the only measure being robust to false negative as well as false positive spikes. Analyzing the experimental data set revealed that all measures were able to capture the effect of BIC in a statistically significant way, with Spike-contrast showing the highest statistical significance even at low spike detection thresholds. In summary, we suggest the usage of Spike-contrast to complement established synchrony measures, as it is time-scale independent and robust to erroneous spike trains.

4.1 Introduction

Synchrony is generally accepted to be an important feature of basic brain functions (Engel et al., 2001; Ward, 2003; Rosenbaum et al., 2014) and pathological states (Pare et al., 1990; Fisher et al., 2005; Truccolo et al., 2014; Arnulfo et al., 2015). Measuring synchrony between neural spike trains is a common method to analyze experimental data e.g. recordings from *in vitro* neuronal cell cultures with microelectrode arrays (MEA) (Selinger et al., 2004; Chiappalone et al., 2006b, 2007b; Eisenman et al., 2015; Flachs and Ciba, 2016) or from *in vivo* experiments (Li et al., 2011). As an example for *in vitro* neuronal cell cultures on MEA chips, Sokal et al. (2000) reported that synchrony reliably increased due to the substance bicuculline (BIC), while the usual applied quantification method "spike rate" increased or decreased. In order to quantify synchrony, many spike train synchrony measures have been proposed based on different approaches. Some of them belong to the class of time-scale dependent measures. This means that at the beginning of the analysis the user has to select the desired time scale (e.g. bin size) (Selinger et al., 2004; Cutts and Eglen, 2014). The second class contains time-scale independent measures, which automatically adapt their time-scale parameter according to the data (Satuvuori et al., 2017; Ciba et al., 2018). However, there is no gold standard for the evaluation of synchrony in experimental data. This is because there is no common definition of synchrony between spike trains. To be more specific, each synchrony measure can be considered as its own definition of synchrony, extracting different features from the data. This situation is unsatisfactory as data interpretations are not comparable. Therefore, a guidance would be desirable on which synchrony measure to use for specific data.
When it comes to the analysis of experimental spike train data, the data are likely to suffer from erroneous spike detection. For example, spikes are missed as they are buried in noise (false negative) or noise is misinterpreted as spikes (false positive). At low signal-to-noise ratios (SNR), even advanced spike detection methods are affected by missed or misinterpreted spikes (Lieb et al., 2017).
Hence, a synchrony measure that operates on spike trains from experimental data should be as robust as possible to such erroneous spike trains.

In order to approach a guidance to analyze epileptiform spike trains from *in vitro* neuronal networks, the performance of different synchrony measures was compared with the focus on robustness to erroneous spike trains. Well known time-scale dependent measures, like cross-correlation (CC), mutual information (MI), and spike time tiling coefficient (STTC) and time-scale independent measures, like Spike-contrast, phase synchronization (PS), A-SPIKE-synchronization, A-ISI-distance, A-SPIKE-distance, and ARI-SPIKE-distance were applied to two types of data sets: (1) *in silico* manipulated data and (2) experimental data.
(1) The in silico manipulated data are based on the experimental data and were used to simulate erroneous spike train data by randomly adding spikes (false positive) or deleting spikes (false negative). As a requirement, the synchrony measures should be robust to added and deleted spikes.
(2) The experimental data were recorded from primary cortical networks grown *in vitro* on MEA chips. Neuronal networks were exposed to the γ-aminobutyric acid

($GABA_A$) receptor antagonist bicuculline (BIC) in order to increase the synchrony level of the network activity. Spike detection threshold factor was varied in order to vary the level of false positive and false negative spikes. The synchrony measures were tested for their ability to find significant synchrony changes induced by BIC.

4.2 Material and methods

4.2.1 Synchrony measures

In this section the synchrony measures used in this study are briefly described. To consider a wide range of synchronization measures, a representative group of linear and nonlinear methods as well as time-scale dependent and independent methods were chosen. For a detailed definition see the respective original publication. Since there is no specific publication on how to apply MI and PS to spike train data, their definitions are provided in appendix 4.4.

Time-scale dependent:

- **Cross-correlation (CC)** based methods are probably most popular to measure synchrony (Cutts and Eglen, 2014). Here we use a definition by Selinger et al. (2004) that was specially proposed for *in vitro* experiments and had also been used by Chiappalone et al. (2006b). According to the definition, synchrony between two spike trains is measured by binning the spike trains into a binary signal and then calculating the cross-correlation without shifting the signals. Selinger et al. (2004) proposed a bin size of 500 ms and was able to detect synchrony changes in spinal-cord cultures mediated by the chemicals BIC, strychnin, and 2,3-dioxo-6-nitro-l,2,3,4-tetrahydrobenzoquinoxaline-7-sulphonamide (NBQX). Due to the bin size parameter, CC is time-scale dependent. A bin size of 500 ms is also used in this study (see Section 4.2.4).

- **Mutual information (MI)** is a measure from the field of information theory and is – in contrast to CC – able to capture non-linear dependencies. In this work, MI measures the synchrony between two spike trains by binning the spike trains into binary signals and quantifying the redundant information (Cover and Thomas, 2012). Therefore, this version of MI is time-scale dependent using a bin size of 500 ms (see Section 4.2.4).

- **Spike time tiling coefficient (STTC)** measures the synchrony between two spike trains and has been proposed by Cutts and Eglen (2014) as a spike rate independent replacement of a synchrony measure called “correlation index” by Wong et al. (1993). Reanalysis of a study of retinal waves using STTC instead of the “correlation index” significantly changed the result and conclusion (Cutts and Eglen, 2014). STTC is a time-scale dependent measures as it needs a predefined time window Δt in which spikes are considered synchronous. Referring to the work of Cutts and Eglen (2014), a time window of 100 ms was used in this work (see Section 4.2.4).

Time-scale independent:

- **Phase synchronization (PS)** measures the synchrony between spike trains in two steps. First step is to assign a linear phase procession from 0 and 2π to every interspike interval (ISI). Second step is quantifying the common phase evolution of all spike trains via an order parameter defined by Pikovsky et al. (2003). PS is time-scale independent and – to the best of our knowledge – has not been systematically compared with other measurements in studies of spike train synchrony yet or has even never been used to measure synchrony of neural spike trains.

- **Spike-contrast** is a time-scale independent synchrony measure based on the temporal "contrast" of the spike raster plot (activity vs. non-activity in certain temporal bins) and not only provides a single synchrony value, but also a synchrony curve as a function of the bin size, or in other words, as a function of the time-scale (Ciba et al., 2018). Here, instead of the synchrony curve only the single synchrony value was used.

- **A-SPIKE-synchronization** is a time-scale independent and parameter free coincidence detector (Satuvuori et al., 2017). It measures the similarity between spike trains and is the adaptive generalization of SPIKE-synchronization (Kreuz et al., 2015). In the adaptive versions a decision is made if the spike trains are compared considering their local or global time-scale, which is advantageous for data containing different time-scales like regular spiking and bursts.

- **A-ISI-distance** is a time-scale independent and parameter free distance measure (Satuvuori et al., 2017). It measures the instantaneous rate difference between spike trains and is the adaptive generalization of ISI-distance (Kreuz et al., 2007a).

- **A-SPIKE-distance** is a time-scale independent and parameter free distance measure (Satuvuori et al., 2017). It measures the accuracy of spike times between spike trains relative to local firing rates and is the adaptive generalization of SPIKE-distance (Kreuz et al., 2011, 2013).

- **ARI-SPIKE-distance** is the rate independent version of A-SPIKE-distance (Satuvuori et al., 2017). It measures the accuracy of spike times between spike trains without using the relative local firing rate. Some of the original version have already been applied to experimental neuronal data. For example Andrzejak et al. (2014) used ISI-distance and SPIKE-distance and Dura-Bernal et al. (2016) used SPIKE-distance and SPIKE-synchronization. Espinal et al. (2016) applied SPIKE-distance to simulated data.

In order to get a final synchrony value over all recorded spike trains, synchrony between all spike train pairs was calculated and averaged. With the exception of Spike-contrast, which already yields a single synchrony value between all spike trains due to its multivariate nature.

Note that all synchrony measures are designed to provide a value between 0 (miminum synchrony) and 1 (maximum synchrony). Only CC and STTC are

able to yield negative values in case of anticorrelation. The distance measures A-ISI-distance, A-SPIKE-distance, and ARI-SPIKE-distance naturally provide values between 0 (minimal distance or maximum synchrony) and 1 (maximum distance or minimum synchrony). Therefore, their values were substracted from 1 to make the distance measures comparable to the synchrony measures. The MATLAB® (MATLAB 2016a, MathWorks, Inc., Natick, Massachusetts, USA) source code of A-SPIKE-synchronization, A-ISI-distance, A-SPIKE-distance, and ARI-SPIKE-distance was downloaded along with the tool called *cSPIKE*[1]. The Spike-contrast[2] and MI[3] MATLAB source code also was taken from online sources. STTC python code[4] was translated into MATLAB code. MATLAB code for PS was specifically programmed for this work. All MATLAB functions and scripts used for this work are provided online[5].

4.2.2 *In silico* manipulated data

Two sets of *in silico* manipulated data were generated featuring added spikes (=false positive spikes) and deleted spikes (=false negative spikes). As the measures CC, MI, and STTC are time-scale dependent, the *in silico* manipulated data are based on the experimental data (see Section 4.2.3) in order to obtain realistic time-scales. In total, 10 recordings from 5 independent networks (N = 5) were used (5 without and 5 with 10 μM BIC). Each recording had a length of 300 s and up to 60 active electrodes. The following procedures were applied for every active electrode (active if at least 6 spikes per minute, see Section 4.2.3) with X being the spike train of the original electrode and Y being the manipulated spike train:

1) **Added spikes:** Spike train Y was generated by copying spike train X and adding N_{add} spikes to Y with temporal positions randomly assigned in the range of $(0, 300]$ seconds. In case of identical spike times, new random spike times were generated until all spike times were unique. Depending on the manipulation level the number of added spikes was

$$N_{add} = L \cdot 0.1 \cdot N_X, \tag{4.1}$$

with N_X being the number of spikes in spike train X and L being the manipulation level in the range of $L = [0, 0.1, 0.2...1]$ ($L = 0$: No manipulation, $L = 1$: 10% random spikes were added). For each L, 40 independent random manipulations ($n_{manipulated} = 40$) were performed (see Fig. 4.1 (b 2) for example spike trains).

2) **Deleted spikes:** Spike train Y was generated by copying spike train X and deleting N_{delete} randomly selected spikes from Y. Depending on the manipulation level the number of deleted spikes was

$$N_{delete} = L \cdot 0.9 \cdot N_X, \tag{4.2}$$

[1] http://wwwold.fi.isc.cnr.it/users/thomas.kreuz/Source-Code/cSPIKE.html
[2] https://github.com/biomemsLAB/Spike-Contrast
[3] https://de.mathworks.com/matlabcentral/fileexchange/28694-mutual-information
[4] http://neuralensemble.org/elephant/
[5] https://github.com/biomemsLAB/SynchronyMeasures-Robustness

where N_X is the number of spikes in spike train X and L is the manipulation level in the range of $L = [0, 0.1, 0.2, ...1]$ ($L = 0$: No manipulation, $L = 1$: 90% of all spikes were deleted). Note that the maximum range was restricted to 90% of N_X as some of the tested synchrony measures were not defined for empty spike trains. For each L, 40 independent random manipulations ($n_{manipulated} = 40$) were performed (see Fig. 4.1 (b 3) for example spike trains).

A single synchrony value was then calculated for every recording ($N = 10$) and every random manipulation ($n_{manipulated} = 40$). Overall, for every manipulation level 400 synchrony values were calculated per synchrony measure.

As some of the synchrony measures differ in terms of their minimum value for Poisson spike trains with equal rate (e.g. 0.295 for SPIKE-distance and 0.5 for ISI-distance (Kreuz et al., 2013)), they could not be compared directly. Therefore, synchrony values of each measure were rescaled to their lowest possible synchrony value defined as synchrony of a data set made of Poisson spike trains $Y_{L,random}$ at the manipulation level L. The number of spikes in $Y_{L,random}$ was equal to the number of spikes in Y_L (being the manipulated spike train Y at the manipulation level L), to account for the spike rate dependence of some synchrony measures, as reported in Cutts and Eglen (2014). The scaling was done with

$$s'_L = \frac{s_L - \bar{s}_{L,random}}{1 - \bar{s}_{L,random}}, \tag{4.3}$$

where s_L is the synchrony value at a manipulation level L, $\bar{s}_{L,random}$ is the mean synchrony value of the data set consisting of Poisson spike trains $Y_{L,random}$, and value "1 " representing the largest possible synchrony value (all synchrony measures were able to yield "1 " for identical spike trains). As ten different recordings with different synchrony level were used, all synchrony values were normalized, allowing to calculate the mean over all recordings and all random realizations. The normalization was done with

$$s''_L = \frac{s'_L}{s'_{L=0}}, \tag{4.4}$$

where $s'_{L=0}$ is the synchrony of the orginal spike train (manipulation level $L = 0$), and s''_L the normalized synchrony value. All normalized synchrony values of all recordings and all random realizations taken together are denoted as $s''_{L,all}$. In order to ease the comparison between the different synchrony measures, the total deviation of the normalized synchrony (TDNS) over the manipulation level was calculated as

$$TDNS = \sum_{L=0}^{1} std(s''_{L,all}), \tag{4.5}$$

where $std()$ is the standard deviation. The lower the TDNS, the more robust the synchrony measure against the spike train manipulation procedure.

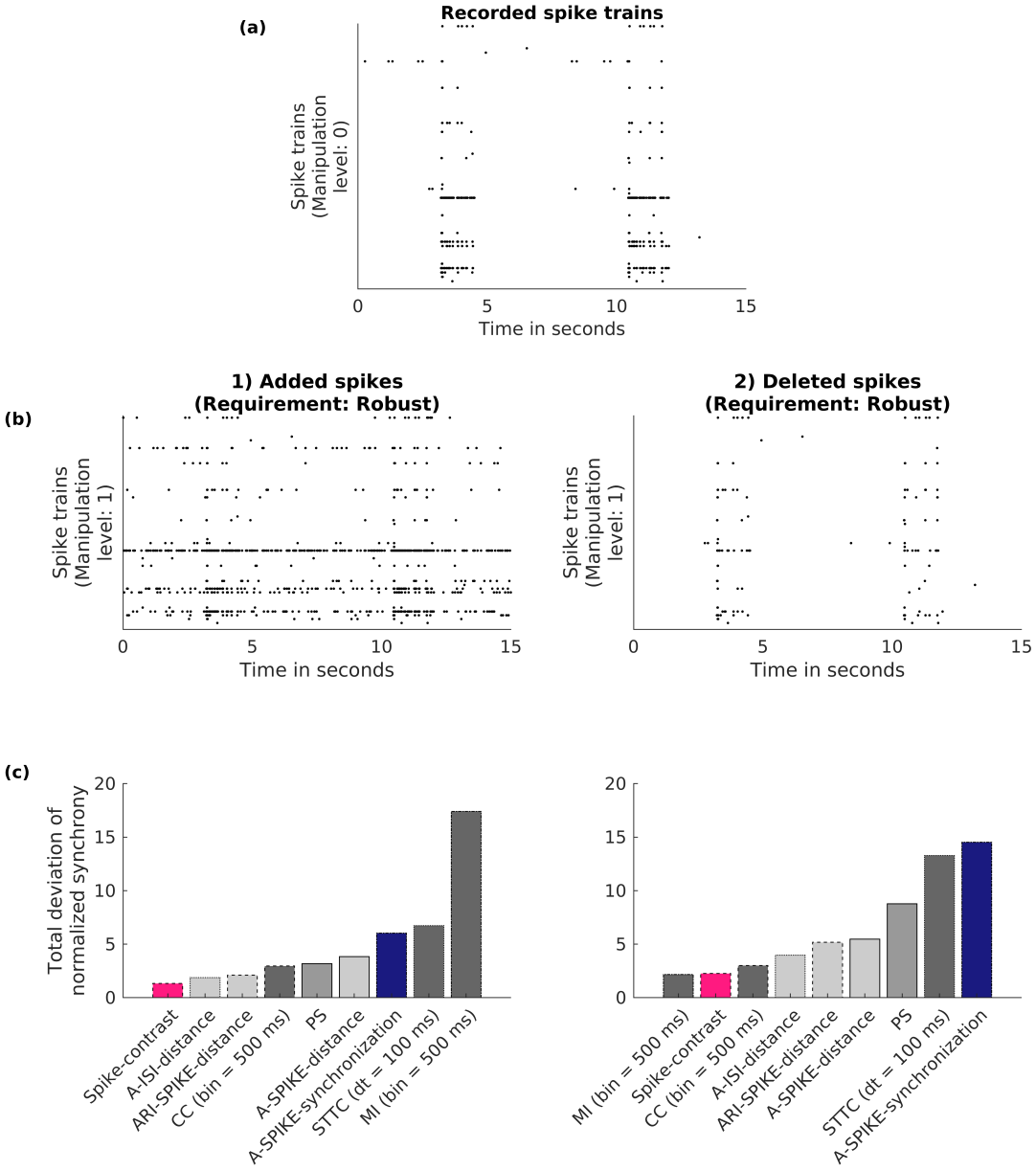

Figure 4.1: **Comparison of different synchrony measures regarding their robustness to erroneous spike trains. (a)** Spike trains recorded from 60 electrodes with 10 μM BIC. Each line represents the spike train of one electrode (only first 15 s of 300 s are displayed). **(b)** Same as (a) but with maximum manipulation level applied (left: Simulation of false positive spikes, right: Simulation of false negative spikes). In total 10 different recordings were used to generate the *in silico* manipulated data (for details see Sec. 4.2.2). **(c)** Sum of synchrony deviation over all manipulation levels (denoted as total deviation of the normalized synchrony (TDNS), see Eq. 4.5). The lower the TDNS value of a synchrony measure, the more robust it is to spike train manipulation.

4.2.3 Experimental data

Cell culture and electrophysiological recordings

Experimental data used for this study were recorded from primary cortical neurons (Lonza Ltd, Basel, Switzerland) harvested from embryonic rats (E18 and E19). Cell cultivation followed a modified protocol based on Otto et al. (2003). Briefly, vials containing 4×10^6 cells were stored in liquid nitrogen at -196^{0}C. After thawing, cells were diluted drop-wise with pre-warmed cell culture medium and seeded at a density of 5000 cells/mm^2 onto Poly-D-Lysine and Laminin coated (Sigma Aldrich Co. LLC, St. Louis, USA) microelectrode arrays (60MEA200/30iR-Ti, Multichannel Systems MCS GmbH, Reutlingen, Germany). Twice a week, half of the medium was replaced with fresh, pre-warmed medium.
Neuronal signals were recorded extracellularly at a sampling rate of 10 kHz outside the incubator at 37^{0}C employing a temperature-controller (Multichannel Systems MCS GmbH). For drug-induced increase of network synchronization, bicuculline (BIC) (Sigma Aldrich Co. LLC) was applied to the neuronal cell culture after 21 days *in vitro* (div) at a concentration of 10 μM. BIC is a competitive antagonist of the GABA$_A$ receptor. Since it blocks the inhibitory function of GABA$_A$ receptors, its application yields an increased incidence of synchronized burst events (Jungblut et al., 2009), see Fig. 4.2 (b) and (c). Neuronal activity was recorded for 5 minutes before and 5 minutes during the application of BIC.

Spike detection

Raw data were stored for offline spike detection with *DrCell*, a custom-made Matlab (MathWorks Inc., Natick, Massachusetts, U.S.A.) software tool, developed by Nick et al. (2013). After applying a high-pass filter with a cutoff frequency of 50 Hz, spikes were separated from noise using a threshold-based algorithm, with a threshold calculated by multiplying the standard deviation of the noise by a factor of 5 (or more precisely -5 as only negative spikes were used for analysis). As soon as the raw signal underran the threshold, the time of the minimum voltage value was defined as a spike time stamp (Fig. 4.2 (a)). Additionally, in order to alter the level of false positive and false negative spikes, spike detection was also conducted using threshold factors of 4, 6, and 7. For subsequent spike train analysis, only electrodes with more than 5 spikes per minute were considered active and used for analysis (Novellino et al., 2011).

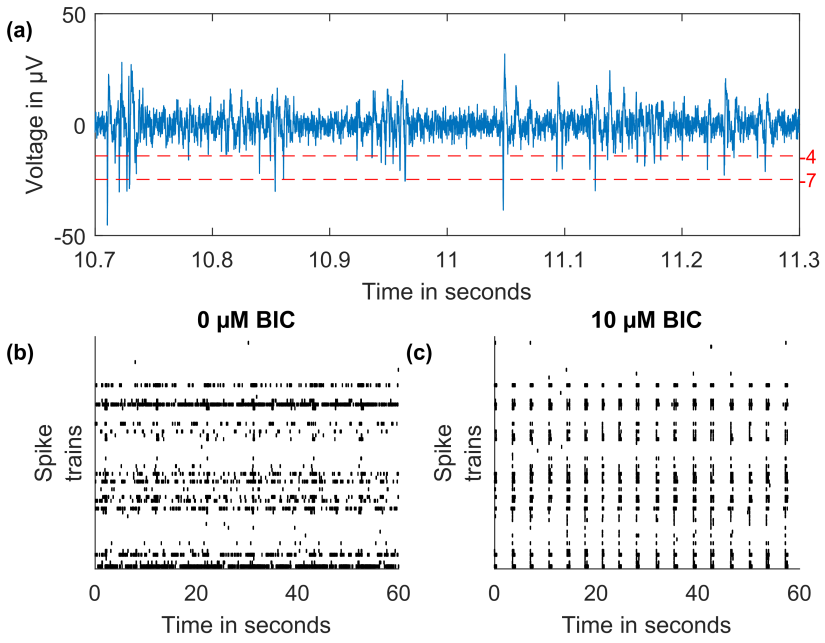

Figure 4.2: **Exemplary illustration of the experimental data. (a)** Signal recorded from one MEA electrode (50 Hz high-pass filtered). Thresholds are displayed for the lowest (4) and highest (7) threshold factors used for spike detection. The higher the threshold factor, the less spikes are detected. **(b)** Rasterplot of the spontaneous activity of one MEA chip without BIC (only first 60 s of 300 s are shown). **(c)** Same as (b) but with 10 μM BIC. Spontaneous activity was recorded with a 60 electrode MEA chip at 23 div. Compared to the native state, the administration of 10 μM BIC increased the level of synchrony.

Statistical analysis

Since it is known that BIC causes an increase of network synchrony in cortical neurons *in vitro* (Sokal et al., 2000; Chiappalone et al., 2007a; Eisenman et al., 2015), a one-tailed statistical test was applied. More specifically, a paired t-test was applied under the null hypothesis that BIC does not increase synchrony. The lower the p-value, the lower the probability that there is no synchrony change, and hence the better the synchrony measure's sensitivity to BIC.

4.2.4 Parameter choice

As the synchrony measures CC, MI, and STTC depend on a time-scale parameter that directly influences the synchrony definition, an appropriate parameter value had to be chosen. Therefore, we analyzed the experimental BIC data using different parameter values and conducted a statistical hypothesis test. The lower the p-value, the higher the probability that an increase in synchrony occurred. Parameter values that lead to low p-values are therefore desirable (given that BIC results in increased level of synchrony). CC proposed by Selinger et al. (2004) chose a bin size of 500 ms, which also gave reasonable low p-values in our analysis (Fig. 4.3). Even if smaller

bin sizes yielded lower p-values in our data, we stuck to the predefined 500 ms. For MI, we also chose a bin size of 500 ms as for smaller bin sizes the p-value only improved slightly. The parameter dt of STTC was set to 100 ms according to the original publication from Cutts and Eglen (2014). Note that in our cortical data a larger dt value would only slightly improve the p-value.

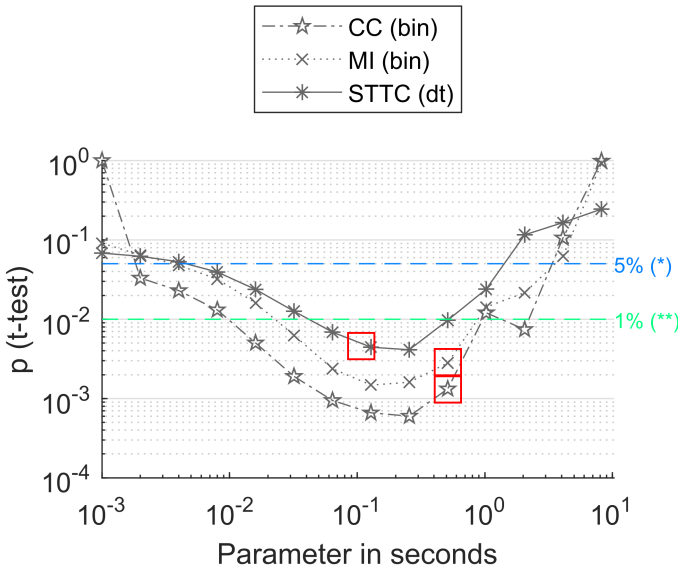

Figure 4.3: **Influence of the parameter choice on the statistical significance of the experimental data.** The synchrony measures CC, MI, and STTC depend on a parameter which has to be chosen by the user. For each synchrony measure, the experimental data described in Section 4.2.3 were analyzed using different parameter values. After that, a t-test was applied to the data with the null hypothesis that synchrony values of the data with BIC are lower or equal to synchrony values of the data without BIC. In this work, a bin size of 500 ms was used for CC and a dt of 100 ms for STTC (red squares), as these values were suggested in their original publications. For MI, the same bin size as for CC was used due to the identical binning procedure.

4.3 Results

4.3.1 Comparison of synchrony measures for *in silico* manipulated data

1) **Added spikes:** The robustness of measures was studied by randomly adding false positive spikes to the basic signals. For a robust synchrony measure low sensitivity to false positive spikes is desirable as such noise may falsify the results. As displayed in Fig. 4.1 (c, left) Spike-contrast was most robust to false positive spikes indicated by the small TDNS value of around 1, closely followed by A-ISI-distance and ARI-SPIKE-distance. MI showed by far the largest synchrony deviation indicated by a TDNS value of around 17.

2) **Deleted spikes:** A similar picture occurs after increasingly deleting spikes in order to simulate false negative spikes, as robustness to false negative spikes was required. In Fig. 4.1 (c, right) results of synchrony measure dependency to false negative spikes are shown. Here, MI and Spike-contrast were most robust to false negative spikes yielding the smallest TDNS value of around 2. STTC and A-SPIKE-synchronization showed largest TDNS value of around 14.

4.3.2 Comparison of synchrony measures for experimental data

In addition to the evaluation with *in silico* manipulated data, all synchrony measures were applied to experimental data recorded from cortical neurons by MEA chips with and without the application of 10 μM BIC. Fig. 4.4 (a) shows the absolute synchrony values for each synchrony measure and for all different cell cultures ($N = 5$), before and after the application of BIC. Generally all measures showed a significant synchrony increase due to the BIC application with p-values of 5% and below, where A-SPIKE-synchronization, A-ISI-distance, and A-SPIKE-distance failed to reach the high significance level of 1%.

In order to alter the level of false positive and false negative spikes in the experimental data, different spike detection threshold factors (4 to 7) were applied. Where low thresholds are likely to correspond to additional false spikes (false positive) and high thresholds to missed spikes (false negative). Increasing the threshold factor is comparable with deleting spikes from the spike train as already done in the *in silico* manipulated data evaluation (Section 4.3.1). For the *in silico* manipulated data, the synchrony measures STTC and A-SPIKE-synchronization were most sensitive to deleted spikes. This behavior was also evident within the experimental data (Fig. 4.5). As the spike detection threshold factor increased, STTC and A-Spike-synchronization lose their statistical significance (above 5% level), while all others remained stable indicating statistical significance (below 5% level). Spike-contrast yielded the highest statistical significance across all tested threshold factors, and was the only measures that still indicated a statistical significance (at 5% level) at the smallest threshold factor of 4, where a high level of noise spikes is assumable.

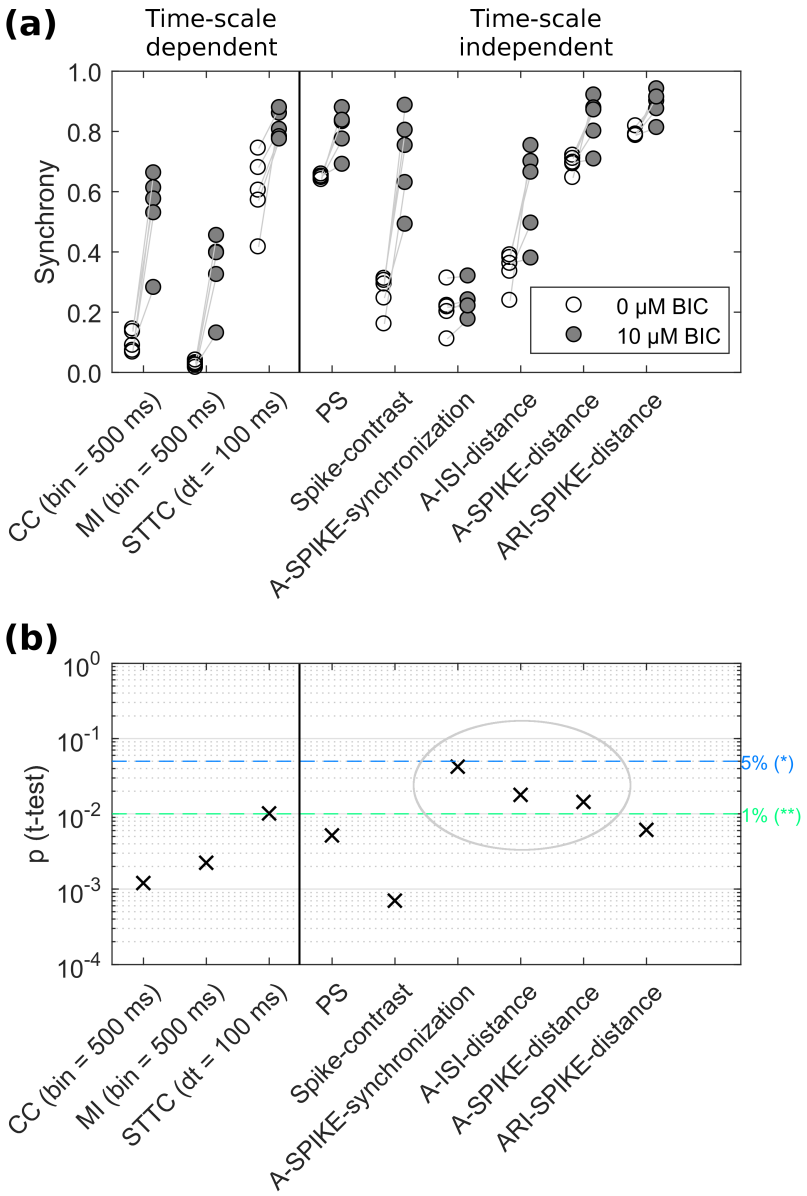

Figure 4.4: **Results of the application of different time-scale dependent and time-scale independent synchrony measures to a set of experimental data.** Experimental data were recorded from cortical cell cultures on MEA chips ($N = 5$) in the absence and presence of 10 μM BIC. **(a)** Absolute synchrony values of each synchrony measure for data without BIC (white circles) and with BIC (gray circles). **(b)** P-values for each synchrony measure from a one-tailed paired t-test assuming an increase in synchrony. The lower the p-value, the better the synchrony measure's ability to capture the effect of BIC. Grey ellipse marks synchrony measures that were not able to indicate high significant effects below p-values of 1%. Spike detection threshold factor was 5.

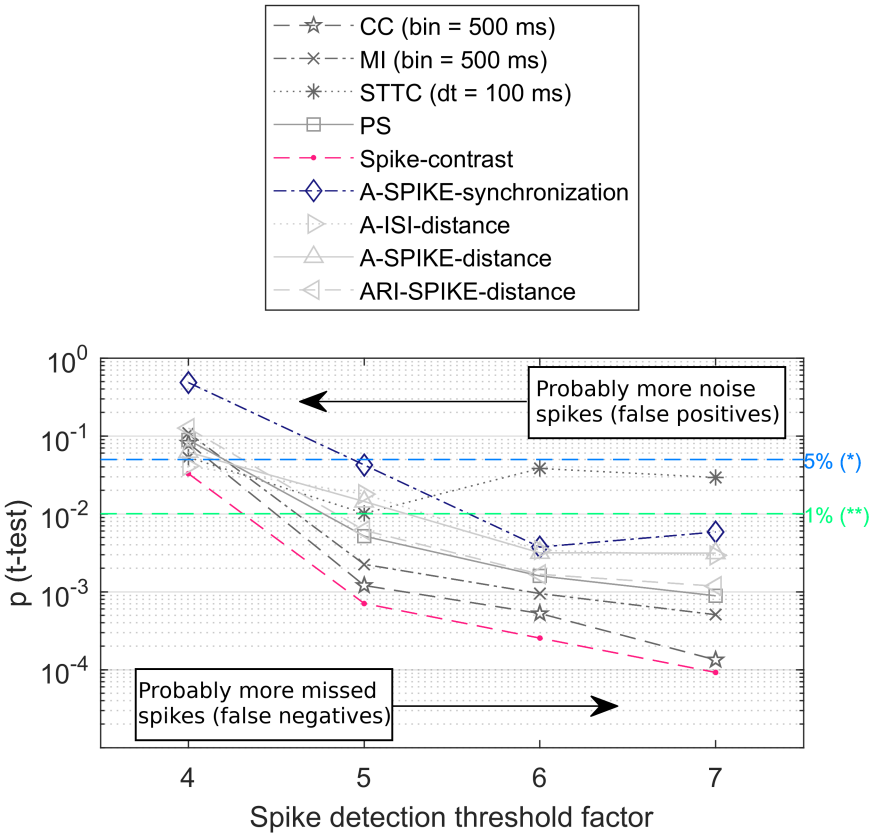

Figure 4.5: **Influence of the spike detection threshold on the statistical significance of the experimental data.** Synchrony and statistical significance of the experimental data were analyzed like in Fig. 4.4 applying different thresholds to detect spikes from the recorded signals. Assumably, the higher the spike detection threshold factor, the less noise were detected but also more real spikes were missed. The lower the p-value, the better the synchrony measure's ability to capture the effect of BIC.

4.4 Discussion and conclusion

In this work we compared different spike train synchrony measures regarding their robustness to false positive and false negative spikes in epileptiform signals. Such robustness is particularly relevant for experimental data with error prone spike detection, especially at low signal-to-noise ratios. Representative synchrony measures were chosen from different categories such as time-scale dependent (CC, MI, STTC), or time-scale independent (Spike-contrast, PS, A-SPIKE-synchronization, A-ISI-distance, A-SPIKE-distance, ARI-SPIKE-distance). In order to perform a comparison, we proposed a procedure based on a set of *in silico* manipulated spike trains with defined manipulation of features. Two data sets were generated based on experimental data by adding spikes, representing noise (false positive), and deleting spikes, representing missed spikes (false negative). Synchrony

of the experimental data was increased by applying BIC to cortical *in vitro* networks. The code and data used in this work are publicly available (see Section 4.2.1).

For the *in silico* manipulated data, the results showed that Spike-contrast was most robust to added spikes and very robust to deleted spikes. All other measures showed either comparable high robustness for added or deleted spikes, but not for both cases. Furthermore, CC, MI, and Spike-contrast work with binnend spike trains, which explains their robustness to deleted spikes as long as bursts (=many spikes occuring within a small time period) are still present in the data (see Fig. 4.1, (b 2)). A binned spike train will almost not change if only some spikes are deleted from a burst and if the bin size and burst duration are similar. As Spike-contrast automatically adapts its bin-size to the data, it is preferable over CC and MI for exploratory studies, where the time-scale is not known beforehand.
For the experimental data, all synchrony measures captured the synchrony increase mediated by BIC in a statistical significant way (below a p-value of 5%). However, there were differences in performance as the synchrony measures CC, MI, PS, Spike-contrast, and ARI-SPIKE-distance yielded values leading to a high statistical significance below p-values of 1%. Note that for CC the proposed bin size of 500 ms was used, but smaller bin sizes of around 300 ms would have overperformed Spike-contrast (Fig. 4.3). Referring to our assumption "the lower the p-value, the better the synchrony measure" defined in Section 4.2.3, it must be taken into account that this assumption is controversial since the actual synchrony increase (=ground truth) is not known for the experimental data. Thus, a synchrony measure that overestimates the synchrony increase mediated by BIC would incorrectly lead to a low p-value.

For small sample sizes, as in our experiment ($N = 5$), parameter-free statistics like the Wilcoxon signed-rank test are generally used to avoid assumptions about population distribution. Application of the Wilcoxon signed-rank test to our data yielded almost identical p-values for all synchrony measures (data not shown). In contrast, the t-test used in this work resulted in different p-values for each synchrony measure. So, it also depends on the choice of statistical test whether the choice of synchrony measures affects the final results.
Considering the results of the *in silico* manipulated data, the measures CC, MI, Spike-contrast, and ARI-SPIKE-distance were most robust to deleted spikes (=false negative spikes). As mentioned above, these synchrony measures also showed the best performance in the experimental data. This suggests that robustness to false negative spikes correlates with the ability to quantify synchrony changes in experimental data. If so, it would also imply that the experimental data used in this work were more affected by false negative spikes, than by false positive spikes. In other words, more spikes were missed than noise was misinterpreted as spikes. This behavior could be used to draw conclusions about the quality of an experimental spike train from the rank of the p-values of different synchrony measures.
Like already mentioned, there were some synchrony measures, whose results of the *in silico* manipulated data and experimental data did not correlate. This suggests, that robustness to false positive or false negative spikes is not the only factor to effectively capture synchrony changes in experimental data. Factors like robust-

ness to temporal non-stationarity of the recording could also be different among the synchrony measures. For instance, PS, A-SPIKE-distance, ARI-SPIKE-distance, A-ISI-distance, and A-SPIKE-synchronization are more adaptive to changes in time scales inside a spike train as they dynamically define their time scales considering nearby spikes. In contrast, CC, MI, STTC, and Spike-contrast use equally spaced time scales along the entire spike train duration.
Overall, for our specific data set, Spike-contrast was the only time-scale independent measure being robust to noise (false positive spikes) as well as missed spikes (false negative spikes). This desirable performance was confirmed by the ability of the Spike-contrast measure to detect biochemically induced synchrony with a high significance, even for different spike detection threshold factors. It should be mentioned that the measures A-SPIKE-synchronization, A-ISI-distance, A-SPIKE-distance, and ARI-SPIKE-distance are able to produce a synchrony profile over time, which complements the synchrony profile over time-scale of Spike-contrast.
Summarizing, we suggest to include the Spike-contrast synchrony measure into synchrony studies of epileptiform experimental neuronal data sets in addition to established synchrony measures.

Acknowledgments

F.A.R. acknowledge CNPq (grant 305940/2010-4), Fapesp (grant 2012/51301-8 and 2013/26416-9) and NAP eScience - PRP - USP for financial support. L.F.C. thanks CNPq (grant 307085/2018-0) and FAPESP (grant 15/22308-2) for sponsorship. G.F.A. acknowledges FAPESP (grant 2012/25219-2). T.P. acknowledges FAPESP (grant 2016/23827-6). C.C.H. acknowledges FAPESP (grant 18/09125-4). C.T. and M.C. acknowledges Bayerisches Staatsministerium für Bildung und Kultus, Wissenschaft und Kunst for financial support in the frame of ZEWIS, BAYLAT, the BMBF (grant 03FH061PX3), and INeuTox (grant 13FH516IX6). C.N. would like to acknowledge support from the Studienstiftung des Deutschen Volkes.

Appendix

Synchrony measure description

Mutual Information MI measures how two random variables X and Y are related (Cover and Thomas, 2012) and is based on the concept of entropy, which is a fundamental concept in information theory (Shannon and Weaver, 1948; Cover and Thomas, 2012). The Shannon entropy (Cover and Thomas, 2012) of a random variable X is defined as

$$H(X) = -\sum_i p_x(i) \log(p_x(i)), \tag{4.6}$$

where $p_x(i) = P(X = i)$ and the $\log$ function is taken to the base 2 (see Fig. 4.6 a for an example calculation). $H(X)$ measures the uncertainty about a random variable X. The conditional entropy quantifies the information necessary to describe the random variable Y given that the information about X is known (Cover and Thomas, 2012). Formally, it is defined by

$$\begin{aligned} H(Y|X) &\equiv \sum_{x\in X} p(x)\, H(Y|X=x) \\ &= \sum_{x\in X} \left(p(x) \sum_{y\in Y} p(y|x)\ \log\ \frac{1}{p(y|x)} \right) \\ &= -\sum_{x\in X}\sum_{y\in Y} p(x,y)\ \log\ p(y|x) \\ &= -\sum_{x\in X, y\in Y} p(x,y) \log\ p(y|x) \\ &= \sum_{x\in X, y\in Y} p(x,y) \log \frac{p(x)}{p(x,y)}. \end{aligned} \tag{4.7}$$

MI is defined as

$$I(X;Y) = \sum_{y\in Y}\sum_{x\in X} p(x,y) \log \left(\frac{p(x,y)}{p(x)\, p(y)} \right). \tag{4.8}$$

Additionally, the MI can be expressed in terms of the entropy and the conditional entropy of random variables X and Y as

$$\begin{aligned} I(X;Y) &= H(X) - H(X|Y) \\ &= H(Y) - H(Y|X) \\ &= H(X) + H(Y) - H(X,Y) \\ &= H(X,Y) - H(X|Y) - H(Y|X). \end{aligned} \tag{4.9}$$

Aside from the analytic expressions, it is possible to interpret those quantities graphically, as depicted in Fig. 4.6b. MI is more general than the correlation coefficient and quantifies how the joint distribution $p(x, y)$ is similar to the products of marginal distributions $p(x)p(y)$ (Cover and Thomas, 2012). Compared to the cross-correlation measure, mutual information also captures non-linear dependencies.

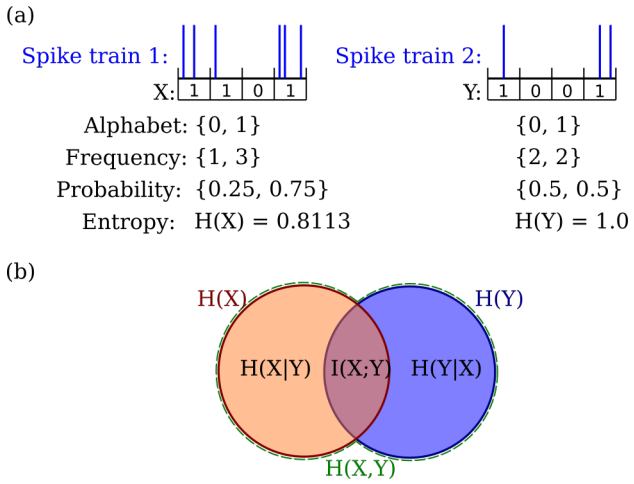

Figure 4.6: **Example entropy calculation of two spike trains and illustration of the mutual information (MI) measure.** (a) Two different spike trains are binned in a binary way resulting in X and Y. Each value is considered a character building the alphabet of the signal. The probability of each character is obtained by dividing its incidence by the length of the signal. The entropy of each signal (H(X), H(Y)) is calculated using Eq. (4.6) with the probabilities given above. (b) Visualization of the mutual information I(X;Y) using the joint entropy H(X,Y), the entropies H(X), H(Y), and conditional entropies H(X|Y), H(Y|X) like calculated in Eq. (4.9). The mutual information value I(X;Y) increases with increasing synchrony between signal X and Y.

For comparison, the value of mutual information needs to be normalized. Many possible approaches have been proposed (Cover and Thomas, 2012), such as

$$M(X;Y) = \frac{I(X;Y)}{\min\left[H(X), H(Y)\right]}, \tag{4.10}$$

because $I(X;Y) \leq \min\left[H(X), H(Y)\right]$ and, consequently, $0 \leq M(X;Y) \leq 1$. This formulation has been used before in the context of neuronal signal analysis (Bettencourt et al., 2007, 2008; Ham et al., 2010). Another possible normalization is the so-called symmetric uncertainty (Witten and Frank, 2000), defined as

$$M^*(X;Y) = 2\frac{I(X;Y)}{H(X) + H(Y)}, \tag{4.11}$$

where $0 \leq M^*(X;Y) \leq 1$. In this work the latter normalization were used as it performed better than the first one when applied to the experimental data (data not shown).

In order to estimate the MI between two spike trains, both spike trains were transformed into binary binned signals. A spike train i is binnend as

$$x_i(t) = \begin{cases} 1, \text{ if spike train } i \text{ shows at least one spike in time interval } t \text{ to } t + \Delta t. \\ 0, \text{ if spike train } i \text{ shows no spike in time interval } t \text{ to } t + \Delta t. \end{cases} \tag{4.12}$$

using a bin size $\Delta t = 500\,\text{ms}$ and $t = 0\Delta t, 1\Delta t, 2\Delta t, ...$ (also see Fig. 4.6 a). The

choice of the bin size of 500 ms is justified in Section 4.2.4).

Phase Synchronization Since synchronization processes are related with rhythm adjustment, it is natural to introduce the concept of phase of an oscillator, a quantity that increases by 2π within an oscillation cycle and determines unambiguously the state of a periodic oscillator (Pikovsky et al., 2003). For instance, consider a harmonic oscillator described by the variable $x(t) = A\sin(\omega_0 t + \phi_0)$. In this case, ω_0 denotes the angular frequency, which is related to the oscillation period $\omega_0 = 2\pi/T$, A is the amplitude of oscillation, and the quantity $\phi(t) = \omega_0 t + \phi_0$ is the phase of this oscillator. Two or more oscillators are synchronized when they present the same phase evolution (Pikovsky et al., 2003).
The measurement of the synchronization level of self-sustained oscillators can be done by considering the phases as rotating points in the unit cycle of the complex plane (Pikovsky et al., 2003; Strogatz, 2000). If an oscillator has a phase $\phi(t)$, then its trajectory in the complex plane is described by the vector $e^{i\phi(t)}$. For instance, if two oscillators have phases $\phi_1(t) = \phi_2(t) = \phi(t)$, then they will have the same trajectory in the complex plane and thus the modulus of the resultant vector will be $|e^{i\phi_1(t)} + e^{i\phi_2(t)}|/2 = 1$, meaning that the oscillators are perfectly synchronized. Supposing now a population of N interacting phase oscillators whose phases are described by the variable $\phi_i(t)$, $i = 1, ..., N$. The synchronization order parameter is defined as (Strogatz, 2000)

$$re^{i\psi(t)} = \frac{1}{N}\sum_{j=1}^{N} e^{i\phi_j(t)}, \tag{4.13}$$

where $\psi(t)$ is the average phase of the system at time t. When $r \approx 0$, the phases are distributed uniformly over $[0, 2\pi]$ corresponding to the asynchronous state. When $r \approx 1$ the phases rotate together corresponding to fully synchronized state (Fig. 4.7).

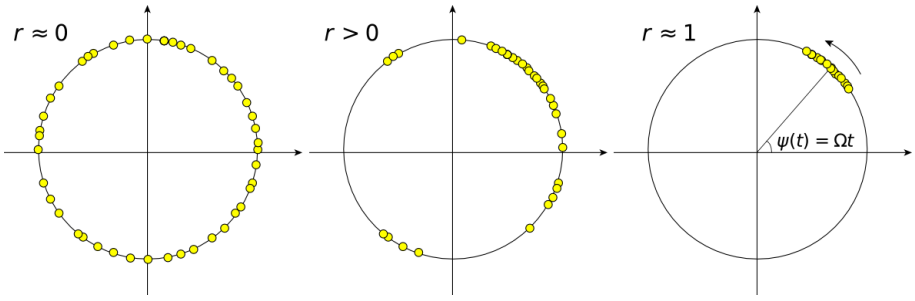

Figure 4.7: **Example for distribution of phase vectors $e^{i\phi(t)}$ in complex plane.** (a) Randomly distributed phase vectors over $[0, 2\pi]$, implying $r \approx 0$; in other words the oscillators are completely asynchronous. (b) Regime of partial synchronization; phase vectors of some oscillators are grouped in a synchronous cluster equivalent to $r > 0$. (c) Strongly synchronized state, where all oscillators group into a single synchronous cluster rotating with average frequency Ω, thus $r \approx 1$.

Neurons can also be considered as self-sustained oscillators (Arenas et al., 2008) and are often modeled as integrate-and-fire oscillators, where the rhythmic quantity

is the rate at which spikes are fired. The synchronization process in this case is the adjustment of the spiking patterns, i.e., if two interacting integrate-and-fire oscillators discharge their spikes jointly, then they are synchronized. Therefore, in order to quantify the synchronization between interacting integrate-and-fire oscillators, the phases associated to the respective spike signals have to be defined.

The time series recorded by an electrode can be considered as a sequence of point events taking place at time t_k, with $k = 1, 2, ..., N_{\text{spikes}}$. The time interval between two spikes can be treated as a complete cycle. In this case, the phase increase during this time interval is exactly 2π. Hence, the values of $\phi(t_k) = 2\pi k$ are assigned to the times t_k, and for an arbitrary instant of time ($t_k < t < t_{k+1}$), the phase is considered as a linear interpolation between these values (Pikovsky et al., 2003; Neiman et al., 1998; Pikovsky et al., 1997; Tass et al., 1998; Hu and Zhou, 2000), as

$$\phi(t) = 2\pi \frac{t - \tau_k}{\tau_{k+1} - \tau_k} + 2\pi k. \tag{4.14}$$

This method can be applied to any process containing time series of spikes and it is widely used in the study of synchronization in neuronal dynamics (Pikovsky et al., 2003). Fig. 4.8 exemplifies the calculation of phases $\phi(t)$ of two spike signals and their respective sum of the phase vectors $e^{i\phi(t)}$ in the complex plane.

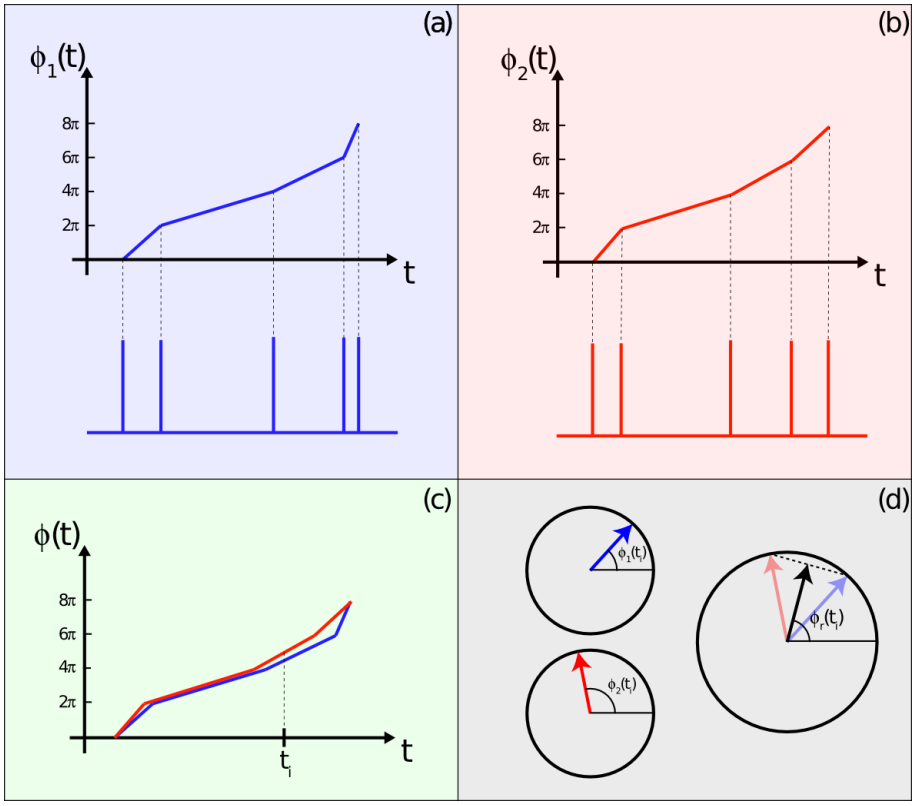

Figure 4.8: **Example of phase vector construction.** (a) $\phi_1(t)$ and (b) $\phi_2(t)$ are calculated using the respective spike signals according to Equation (4.14). (c) Superposition of temporal evolution of phases and (d) phase vectors $e^{i\phi_1(t_i)}$, $e^{i\phi_2(t_i)}$ as well as the resultant vector at time $t = t_i$, $r \cdot e^{i\phi_r(t_i)} = (e^{i\phi_1(t_i)} + e^{i\phi_2(t_i)})/2$.

For a system composed of N oscillators, the instant phase synchronization is quantified by the order parameter defined in Eq. (4.13). However, to quantify the level of synchronization of the neurons, we consider the average over the recorded time

$$\bar{r} = \left\langle \left| \frac{1}{N} \sum_{j=1}^{N} e^{i\phi_j(t)} \right| \right\rangle_t , \tag{4.15}$$

where $\langle \cdots \rangle_t$ stands for the temporal average and N stands for the number of electrodes used to compute the order parameter.

Author contributions

M.C.: Conception, design, generation, and analysis of *in silico* manipulated data. Application of the synchrony measures STTC, Spike-contrast, A-SPIKE-synchronization, A-ISI-distance, A-SPIKE-distance, ARI-SPIKE-distance to experimental data. Statistical tests and spike detection with varying thresholds. Preparation of figure 1 to 6. Draft of the manuscript. R.B.: Initial conception and design of synchrony measure comparison using experimental data. C.N.: Initial conception and design of synchrony measure comparison using experimental data. Performed cell experiments and spike detection of raw data. G.F.A.: Implementation and application of the synchrony measure MI to experimental data and MI description in appendix. T.P.: Implementation and application of the synchrony measure PS to experimental data and PS description in appendix. Preparation of figure 7 and 8. C.C.H.: Implementation and application of the synchrony measures CC to experimental data. L.F.C.: Helped in the initial conception, discussions and revision. F.A.R.: Conception and design of research. C.T.: Conception and design of research. ALL: Interpreted and discussed results of experiments. Edited and revised manuscript. Approved final version of manuscript.

Chapter 5

General discussion

The aim of this work is to identify the most appropriate connectivity estimators and synchrony measures for spike train signals from *in vitro* neuronal networks. Especially, attention was paid to

(a) the choice of appropriate parameter values,

(b) the suitability for massively parallel spike trains such as from HDMEAs, and

(c) the characteristics of experimental data such as different time scales or erroneous spike trains.

As a result, evaluation frameworks were developed considering the characteristics of experimental data in order to compare known methods from the literature. In addition, two new methods were developed. A connectivity estimator called total spiking probability edges (TSPE) and a synchrony measure called Spike-contrast. The comparison showed that the two new methods outperformed the methods known from the current literature.
In the following, this chapter is divided into discussions about connectivity estimators (section 5.1) and synchrony measures (section 5.2). The connectivity estimator section refers to the manuscript in chapter 2 and the synchrony measure section to the manuscripts in chapter 3 and chapter 4.

5.1 Connectivity estimation

Parameter value optimization (a): In order to identify appropriate connectivity estimators, different methods were selected from the literature based on cross-correlation and on transfer entropy. The newly introduced method, TSPE, is based on cross-correlation and not only estimates functional connections but also effective connections. The difference to other cross-correlation based methods, is the additional analysis of the cross-correlogram. More specifically, negative and positive peaks of the cross-correlogram are emphasized by a filter, which enables a distinction between inhibitory and excitatory connections. This filtering procedure is performed for various filter lengths to cover different time constants of neurons. All filtered cross-correlograms are then averaged to a new curve. The extreme value of this curve is the value of the estimated connection strength (see Fig. 3 in chapter 2).

Note that a very similar approach called FNCCH was developed independently at about the same time by Pastore et al. (2018c). This method uses a simpler filter approach for the cross-correlogram and does not vary the filter length.

HDMEA suitability (b): The calculation speed comparison for massively parallel spike trains showed that cross-correlation based methods are the fastest connectivity estimators (see Fig. 10 in chapter 2). The calculation of transfer entropy based methods took at least ten times as long. Despite the additional filter procedure, the computing time of TSPE was only about twice as much as for the cross-correlation based connectivity estimators from the literature. This is due to the fact that the calculation of cross-correlation as well as the filtering is performed in parallelizable matrix operations. TSPE is therefore suitable for massively parallel spike trains.

Complexity of experimental data (c): TSPE was evaluated using simulated data from *in silico* networks with different topologies. In contrast to other comparative studies, not only random networks were used for the simulations, but also small-world and scale-free networks. Since small-world and scale-free networks are more similar to biological neuronal networks, this evaluation approach better captured the complexity of experimental data. As a result, the classification accuracy of TSPE outperformed the compared methods for all simulated network topologies (see Fig. 5 in chapter 2). Because of the high accuracy and the ability to discriminate betweeen excitatory and inhibitory connections, TSPE is considered the most appropriate connectivity estimator.

Limitations and future work: A limitation of TSPE is that it is not possible to detect self-connections or parallel connections, which is generally true for all other connectivity measures evaluated in this work. It should also be noted that the accuracy for estimated inhibitory connections is significantly lower than for excitatory connections. This is a general issue, since inhibitory effects are only visible if the target neuron already exhibits high firing rates.
Another limitation is that TSPE uses predefined values to vary the filter length. While the selected values proved to be suitable for the test data, this does not necessarily apply to all data. It should be kept in mind, that the test data was generated using Izhikevich networks, which are motivated by the anatomy of a mammalian cortex (Izhikevich et al., 2003). For the analysis of neuronal networks from brain regions other than the cortex, a re-evaluation of the predefined values is recommended.
An additional point for future work is the threshold selection. Connectivity estimators provide an estimated connectivity value between all pairs of spike trains. However, depending on the postprocessing of these values, it can be desireable to only consider the most relevant connections. A preliminary study for the threshold selection based on the connectivity matrix distribution or on surrogate data are decribed in De Blasi (2018b).

5.2 Synchrony measurement

Parameter value optimization (a): In order to identify the most appropriate synchrony measure, different time scale dependent and time scale inepended synchrony measures were compared. The novel method Spike-contrast is a time scale independent synchrony measure as it optimizes itself to the time scale of the data. The automatic optimization is based on an intuitive approach, when observing spike raster plots. In raster plots, synchronized network activity appears as vertical lines. The higher the synchrony level, the more distinct the vertical lines appear – or in other words – the visual contrast increases (see Fig. 1 in chapter 3 If, additionally to a high contrast, the number of contributing spike trains to the vertical lines is high, a high synchrony is indicated. This calculation is repeated for different bin sizes which reveals the maximum synchrony in the data. In addition to the maximum synchrony value, this approach also provides a synchrony curve as a function of the time scale (see Fig. 2 in chapter 3). This curve is a new feature of time scale independent synchrony measures and complements the synchrony curve over time from known measures such as SPIKE-distance.
It was shown that Spike-contrast yields similar results to the established time scale independent measure SPIKE-distance for most data (see Fig. 3 in chapter 3). The similarity was surprising, as both methods are based on fundamentally different approaches. The main difference, however, was visible in spike trains with self-similar[1] bursts ("parent bursts") consisting of smaller bursts ("sub-bursts"). In this case, Spike-contrast only emphasizes synchronization changes in the parent bursts or more exactly the largest available time scale. This property is desirable for the analysis of experimental data (see also Ciba et al. (2017)). For example, Satuvuori et al. (2017) modified time scale independent methods to be less sensitive to small time scales. Such modifications are not necessary for Spike-contrast, as it is not only "less sensitive" for small time scales, but "not sensitive at all" which is an advantage over other time scale independent methods.

HDMEA suitability (b): The calculation time for Spike-contrast takes longer than the established measures (e.g. SPIKE-distance) for MEA data with a small number of electrodes. For HDMEA data containing several hundred or thousands of electrodes, however, the calculation becomes significantly faster (see Fig. 4 in chapter 3). The reason lies in the multivariate nature of Spike-contrast, so that the calculation time is nearly independent from the number of parallel spike trains. Spike-contrast is therefore particularly suitable for massively parallel spike trains.

Complexity of experimental data (c): For the comparison framework, experimental data from *in vitro* recordings were used in order to obtian a test data set featuring more complexity than simulated networks. The level of synchrony was increased using a substance called bicuculline (BIC). In addition, spikes were added or deleted from the recorded data in order to study the robustness of the synchrony measures. As a result, Spike-contrast was the most robust time scale independent measure against erroneous spike trains and similarly robust to time scale dependent

[1] Another term is "fractal". Fractal geometry is a fundamental pattern in nature (Mandelbrot, 1983) and is also present in neuronal networks and their signals (Baker et al., 2006)

measures (see Fig. 1 in chapter 4). Furthermore, Spike-contrast was the most sensitive measure to synchrony changes mediated by the substance BIC (see Fig. 4 in chapter 4). The resason for that was the binning procedure within Spike-contrast. All synchrony measures which contain a binning procedure, showed high robustness to the error case of missed spikes and high sensitivity to the substance BIC. Overall, it could be demonstrated that Spike-contrast combines the robustness of bin-based time scale dependent measures, with the flexibility of time scale independent measures. Spike-contrast is therefore considered as the most appropriate measure for experimental data.

Limitations and future work: As a limitation of Spike-contrast it should be noted that – although it is time scale independent – it is not parameter free compared to other time scale independent measures. Parameter such as the resolution of the bin size sweep and the bin overlap have to be chosen. However, the proposed parameter values were suitable for analyzing both simulated and experimental data (Ciba et al., 2017; Ciba and Thielemann, 2019; Ciba et al., 2019, 2020). Because of the binning procedure of Spike-contrast, "binning-artefacts" may influence the final synchrony value such as observed when analyzing random spike trains. Therefore, further investigations are needed in order to better understand the limitations of Spike-contrast.
In addition to the limitations of Spike-contrast, the fact that not all synchrony measures described in the literature were included can be regarded as a limitation of the comparison. While all time scale independent synchrony measures found in the literature were taken into account, the comparison of time scale dependent methods is not comprehensive. The reason lies in the large number of different methods which are scattered across the literature, inconsistent programming platforms, restricted accessability (e.g. Global-Synchrony-Index used in Eisenman et al. (2015)), or recently published methods (Sihn and Kim, 2019; Sotomayor-Gomez et al., 2020). Moreover, there are further methods in the literature that are modifiable to derive a synchrony value. For example unitary event analysis (UEA) (Grün et al., 2002; Grün and Rotter, 2010), was used to derive a time scale dependent synchrony index by calculating the average number of synchronous events (Kilavik et al., 2009). Such synchrony measures could be included in future work if the focus is on time scale dependent measures.
As a further point for future work, the impact of errors due to incorrect spike sorting could be taken into account. A spike sorting procedure can be used to distinguish between different source neurons contributing to the same spike train. However, such a spike sorting is also prone to errors (Rey et al., 2015). Although this has not been explicitly investigated, it is assumed that Spike-contrast is robust against spike sorting errors, as long as the overall burst patterns are preserved.

Due to the time scale independence, Spike-contrast could also be applied to *in vivo* data or even to other fields. Not only neurons generate spike trains but also cardiomyocytes (Spira and Hai, 2013) or plant roots (Masi et al., 2012). Also beyond biology, all systems that can be reduced to sequences of discrete events may be a potential application. For example, spike train synchrony measures have already been used in social science to study inter-personal synchronization in cooperative

tasks of children (Rabinowitch and Knafo-Noam, 2015), quantifying the regularity of human behaviour, (Williams et al., 2012), or in climate research to identify spatial structure of rainfall fields (Malik et al., 2010).

5.3 Summary and outlook

In summary, an evaluation framework for connectivity estimators and for synchrony measures was developed and two novel methods were proposed which outperformed methods known from the literature. While many methods depend heavily on parameters that have to be selected by the user, the two new methods are designed to require no user interaction, thus avoiding misinterpretation of the data and ensuring comparability of the results. The demand for computationally efficient analysis methods, which arises from the increasing use of HDMEAs, is covered by the two analysis methods as well. In contrast to other comparative studies known from the literature, the evaluation framework of this work takes into account further aspects of the complexity of experimental data, such as more realistic network topologies or pre-processing errors. As the new methods performed best in these evaluation frameworks, they are considered as the most appropriate methods for the analysis of *in vitro* neuronal networks. The developed evaluation framework serves as a step towards a standard benchmark procedure for testing newly developed functional or effective connectivity estimators and synchrony measures. In order to help fill the gap of a missing gold standard, the proposed evaluation framework as well as the new methods were made available online at `https://github.com/biomemsLAB/`.

Due to the discussed advantages of the two new methods, the performance of estimating connectivity and measuring synchrony increased. Since information about the connectivity and synchrony of neuronal networks are fundamental to study neuronal networks, research fields such as pharmacology (Chiappalone et al., 2003; Amin et al., 2016), toxicology (Johnstone et al., 2010; Flachs and Ciba, 2016), and basic research will benefit. For example, the synchrony curve from Spike-contrast has already been applied as a new feature to analyze the synchrony development of a neuronal *in vitro* network during a long-term recording of several days (Ciba and Thielemann, 2019). A first application of Spike-contrast and TSPE to HDMEA data is shown in Ciba et al. (2019) to study the effects of psychedelics with the aim of developing treatments for depression, anxiety, addiction or to explore neural correlates to consciousness. Additionally, TSPE has already found its way into the research community due to its fast calculation. De Filippo et al. (2020) applied it for the estimation of inhibitory connections in order to study the effect of serotonin on slow oscillations in the entorhinal cortex.

Bibliography

M. Abeles. *Local cortical circuits: an electrophysiological study*, volume 6. Springer Science & Business Media, 2012.

A. P. Alivisatos, M. Chun, G. M. Church, R. J. Greenspan, M. L. Roukes, and R. Yuste. The brain activity map project and the challenge of functional connectomics. *Neuron*, 74(6):970–974, 2012.

K. W. Alt, C. Jeunesse, C. H. Buitrago-Téllez, R. Wächter, E. Boës, and S. L. Pichler. Evidence for stone age cranial surgery. *Nature*, 387(6631):360–360, 1997.

H. Amin, A. Maccione, F. Marinaro, S. Zordan, T. Nieus, and L. Berdondini. Electrical responses and spontaneous activity of human ips-derived neuronal networks characterized for 3-month culture with 4096-electrode arrays. *Frontiers in neuroscience*, 10:121, 2016.

A. Amon. A case for more curiosity-driven basic research. *Molecular biology of the cell*, 26(21):3690–3691, 2015.

K. Amunts, C. Ebell, J. Muller, M. Telefont, A. Knoll, and T. Lippert. The human brain project: creating a european research infrastructure to decode the human brain. *Neuron*, 92(3):574–581, 2016.

R. G. Andrzejak, F. Mormann, and T. Kreuz. Detecting determinism from point processes. *Physical Review E*, 90(6):062906, 2014.

A. Arenas, A. Díaz-Guilera, J. Kurths, Y. Moreno, and C. Zhou. Synchronization in complex networks. *Physics Reports*, 469(3):93–153, 2008.

G. Arnulfo, A. Canessa, F. Steigerwald, N. G. Pozzi, J. Volkmann, P. Massobrio, S. Martinoia, and I. U. Isaias. Characterization of the spiking and bursting activity of the subthalamic nucleus in patients with parkinson's disease. In *Advances in Biomedical Engineering (ICABME), 2015 International Conference on*, pages 107–110. IEEE, 2015.

A. Bahmer and G. Langner. Oscillating neurons in the cochlear nucleus: I. experimental basis of a simulation paradigm. *Biological Cybernetics*, 95(4):371–379, 2006.

R. E. Baker, M. A. Corner, and J. van Pelt. Spontaneous neuronal discharge patterns in developing organotypic mega-co-cultures of neonatal rat cerebral cortex. *Brain Research*, 1101(1):29–35, 2006.

A.-L. Barabási and E. Bonabeau. Scale-free networks. *Scientific American*, 288(5): 60–69, 2003. ISSN 0036-8733.

P. Barthó, H. Hirase, L. Monconduit, M. Zugaro, K. D. Harris, and G. Buzsáki. Characterization of neocortical principal cells and interneurons by network interactions and extracellular features. *Journal of neurophysiology*, 92(1):600–608, 2004. ISSN 0022-3077. doi: 10.1152/jn.01170.2003.

P. Bedenbaugh and G. L. Gerstein. Multiunit normalized cross correlation differs from the average single-unit normalized correlation. *Neural computation*, 9(6): 1265–1275, 1997. ISSN 0899-7667.

L. Berdondini, K. Imfeld, A. Maccione, M. Tedesco, S. Neukom, M. Koudelka-Hep, and S. Martinoia. Active pixel sensor array for high spatio-temporal resolution electrophysiological recordings from single cell to large scale neuronal networks. *Lab on a chip*, 9(18):2644–2651, 2009a. ISSN 1473-0197. doi: 10.1039/b907394a.

L. Berdondini, K. Imfeld, A. Maccione, M. Tedesco, S. Neukom, M. Koudelka-Hep, and S. Martinoia. Active pixel sensor array for high spatio-temporal resolution electrophysiological recordings from single cell to large scale neuronal networks. *Lab on a Chip*, 9(18):2644–2651, 2009b.

L. Berdondini, P. Massobrio, M. Chiappalone, M. Tedesco, K. Imfeld, A. Maccione, M. Gandolfo, M. Koudelka-Hep, and S. Martinoia. Extracellular recordings from locally dense microelectrode arrays coupled to dissociated cortical cultures. *Journal of neuroscience methods*, 177(2):386–396, 2009c. ISSN 0165-0270. doi: 10.1016/j.jneumeth.2008.10.032.

L. Bettencourt, G. Stephens, M. Ham, and G. Gross. Functional structure of cortical neuronal networks grown in vitro. *Physical Review E*, 75(2):021915, Feb. 2007. ISSN 1539-3755. doi: 10.1103/PhysRevE.75.021915. URL http://link.aps.org/doi/10.1103/PhysRevE.75.021915.

L. M. A. Bettencourt, V. Gintautas, and M. I. Ham. Identification of Functional Information Subgraphs in Complex Networks. *Phys. Rev. Lett.*, 100:238701, Jun 2008. doi: 10.1103/PhysRevLett.100.238701. URL http://link.aps.org/doi/10.1103/PhysRevLett.100.238701.

S. C. Bondy and A. Campbell. Developmental neurotoxicology. *Journal of neuroscience research*, 81(5):605–612, 2005.

P. Bonifazi, M. Goldin, M. A. Picardo, I. Jorquera, A. Cattani, G. Bianconi, A. Represa, Y. Ben-Ari, and R. Cossart. Gabaergic hub neurons orchestrate synchrony in developing hippocampal networks. *Science (New York, N.Y.)*, 326(5958):1419–1424, 2009. ISSN 1095-9203. doi: 10.1126/science.1175509.

D. Botstein. Why we need more basic biology research, not less. *Molecular biology of the cell*, 23(21):4160–4161, 2012.

A. P. Bradley. The use of the area under the roc curve in the evaluation of machine learning algorithms. *Pattern recognition*, 30(7):1145–1159, 1997.

M. Brosch and C. E. Schreiner. Correlations between neural discharges are related to receptive field properties in cat primary auditory cortex. *The European journal of neuroscience*, 11(10):3517–3530, 1999. ISSN 0953-816X.

E. N. Brown, R. E. Kass, and P. P. Mitra. Multiple neural spike train data analysis: state-of-the-art and future challenges. *Nature Neuroscience*, 7(5):456–461, 2004.

G. Buzsaki. *Rhythms of the Brain*. Oxford University Press, 2006.

G. Buzsáki and A. Draguhn. Neuronal oscillations in cortical networks. *Science*, 304 (5679):1926–1929, 2004.

G. Buzsáki, C. A. Anastassiou, and C. Koch. The origin of extracellular fields and currents—eeg, ecog, lfp and spikes. *Nature Reviews Neuroscience*, 13(6):407–420, 2012.

G. Buzsáki, N. Logothetis, and W. Singer. Scaling brain size, keeping timing: evolutionary preservation of brain rhythms. *Neuron*, 80(3):751–764, 2013.

J. Cambray. Synchronicity and emergence. *American Imago*, 59(4):409–434, 2002.

M. Catanzaro, M. Boguñá, and R. Pastor-Satorras. Generation of uncorrelated random scale-free networks. *Physical review. E, Statistical, nonlinear, and soft matter physics*, 71(2 Pt 2):027103, 2005. ISSN 1539-3755. doi: 10.1103/PhysRevE.71.027103.

M. Chiappalone, A. Vato, M. Marcoli, F. Davide, S. Martinoia, et al. Networks of neurons coupled to microelectrode arrays: a neuronal sensory system for pharmacological applications. *Biosensors and Bioelectronics*, 18(5-6):627–634, 2003.

M. Chiappalone, M. Bove, A. Vato, M. Tedesco, and S. Martinoia. Dissociated cortical networks show spontaneously correlated activity patterns during in vitro development. *Brain research*, 1093(1):41–53, 2006a. ISSN 0006-8993. doi: 10.1016/j.brainres.2006.03.049.

M. Chiappalone, M. Bove, A. Vato, M. Tedesco, and S. Martinoia. Dissociated cortical networks show spontaneously correlated activity patterns during in vitro development. *Brain research*, 1093(1):41–53, 2006b.

M. Chiappalone, A. Vato, L. Berdondini, M. Koudelka-Hep, and S. Martinoia. Network dynamics and synchronous activity in cultured cortical neurons. *International Journal of Neural Systems*, 17(02):87–103, 2007a.

M. Chiappalone, A. Vato, L. Berdondini, M. Koudelka-Hep, and S. Martinoia. Network dynamics and synchronous activity in cultured cortical neurons. *International Journal of Neural Systems*, 17(02):87–103, 2007b.

D. Chicharro, T. Kreuz, and R. G. Andrzejak. What can spike train distances tell us about the neural code? *Journal of neuroscience methods*, 199(1):146–165, 2011.

M. Ciba and C. Thielemann. Synchrony changes on different time-scales during in vitro neuronal network development. *Conference Abstract: MEA Meeting 2018 — 11th International Meeting on Substrate Integrated Microelectrode Arrays*, 2019. doi: doi:10.3389/conf.fncel.2018.38.00081.

M. Ciba, A. Bahmer, and C. Thielemann. Application of spike train synchrony measure spike-contrast to quantify the effect of bicuculline on cortical networks grown on microelectrode arrays. volume 18, page P269. BioMed Central, Aug 2017. doi: 10.1186/s12868-017-0372-1. URL https://doi.org/10.1186/s12868-017-0372-1.

M. Ciba, T. Isomura, Y. Jimbo, A. Bahmer, and C. Thielemann. Spike-contrast: A novel time scale independent and multivariate measure of spike train synchrony. *Journal of Neuroscience Methods*, 293(Supplement C):136 – 143, 2018. ISSN 0165-0270. doi: https://doi.org/10.1016/j.jneumeth.2017.09.008. URL http://www.sciencedirect.com/science/article/pii/S0165027017303370.

M. Ciba, M. Mayer, and C. Thielemann. Experimental setup to investigate the effect of psychedelics on in vitro neuronal networks. INSIGHT2019, Berlin, Sept. 2019.

M. Ciba, R. Bestel, C. Nick, G. F. de Arruda, T. Peron, C. C. Henrique, L. d. F. Costa, F. A. Rodrigues, and C. Thielemann. Comparison of different spike train synchrony measures regarding their robustness to erroneous data from bicuculline-induced epileptiform activity. *Neural Computation*, 32(5):887–911, 2020.

J. R. Cooper, F. E. Bloom, and R. H. Roth. *The biochemical basis of neuropharmacology*. Oxford University Press, USA, 2003.

T. M. Cover and J. A. Thomas. *Elements of information theory*. John Wiley & Sons, 2012.

C. S. Cutts and S. J. Eglen. Detecting pairwise correlations in spike trains: an objective comparison of methods and application to the study of retinal waves. *The Journal of Neuroscience*, 34(43):14288–14303, 2014.

J. Dauwels, F. Vialatte, T. Musha, and A. Cichocki. A comparative study of synchrony measures for the early diagnosis of alzheimer's disease based on eeg. *NeuroImage*, 49(1):668–693, 2010.

S. De Blasi. Simulation of large scale neural networks for evaluation applications. *Proceedings of the International Student Scientific Conference POSTER 2018 : May 10, 2018, Prague*, 22, 2018a.

S. De Blasi. Connectivity estimation of high dimensional data recorded from neuronal cells. Master's thesis, University of Applied Sciences Aschaffenburg, 2018b.

S. De Blasi, M. Ciba, A. Bahmer, and C. Thielemann. Total spiking probability edges: A cross-correlation based method for effective connectivity estimation of cortical spiking neurons. *Journal of neuroscience methods*, 312:169–181, 2019.

R. De Filippo, B. Rost, A. Stumpf, C. Cooper, J. Tukker, C. Harms, P. Beed, and D. Schmitz. Serotonin suppresses slow oscillations by activating somatostatin interneurons via the 5-ht2a receptor. *BioRxiv*, 2020.

E. R. De Kloet, M. Joëls, and F. Holsboer. Stress and the brain: from adaptation to disease. *Nature reviews neuroscience*, 6(6):463–475, 2005.

S. Dehaene. *Consciousness and the brain: Deciphering how the brain codes our thoughts*. Penguin, 2014.

T. B. DeMarse, L. Pan, S. Alagapan, G. J. Brewer, and B. C. Wheeler. Feed-forward propagation of temporal and rate information between cortical populations during coherent activation in engineered in vitro networks. *Frontiers in Neural Circuits*, 10:32, 2016.

C. Diekman, K. Dasgupta, V. Nair, and K. P. Unnikrishnan. Discovering functional neuronal connectivity from serial patterns in spike train data. *Neural computation*, 26(7):1263–1297, 2014. ISSN 0899-7667. doi: $10.1162/\mathrm{NECO\_a\_00598}$.

F. Dörfler, M. Chertkov, and F. Bullo. Synchronization in complex oscillator networks and smart grids. *Proceedings of the National Academy of Sciences*, 110(6):2005–2010, 2013.

J. Dragas, V. Viswam, A. Shadmani, Y. Chen, R. Bounik, A. Stettler, M. Radivojevic, S. Geissler, M. E. J. Obien, J. Müller, et al. In vitro multi-functional microelectrode array featuring 59760 electrodes, 2048 electrophysiology channels, stimulation, impedance measurement, and neurotransmitter detection channels. *IEEE Journal of Solid-state Circuits*, 2017.

E. J. Dropcho. Neurotoxicity of radiation therapy. *Neurologic clinics*, 28(1):217–234, 2010.

G. Dumas, F. Lachat, J. Martinerie, J. Nadel, and N. George. From social behaviour to brain synchronization: review and perspectives in hyperscanning. *Irbm*, 32(1): 48–53, 2011.

S. Dura-Bernal, K. Li, S. A. Neymotin, J. T. Francis, J. C. Principe, and W. W. Lytton. Restoring behavior via inverse neurocontroller in a lesioned cortical spiking model driving a virtual arm. *Frontiers in Neuroscience*, 10, 2016.

L. N. Eisenman, C. M. Emnett, J. Mohan, C. F. Zorumski, and S. Mennerick. Quantification of bursting and synchrony in cultured hippocampal neurons. *Journal of Neurophysiology*, 114(2):1059–1071, 2015.

A. K. Engel and W. Singer. Temporal binding and the neural correlates of sensory awareness. *Trends in cognitive sciences*, 5(1):16–25, 2001.

A. K. Engel, P. Fries, and W. Singer. Dynamic predictions: oscillations and synchrony in top–down processing. *Nature Reviews Neuroscience*, 2(10):704–716, 2001.

P. Erdös and A. Rényi. On random graphs, i. *Publicationes Mathematicae (Debrecen)*, 6:290–297, 1959.

A. Espinal, H. Rostro-Gonzalez, M. Carpio, E. I. Guerra-Hernandez, M. Ornelas-Rodriguez, H. Puga-Soberanes, M. A. Sotelo-Figueroa, and P. Melin. Quadrupedal robot locomotion: a biologically inspired approach and its hardware implementation. *Computational Intelligence and Neuroscience*, 2016, 2016.

D. Eytan, A. Minerbi, N. Ziv, and S. Marom. Dopamine-induced dispersion of correlations between action potentials in networks of cortical neurons. *Journal of neurophysiology*, 92(3):1817–1824, 2004. ISSN 0022-3077. doi: $10.1152/\mathrm{jn}.00202.2004$.

R. S. Fisher, W. v. E. Boas, W. Blume, C. Elger, P. Genton, P. Lee, and J. Engel. Epileptic seizures and epilepsy: definitions proposed by the international league against epilepsy (ilae) and the international bureau for epilepsy (ibe). *Epilepsia*, 46(4):470–472, 2005.

D. Flachs and M. Ciba. Cell-based sensor chip for neurotoxicity measurements in drinking water. *Lékař a technika - Clinician and Technology*, 46(2):46–50, 2016.

K. C. Fox, S. Nijeboer, M. L. Dixon, J. L. Floman, M. Ellamil, S. P. Rumak, P. Sedlmeier, and K. Christoff. Is meditation associated with altered brain structure? a systematic review and meta-analysis of morphometric neuroimaging in meditation practitioners. *Neuroscience & Biobehavioral Reviews*, 43:48–73, 2014.

K. Friston. The free-energy principle: a unified brain theory? *Nature reviews neuroscience*, 11(2):127–138, 2010.

K. J. Friston. Functional and effective connectivity in neuroimaging: A synthesis. *Human Brain Mapping*, 2(1-2):56–78, 1994a. ISSN 10659471. doi: 10.1002/hbm.460020107.

K. J. Friston. Functional and effective connectivity in neuroimaging: a synthesis. *Human brain mapping*, 2(1-2):56–78, 1994b.

K. J. Friston. Functional and effective connectivity: a review. *Brain connectivity*, 1(1): 13–36, 2011.

K. J. Friston, B. Li, J. Daunizeau, and K. E. Stephan. Network discovery with dcm. *NeuroImage*, 56(3):1202–1221, 2011. ISSN 1095-9572. doi: 10.1016/j.neuroimage.2010.12.039.

M. Garofalo, T. Nieus, P. Massobrio, and S. Martinoia. Evaluation of the performance of information theory-based methods and cross-correlation to estimate the functional connectivity in cortical networks. *PloS one*, 4(8):e6482, 2009a. ISSN 1932-6203. doi: 10.1371/journal.pone.0006482.

M. Garofalo, T. Nieus, P. Massobrio, and S. Martinoia. Evaluation of the performance of information theory-based methods and cross-correlation to estimate the functional connectivity in cortical networks. *PloS One*, 4(8):e6482, 2009b.

G. Gerstein. Gravitational clustering. In *Analysis of Parallel Spike Trains*, pages 157–172. Springer, 2010.

B. Gourévitch and J. J. Eggermont. Evaluating information transfer between auditory cortical neurons. *Journal of neurophysiology*, 97(3):2533–2543, 2007a. ISSN 0022-3077. doi: 10.1152/jn.01106.2006.

B. Gourévitch and J. J. Eggermont. A simple indicator of nonstationarity of firing rate in spike trains. *Journal of Neuroscience Methods*, 163(1):181–187, 2007b.

B. Gourévitch and J. J. Eggermont. Evaluating information transfer between auditory cortical neurons. *Journal of neurophysiology*, 97(3):2533–2543, 2007c.

S. Grün. Data-driven significance estimation for precise spike correlation. *Journal of Neurophysiology*, 101(3):1126–1140, 2009.

S. Grün and S. Rotter. *Analysis of parallel spike trains*, volume 7. Springer, 2010.

S. Grün, M. Diesmann, and A. Aertsen. Unitary events in multiple single-neuron spiking activity: Ii. nonstationary data. *Neural computation*, 14(1):81–119, 2002.

A. Gustavsson, M. Svensson, F. Jacobi, C. Allgulander, J. Alonso, E. Beghi, R. Dodel, M. Ekman, C. Faravelli, L. Fratiglioni, et al. Cost of disorders of the brain in europe 2010. *European neuropsychopharmacology*, 21(10):718–779, 2011.

A. Hagberg, P. Swart, and D. S Chult. Exploring network structure, dynamics, and function using networkx. Technical report, Los Alamos National Lab.(LANL), Los Alamos, NM (United States), 2008.

M. I. Ham, V. Gintautas, M. a. Rodriguez, R. a. Bennett, C. L. S. Maria, and L. M. a. Bettencourt. Density-dependence of functional development in spiking cortical networks grown in vitro. *Biological cybernetics*, 102(1):71–80, Jan. 2010. ISSN 1432-0770. doi: 10.1007/s00422-009-0351-4. URL http://www.ncbi.nlm.nih.gov/pubmed/20012546.

S. Haufe, V. V. Nikulin, K.-R. Müller, and G. Nolte. A critical assessment of connectivity measures for eeg data: a simulation study. *Neuroimage*, 64:120–133, 2013.

B. Hu and C. Zhou. Phase synchronization in coupled nonidentical excitable systems and array-enhanced coherence resonance. *Phys. Rev. E*, 61:R1001–R1004, Feb 2000. doi: 10.1103/PhysRevE.61.R1001. URL http://link.aps.org/doi/10.1103/PhysRevE.61.R1001.

M. D. Humphries, K. Gurney, and T. J. Prescott. The brainstem reticular formation is a small-world, not scale-free, network. *Proceedings of the Royal Society of London B: Biological Sciences*, 273(1585):503–511, 2006.

T. Isomura, A. Takeuchi, K. Shimba, K. Kotani, and Y. Jimbo. Connection-strength estimation of neuronal networks by fitting for izhikevich model. *Electrical Engineering in Japan*, 187(4):42–50, 2014a. ISSN 04247760. doi: 10.1002/eej.22517.

T. Isomura, A. Takeuchi, K. Shimba, K. Kotani, and Y. Jimbo. Connection-strength estimation of neuronal networks by fitting for izhikevich model. *Electrical Engineering in Japan*, 187(4):42–50, 2014b.

T. Isomura, Y. Ogawa, K. Kotani, and Y. Jimbo. Accurate connection strength estimation based on variational bayes for detecting synaptic plasticity. *Neural computation*, 27(4):819–844, 2015. ISSN 0899-7667. doi: 10.1162/NECO_a_00721.

S. Ito, M. E. Hansen, R. Heiland, A. Lumsdaine, A. M. Litke, and J. M. Beggs. Extending transfer entropy improves identification of effective connectivity in a spiking cortical network model. *PloS one*, 6(11):e27431, 2011. ISSN 1932-6203. doi: 10.1371/journal.pone.0027431.

E. M. Izhikevich. Simple model of spiking neurons. *IEEE transactions on neural networks*, 14(6):1569–1572, 2003. ISSN 1045-9227. doi: 10.1109/TNN.2003.820440.

E. M. Izhikevich. Polychronization: computation with spikes. *Neural computation*, 18 (2):245–282, 2006. ISSN 0899-7667. doi: 10.1162/089976606775093882.

E. M. Izhikevich et al. Simple model of spiking neurons. *IEEE Transactions on Neural Networks*, 14(6):1569–1572, 2003.

L. A. Jeffress. A place theory of sound localization. *Journal of Comparative and Physiological Psychology*, 41(1):35, 1948.

Y. Jimbo, T. Tateno, and H. Robinson. Simultaneous induction of pathway-specific potentiation and depression in networks of cortical neurons. *Biophysical Journal*, 76(2):670–678, 1999. ISSN 00063495. doi: 10.1016/S0006-3495(99)77234-6.

A. F. Johnstone, G. W. Gross, D. G. Weiss, O. H.-U. Schroeder, A. Gramowski, and T. J. Shafer. Microelectrode arrays: a physiologically based neurotoxicity testing platform for the 21st century. *Neurotoxicology*, 31(4):331–350, 2010.

R. Jolivet, R. Kobayashi, A. Rauch, R. Naud, S. Shinomoto, and W. Gerstner. A benchmark test for a quantitative assessment of simple neuron models. *Journal of Neuroscience Methods*, 169(2):417–424, 2008.

E. Juergens and R. Eckhorn. Parallel processing by a homogeneous group of coupled model neurons can enhance, reduce and generate signal correlations. *Biological cybernetics*, 76(3):217–227, 1997. ISSN 0340-1200. doi: 10.1007/s004220050334.

C. G. Jung. *Jung on Synchronicity and the Paranormal*. psychology press, 1997.

M. Jungblut, W. Knoll, C. Thielemann, and M. Pottek. Triangular neuronal networks on microelectrode arrays: an approach to improve the properties of low-density networks for extracellular recording. *Biomedical microdevices*, 11(6):1269–1278, 2009.

B. Kadirvelu, Y. Hayashi, and S. J. Nasuto. Inferring structural connectivity using ising couplings in models of neuronal networks. *Scientific reports*, 7(1):8156, 2017.

A. K. Kar. Bio inspired computing–a review of algorithms and scope of applications. *Expert Systems with Applications*, 59:20–32, 2016.

T. Kiemel and A. H. Cohen. Estimation of coupling strength in regenerated lamprey spinal cords based on a stochastic phase model. *Journal of computational neuroscience*, 5(3):267–284, 1998. ISSN 1573-6873.

B. E. Kilavik, S. Roux, A. Ponce-Alvarez, J. Confais, S. Grün, and A. Riehle. Long-term modifications in motor cortical dynamics induced by intensive practice. *Journal of Neuroscience*, 29(40):12653–12663, 2009.

W. Klimesch. Eeg alpha and theta oscillations reflect cognitive and memory performance: a review and analysis. *Brain research reviews*, 29(2-3):169–195, 1999.

T. Kreuz, J. S. Haas, A. Morelli, H. D. Abarbanel, and A. Politi. Measuring spike train synchrony. *Journal of Neuroscience Methods*, 165(1):151–161, 2007a.

T. Kreuz, F. Mormann, R. G. Andrzejak, A. Kraskov, K. Lehnertz, and P. Grassberger. Measuring synchronization in coupled model systems: A comparison of different approaches. *Physica D: Nonlinear Phenomena*, 225(1):29–42, 2007b.

T. Kreuz, D. Chicharro, R. G. Andrzejak, J. S. Haas, and H. D. Abarbanel. Measuring multiple spike train synchrony. *Journal of Neuroscience Methods*, 183(2):287–299, 2009.

T. Kreuz, D. Chicharro, M. Greschner, and R. G. Andrzejak. Time-resolved and time-scale adaptive measures of spike train synchrony. *Journal of Neuroscience Methods*, 195(1):92–106, 2011.

T. Kreuz, D. Chicharro, C. Houghton, R. G. Andrzejak, and F. Mormann. Monitoring spike train synchrony. *Journal of Neurophysiology*, 109(5):1457–1472, 2013.

T. Kreuz, M. Mulansky, and N. Bozanic. Spiky: A graphical user interface for monitoring spike train synchrony. *Journal of Neurophysiology*, 113(9):3432–3445, 2015.

T. Kreuz, E. Satuvuori, M. Pofahl, and M. Mulansky. Leaders and followers: Quantifying consistency in spatio-temporal propagation patterns. *New Journal of Physics*, 19(4):043028, 2017.

W. Li, W. M. Doyon, and J. A. Dani. Acute in vivo nicotine administration enhances synchrony among dopamine neurons. *Biochemical pharmacology*, 82(8):977–983, 2011.

Z. Li, M. Gao, and Y. Wang. The orientation selectivity of spike-lfp synchronization in macaque v1 and v4. *Frontiers in computational neuroscience*, 13, 2019.

F. Lieb, H.-G. Stark, and C. Thielemann. A stationary wavelet transform and a time-frequency based spike detection algorithm for extracellular recorded data. *Journal of neural engineering*, 14(3):036013, 2017.

A. Litke, N. Bezayiff, E. Chichilnisky, W. Cunningham, W. Dabrowski, A. Grillo, M. Grivich, P. Grybos, P. Hottowy, S. Kachiguine, et al. What does the eye tell the brain?: Development of a system for the large-scale recording of retinal output activity. *IEEE Transactions on Nuclear Science*, 51(4):1434–1440, 2004.

M. Lungarella and O. Sporns. Mapping information flow in sensorimotor networks. *PLoS computational biology*, 2(10):e144, 2006. ISSN 1553-7358. doi: 10.1371/journal.pcbi.0020144.

A. Maccione, M. Gandolfo, M. Tedesco, T. Nieus, K. Imfeld, S. Martinoia, and B. Luca. Experimental investigation on spontaneously active hippocampal cultures recorded by means of high-density meas: analysis of the spatial resolution effects. *Frontiers in neuroengineering*, 3:4, 2010.

A. Maccione, M. Garofalo, T. Nieus, M. Tedesco, L. Berdondini, and S. Martinoia. Multiscale functional connectivity estimation on low-density neuronal cultures recorded by high-density cmos micro electrode arrays. *Journal of neuroscience methods*, 207(2):161–171, 2012. ISSN 0165-0270. doi: 10.1016/j.jneumeth.2012.04.002.

Z. F. Mainen and T. J. Sejnowski. Reliability of spike timing in neocortical neurons. *Science*, 268(5216):1503, 1995.

N. Malik, N. Marwan, and J. Kurths. Spatial structures and directionalities in monsoonal precipitation over south asia. *Nonlinear Processes in Geophysics*, 17(5): 371, 2010.

B. B. Mandelbrot. *The fractal geometry of nature*, volume 173. WH freeman New York, 1983.

H. Markram. Seven challenges for neuroscience. *Functional neurology*, 28(3):145, 2013.

E. Masi, M. Fiscella, J. Müller, U. Frey, S. Mancuso, and A. Hierlemann. Investigating electrical network dynamics in plant root cells by means of a high-density cmos-based microelectrode array. In *MEA Meeting 2012*, page 246, 2012.

A. Mason, A. Nicoll, and K. Stratford. Synaptic transmission between individual pyramidal neurons of the rat visual cortex in vitro. *The Journal of neuroscience : the official journal of the Society for Neuroscience*, 11(1):72–84, 1991. ISSN 1529-2401.

M. S. Masud, R. Borisyuk, and L. Stuart. Advanced correlation grid: Analysis and visualisation of functional connectivity among multiple spike trains. *Journal of neuroscience methods*, 286:78–101, 2017. ISSN 0165-0270. doi: 10.1016/j.jneumeth.2017.05.016.

H. S. Mayberg, A. M. Lozano, V. Voon, H. E. McNeely, D. Seminowicz, C. Hamani, J. M. Schwalb, and S. H. Kennedy. Deep brain stimulation for treatment-resistant depression. *Neuron*, 45(5):651–660, 2005.

S. F. Muldoon, E. W. Bridgeford, and D. S. Bassett. Small-world propensity and weighted brain networks. *Scientific reports*, 6:22057, 2016.

S. Muttoni, M. Ardissino, and C. John. Classical psychedelics for the treatment of depression and anxiety: a systematic review. *Journal of affective disorders*, 2019.

A. Neiman, A. Silchenko, V. Anishchenko, and L. Schimansky-Geier. Stochastic resonance: Noise-enhanced phase coherence. *Phys. Rev. E*, 58:7118–7125, Dec 1998. doi: 10.1103/PhysRevE.58.7118. URL http://link.aps.org/doi/10.1103/PhysRevE.58.7118.

C. Nick, M. Goldhammer, R. Bestel, F. Steger, A. Daus, and C. Thielemann. Drcell—a software tool for the analysis of cell signals recorded with extracellular microelectrodes. *Signal Processing: An International Journal (SPIJ)*, 7:96–109, 2013.

A. Novellino, B. Scelfo, T. Palosaari, A. Price, T. Sobanski, T. J. Shafer, A. F. Johnstone, G. W. Gross, A. Gramowski, O. Schroeder, et al. Development of microelectrode array based tests for neurotoxicity: assessment of interlaboratory reproducibility with neuroactive chemicals. *Frontiers in neuroengineering*, 4, 2011.

F. Otto, P. Goertz, W. Fleischer, and M. Siebler. Cryopreserved rat cortical cells develop functional neuronal networks on microelectrode arrays. *Journal of Neuroscience Methods*, 128:173, 2003.

L. A. Overbey and M. D. Todd. Dynamic system change detection using a modification of the transfer entropy. *Journal of Sound and Vibration*, 322(1-2):438–453, 2009. ISSN 0022460X. doi: 10.1016/j.jsv.2008.11.025.

A. R. Paiva, I. Park, and J. C. Príncipe. A comparison of binless spike train measures. *Neural Computing and Applications*, 19(3):405–419, 2010.

D. Pare, R. Curro'Dossi, and M. Steriade. Neuronal basis of the parkinsonian resting tremor: a hypothesis and its implications for treatment. *Neuroscience*, 35(2):217–226, 1990.

V. Pasquale, P. Massobrio, L. L. Bologna, M. Chiappalone, and S. Martinoia. Self-organization and neuronal avalanches in networks of dissociated cortical neurons. *Neuroscience*, 153(4):1354–1369, 2008. ISSN 0306-4522. doi: 10.1016/j.neuroscience.2008.03.050.

V. P. Pastore, D. Poli, A. Godjoski, S. Martinoia, and P. Massobrio. Toolconnect: A functional connectivity toolbox for in vitro networks. *Frontiers in neuroinformatics*, 10:13, 2016. ISSN 1662-5196. doi: 10.3389/fninf.2016.00013.

V. P. Pastore, A. Godjoski, S. Martinoia, and P. Massobrio. Spicodyn: A toolbox for the analysis of neuronal network dynamics and connectivity from multi-site spike signal recordings. *Neuroinformatics*, 16(1):15–30, 2018a.

V. P. Pastore, P. Massobrio, A. Godjoski, and S. Martinoia. Identification of excitatory-inhibitory links and network topology in large-scale neuronal assemblies from multi-electrode recordings. *PLoS computational biology*, 14(8):e1006381, 2018b.

V. P. Pastore, P. Massobrio, A. Godjoski, and S. Martinoia. Identification of excitatory-inhibitory links and network topology in large-scale neuronal assemblies from multi-electrode recordings. *PLoS computational biology*, 14(8):e1006381, 2018c.

D. H. Perkel, G. L. Gerstein, and G. P. Moore. Neuronal spike trains and stochastic point processes. *Biophysical Journal*, 7(4):391–418, 1967. ISSN 00063495. doi: 10.1016/S0006-3495(67)86596-2.

A. Pikovsky, M. Rosenblum, and J. Kurths. *Synchronization: A universal concept in nonlinear sciences*, volume 12. Cambridge University Press, 2003.

A. S. Pikovsky, M. G. Rosenblum, G. V. Osipov, and J. Kurths. Phase synchronization of chaotic oscillators by external driving. *Physica D: Nonlinear Phenomena*, 104 (3):219–238, 1997.

J. Pine. A history of mea development. In *Advances in network electrophysiology*, pages 3–23. Springer, 2006.

D. Poli, V. P. Pastore, and P. Massobrio. Functional connectivity in in vitro neuronal assemblies. *Frontiers in neural circuits*, 9:57, 2015a. ISSN 1662-5110. doi: 10.3389/fncir.2015.00057.

D. Poli, V. P. Pastore, and P. Massobrio. Functional connectivity in in vitro neuronal assemblies. *Frontiers in neural circuits*, 9:57, 2015b.

D. Poli, V. P. Pastore, S. Martinoia, and P. Massobrio. From functional to structural connectivity using partial correlation in neuronal assemblies. *Journal of neural engineering*, 13(2):026023, 2016a. ISSN 1741-2552. doi: $10.1088/1741\text{-}2560/13/2/026023$.

D. Poli, V. P. Pastore, S. Martinoia, and P. Massobrio. From functional to structural connectivity using partial correlation in neuronal assemblies. *Journal of Neural Engineering*, 13(2):026023, 2016b.

K. H. Pribram and E. H. Carlton. Holonomic brain theory in imaging and object perception. *Acta Psychologica*, 63(2):175–210, 1986.

R. Quian Quiroga, T. Kreuz, and P. Grassberger. Event synchronization: a simple and fast method to measure synchronicity and time delay patterns. *Physical Review E*, 66(4):041904, 2002.

T.-C. Rabinowitch and A. Knafo-Noam. Synchronous rhythmic interaction enhances children's perceived similarity and closeness towards each other. *PloS one*, 10(4), 2015.

J.-M. Ramirez, A. K. Tryba, and F. Peña. Pacemaker neurons and neuronal networks: an integrative view. *Current opinion in neurobiology*, 14(6):665–674, 2004.

G. Rees, G. Kreiman, and C. Koch. Neural correlates of consciousness in humans. *Nature Reviews Neuroscience*, 3(4):261, 2002.

T. Reimer, W. Baumann, and J. Gimsa. Spontaneous activity patterns of cortical in vitro networks depend on cellular network composition. In *MEA Meeting 2012*, page 98, 2012.

H. G. Rey, C. Pedreira, and R. Q. Quiroga. Past, present and future of spike sorting techniques. *Brain research bulletin*, 119:106–117, 2015.

F. Rieke. *Spikes: exploring the neural code*. MIT Press, 1999.

F. A. Rodrigues. Network centrality: An introduction. In *A Mathematical Modeling Approach from Nonlinear Dynamics to Complex Systems*, pages 177–196. Springer, 2019.

R. Rosenbaum, T. Tchumatchenko, and R. Moreno-Bote. Correlated neuronal activity and its relationship to coding, dynamics and network architecture. *Frontiers in computational neuroscience*, 8:102, 2014.

E. Satuvuori, M. Mulansky, N. Bozanic, I. Malvestio, F. Zeldenrust, K. Lenk, and T. Kreuz. Measures of spike train synchrony for data with multiple time scales. *Journal of Neuroscience Methods*, 2017.

E. Satuvuori, M. Mulansky, A. Daffertshofer, and T. Kreuz. Using spike train distances to identify the most discriminative neuronal subpopulation. *Journal of neuroscience methods*, 308:354–365, 2018.

H. Scharfman. Synchronization of area ca3 hippocampal pyramidal cells and non-granule cells of the dentate gyrus in bicuculline-treated rat hippocampal slices. *Neuroscience*, 59(2):245–257, 1994.

C. A. Schevon, J. Cappell, R. Emerson, J. Isler, P. Grieve, R. Goodman, G. Mckhann Jr, H. Weiner, W. Doyle, R. Kuzniecky, et al. Cortical abnormalities in epilepsy revealed by local eeg synchrony. *Neuroimage*, 35(1):140–148, 2007.

S. Schreiber, J.-M. Fellous, D. Whitmer, P. Tiesinga, and T. J. Sejnowski. A new correlation-based measure of spike timing reliability. *Neurocomputing*, 52:925–931, 2003.

T. Schreiber. Measuring information transfer. *Physical review letters*, 85(2):461–464, 2000. ISSN 1079-7114. doi: 10.1103/PhysRevLett.85.461.

J. M. Schwartz, H. P. Stapp, and M. Beauregard. Quantum physics in neuroscience and psychology: a neurophysical model of mind–brain interaction. *Philosophical Transactions of the Royal Society B: Biological Sciences*, 360(1458):1309–1327, 2005.

J. V. Selinger, J. J. Pancrazio, and G. W. Gross. Measuring synchronization in neuronal networks for biosensor applications. *Biosensors and Bioelectronics*, 19(7): 675–683, 2004.

M. N. Shadlen and J. A. Movshon. Synchrony unbound: a critical evaluation of the temporal binding hypothesis. *Neuron*, 24(1):67–77, 1999.

C. Shannon and W. Weaver. A mathematical theory of communication. *Bell Syst. Tech. J*, 27(379):623, 1948.

M. Shimono and J. M. Beggs. Functional clusters, hubs, and communities in the cortical microconnectome. *Cerebral Cortex*, 25(10):3743–3757, 2015.

D. Sihn and S.-P. Kim. A spike train distance robust to firing rate changes based on the earth mover's distance. *Frontiers in Computational Neuroscience*, 13, 2019.

W. Singer. Neuronal synchrony: a versatile code for the definition of relations? *Neuron*, 24(1):49–65, 1999.

D. M. Sokal, R. Mason, and T. L. Parker. Multi-neuronal recordings reveal a differential effect of thapsigargin on bicuculline-or gabazine-induced epileptiform excitability in rat hippocampal neuronal networks. *Neuropharmacology*, 39(12):2408–2417, 2000.

P. Song and X.-J. Wang. Angular path integration by moving "hill of activity": a spiking neuron model without recurrent excitation of the head-direction system. *The Journal of neuroscience : the official journal of the Society for Neuroscience*, 25(4):1002–1014, 2005. ISSN 1529-2401. doi: 10.1523/JNEUROSCI.4172-04.2005.

B. Sotomayor-Gomez, F. P. Battaglia, and M. Vinck. A geometry of spike sequences: Fast, unsupervised discovery of high-dimensional neural spiking patterns based on optimal transport theory. *bioRxiv*, 2020.

M. E. Spira and A. Hai. Multi-electrode array technologies for neuroscience and cardiology. *Nature nanotechnology*, 8(2):83, 2013.

O. Sporns, C. J. Honey, and R. Kötter. Identification and classification of hubs in brain networks. *PloS one*, 2(10):e1049, 2007. ISSN 1932-6203. doi: 10.1371/journal.pone.0001049.

O. Stetter, D. Battaglia, J. Soriano, and T. Geisel. Model-free reconstruction of excitatory neuronal connectivity from calcium imaging signals. *PLoS computational biology*, 8(8):e1002653, 2012. ISSN 1553-7358. doi: 10.1371/journal.pcbi.1002653.

S. Strogatz. From Kuramoto to Crawford: exploring the onset of synchronization in populations of coupled oscillators. *Physica D: Nonlinear Phenomena*, 143(1): 1–20, 2000.

H. A. Swadlow. Efferent neurons and suspected interneurons in motor cortex of the awake rabbit: axonal properties, sensory receptive fields, and subthreshold synaptic inputs. *Journal of neurophysiology*, 71(2):437–453, 1994. ISSN 0022-3077.

P. Tass, M. G. Rosenblum, J. Weule, J. Kurths, A. Pikovsky, J. Volkmann, A. Schnitzler, and H.-J. Freund. Detection of n:m Phase Locking from Noisy Data: Application to Magnetoencephalography. *Phys. Rev. Lett.*, 81:3291–3294, Oct 1998. doi: 10.1103/PhysRevLett.81.3291. URL http://link.aps.org/doi/10.1103/PhysRevLett.81.3291.

T. Tchumatchenko, T. Geisel, M. Volgushev, and F. Wolf. Spike correlations–what can they tell about synchrony? *Frontiers in neuroscience*, 5:68, 2011.

J. F. Téllez-Zenteno, R. Dhar, and S. Wiebe. Long-term seizure outcomes following epilepsy surgery: a systematic review and meta-analysis. *Brain*, 128(5):1188–1198, 2005.

C. Tetzlaff, S. Dasgupta, T. Kulvicius, and F. Wörgötter. The use of hebbian cell assemblies for nonlinear computation. *Scientific reports*, 5:12866, 2015.

W. Truccolo, O. J. Ahmed, M. T. Harrison, E. N. Eskandar, G. R. Cosgrove, J. R. Madsen, A. S. Blum, N. S. Potter, L. R. Hochberg, and S. S. Cash. Neuronal ensemble synchrony during human focal seizures. *Journal of Neuroscience*, 34 (30):9927–9944, 2014.

M. C. van Rossum. A novel spike distance. *Neural Computation*, 13(4):751–763, 2001.

F. Vazza and A. Feletti. The strange similarity of neuron and galaxy networks: Your life's memories could, in principle, be stored in the universe's structure. *Nautilus*, 2017.

J. D. Victor and K. P. Purpura. Nature and precision of temporal coding in visual cortex: a metric-space analysis. *Journal of Neurophysiology*, 76(2):1310–1326, 1996.

L. M. Ward. Synchronous neural oscillations and cognitive processes. *Trends in Cognitive Sciences*, 7(12):553–559, 2003.

A. Washburn, I. Román, M. Huberth, N. Gang, T. Dauer, W. Reid, C. Nanou, M. Wright, and T. Fujioka. Musical role asymmetries in piano duet performance influence alpha-band neural oscillation and behavioral synchronization. *Frontiers in neuroscience*, 13:1088, 2019.

D. J. Watts and S. H. Strogatz. Collective dynamics of small-world networks. *Nature*, 393(6684):440, 1998.

WHO. Depression and other common mental disorders: global health estimates. Technical report, World Health Organization, 2017.

M. J. Williams, R. M. Whitaker, and S. M. Allen. Measuring individual regularity in human visiting patterns. In *2012 International Conference on Privacy, Security, Risk and Trust and 2012 International Confernece on Social Computing*, pages 117–122. IEEE, 2012.

R. W. Williams and K. Herrup. The control of neuron number. *Annual review of neuroscience*, 11(1):423–453, 1988.

S. B. Wilson and R. Emerson. Spike detection: a review and comparison of algorithms. *Clinical Neurophysiology*, 113(12):1873–1881, 2002.

I. Witten and E. Frank. *Data Mining. Practical Machine Learning Tools and Techniques with Java Implementations*. Morgan Kaufmann, 2000. ISBN 90-74821-43-X.

R. O. Wong, M. Meister, and C. J. Shatz. Transient period of correlated bursting activity during development of the mammalian retina. *Neuron*, 11(5):923–938, 1993.

H. Yu, X. Guo, Q. Qin, Y. Deng, J. Wang, J. Liu, and Y. Cao. Synchrony dynamics underlying effective connectivity reconstruction of neuronal circuits. *Physica A: Statistical Mechanics and its Applications*, 471:674–687, 2017.

X. Yuan, M. Schröter, M. E. J. Obien, M. Fiscella, W. Gong, T. Kikuchi, A. Odawara, S. Noji, I. Suzuki, J. Takahashi, et al. Versatile live-cell activity analysis platform for characterization of neuronal dynamics at single-cell and network level. *bioRxiv*, 2020.

S. M. Zeki. Functional specialisation in the visual cortex of the rhesus monkey. *Nature*, 274(5670):423–428, 1978.

Appendices

Appendix A

Publications

Talks

M. Ciba: Synchrony and functional connectivity of drug exposed in vitro neuronal networks, 13th GSLS Retreat, Jugendherberge Waldmünchen, 17th – 19th May 2019.

M. Ciba: Methods to quantify synchrony of neuronal signals, 9th GSLS Retreat, Vollmar Akademie Kochel am See, 17th – 19 th March 2017.

Poster and Proceedings

M. Ciba, M. Mayer, C. Thielemann: Experimental setup to investigate the effect of psychedelics on in vitro neuronal networks. Poster at INSIGHT 2019, Berlin, 2019.

M. Ciba and C. Thielemann: Synchrony changes on different time-scales during in vitro neuronal network development. Front. Cell. Neurosci. Conference Abstract: MEA Meeting, 2018.

M. Ciba, A. Bahmer, C. Thielemann: Application of spike train synchrony measure Spike-contrast to quantify the effect of bicuculline on cortical networks grown on microelectrode arrays. CNS Conference, Antwerp, Belgium: BMC Neuroscience, P269, 2017.

M. Ciba: Novel measure of spike train synchrony for large sets of neuronal data. 11th International GSLS Student Symposium, 12th – 13th October, 2016.

Journals

M. Mayer, O. Arrizabalaga, **M. Ciba**, I. S. Schroeder, S. Ritter and C. Thielemann: Novel in Vitro Assay to Investigate Radiation Induced Changes in the Functionality of Human Embryonic Stem Cell-Derived Neurospheres. Accepted for publication in Neurotoxicology, 2020.

M. Ciba, R. Bestel, C. Nick, G. F. Arruda, T. Peron, C. C. Henrique, L. F. Costa, F. A. Rodrigues, C. Thielemann: Comparison of different spike train synchrony measures regarding their robustness to erroneous data from bicuculline-induced epileptiform activity. Neural Computation, Volume 32, Issue 5, 2020.

S. De Blasi, **M. Ciba**, A. Bahmer, C. Thielemann: Total Spiking Probability Edges: A Cross-Correlation based Method for Effective Connectivity Estimation of Cortical Spiking Neurons. Journal of Neuroscience Methods, 312, 169–181, 2019.

T. Köhler, M. Wölfel, **M.Ciba**, U. Bochtler and C. Thielemann: Terrestrial Trunked Radio (TETRA) exposure of neuronal in vitro networks. Environmental Research, Volume 162, Pages 1–7, 2018.

M. Mayer, O. Arrizabalaga, F. Lieb, **M. Ciba**, S. Ritter and C. Thielemann: Electrophysiological investigation of human embryonic stem cell derived neurospheres using a novel spike detection algorithm. Biosensors and Bioelectronics, Volume 100, p. 462–468, 2018.

M. Ciba, T. Isomura, Y. Jimbo, A. Bahmer, C. Thielemann: Spike-Contrast: A novel time scale independent and multivariate spike train synchrony measure. Journal of Neuroscience Methods, Volume 293, Pages 136–143, 2018.

D. Flachs and **M. Ciba**: Cell-based sensor chip for neurotoxicity measurements in drinking water. Lékař a technika-Clinician and Technology, 46(2):46–50, 2016.

Appendix B

Acknowledgments

I thank my supervisor Prof. Dr.-Ing. Christiane Thielemann for encouraging me to start this work, for support throughout the time and the financial means and resources from her lab (biomems lab).

I thank PD Dr. mult Andreas Bahmer for his willingness to support the work as the primary supervisor, for providing me insights into the scientific community, and for valuable neuroscience input.

I thank Prof. Dr. Charlotte Förster for her willingness to support this work as the secondary supervisor and providing me explanations about instrinsic biological rhythms.

I thank Prof. Francisco Aparecido Rodrigues, Dr.-Ing. Robert Bestel, Dr.-Ing. Christoph Nick, Ph.D. Guilherme Ferraz de Arruda, and Ph.D. Thomas Peron for arousing my interest in synchrony measurement and Dr. Margot Mayer for her intensive support in conducting cell culture experiments.
I thank Prof. Yasuhiko Jimbo for giving me the opportunity to work in his lab and Takuya Isomura for his helpful input for the ”Spike-contrast Paper”.

I thank Stefano De Blasi for his hard and impassionate work on his master project leading to the ”TSPE paper”.

I thank all members of the biomems lab for their great collaboration and relaxed lab atmosphere.

I thank the administrative staff of the GSLS for their kind support and for the organization of great events.

This work was financed by the BMBF project *iNeuTox*. Further, I acknowledge support from *BayWISS-Kolleg Digitalisierung*.

Last but not least, I thank my parents (Edith and Joe), my brother (Stefan), my family, and all my friends (scurrr!) for their support and for being so awesome :)

Appendix C

Author declaration

Julius-Maximilians-
UNIVERSITÄT
WÜRZBURG

Graduate School
Life Sciences

"Dissertation Based on Several Published Manuscripts"

Statement of individual author contributions and of legal second publication rights

(If required please use more than one sheet)

Publication (complete reference): Ciba, M., Isomura, T., Jimbo, Y., Bahmer, A., & Thielemann, C. (2018). Spike-contrast: A novel time scale independent and multivariate measure of spike train synchrony. Journal of Neuroscience Methods, 293, 136-143.					
Participated in	**Author Initials,** Responsibility decreasing from left to right				
Study Design Methods Development	MC MC	TI			
Data Collection	MC	TI			
Data Analysis and Interpretation	MC	TI	AB, CT, YJ		
Manuscript Writing Writing of Introduction Writing of Materials & Methods Writing of Discussion Writing of First Draft	 MC MC MC MC	 AB AB AB	 CT CT CT	 TI, YJ TI, YJ TI, YJ	

Explanations (if applicable):

Author contribution statement from the publication: Initiated the idea to find an intuitive synchrony measure: TI YJ. Development of the algorithm: MC. Conceived and designed the experiments: MC TI. Performed the experiments: MC. Analyzed the data: MC. Wrote the paper: MC, TI, YJ, AB, and CT.

Publication (complete reference): Ciba, M., Bestel, R., Nick, C., Ferraz de Arruda, G., Peron, T., Henrique, C. C., Costa, F. L., Rodrigues, A. F., & Thielemann, C. (2020). Comparison of different spike train synchrony measures regarding their robustness to erroneous data from bicuculline induced epileptiform activity. Neural Computation, (Accepted).					
Participated in	**Author Initials,** Responsibility decreasing from left to right				
Study Design Methods Development	MC MC	CN	RB, CT, FAR	LFC	
Data Collection	CN (in vitro) MC (in silico)				
Data Analysis and Interpretation	MC	CN	TP, GFA, CCH	RB	CT, FAR
Manuscript Writing Writing of Introduction Writing of Materials & Methods Writing of Discussion Writing of First Draft	 MC MC MC MC	CN	TP, GFA	CT, RB CT CT	LFC, FAR CCH LFC

Explanations (if applicable):

A study to compare algorithms that measure synchrony was first initiated by CN, RB, CT, FAR, LFC, TP, GFA, and CCH in the course of a BayLat project. The first paper version has been rejected as it turned out that the synchrony measures couldn't been compared that easily. MC adopted the project and added an entirely new aspect to the work by considering the robustness of these measures to

erroneous spike trains. Furthermore, MC developed a new evaluation method that allowed to make the measures comparable and included additional measures into the work.

Author contribution statement from the publication: M.C.: Conception, design, generation, and analysis of in silico manipulated data. Application of the synchrony measures STTC, Spike-contrast, A-SPIKE-synchronization, A-ISI-distance, A-SPIKE-distance, ARI-SPIKE-distance to experimental data. Statistical tests and spike detection with varying thresholds. Preparation of figure 1 to 6. Draft of the manuscript. R.B.: Initial conception and design of synchrony measure comparison using experimental data. C.N.: Initial conception and design of synchrony measure comparison using experimental data. Performed cell experiments and spike detection of raw data. G.F.A.: Implementation and application of the synchrony measure MI to experimental data and MI description in appendix. T.P.: Implementation and application of the synchrony measure PS to experimental data and PS description in appendix. Preparation of figure 7 and 8. C.C.H.: Implementation and application of the synchrony measures CC to experimental data. L.F.C.: Helped in the initial conception, discussions and revision. F.A.R.: Conception and design of research. C.T.: Conception and design of research. ALL: Interpreted and discussed results of experiments. Edited and revised manuscript. Approved final version of manuscript.

Publication (complete reference): De Blasi, S., Ciba, M., Bahmer, A., & Thielemann, C. (2019). Total spiking probability edges: A cross-correlation based method for effective connectivity estimation of cortical spiking neurons. *Journal of neuroscience methods*, *312*, 169-181.

Participated in	**Author Initials,** Responsibility decreasing from left to right				
Study Design Methods Development	SDB SDB	MC			
Data Collection	SDB				
Data Analysis and Interpretation	SDB	MC			
Manuscript Writing Writing of Introduction Writing of Materials & Methods Writing of Discussion Writing of First Draft	 SDB SDB SDB SDB	 MC, AB, CT MC, AB, CT MC, AB, CT MC, AB, CT			

Explanations (if applicable):

MC supervised SDB in the frame of a master thesis. The algorithm is partly inspired by the algorithm introduced in Ciba et. al (2018) considering different time-scales to optimize the result.

Author contribution statement from the publication: Development of the algorithm: SDB. Performed the experiments: SDB. Analyzed the data: SDB, MC. Wrote the paper: SDB, MC, AB, and CT.

Publication (complete reference): Ciba, M., Noise enhances discrimination between different synchrony levels in neuronal signals. (in preparation)					
Participated in	**Author Initials,** Responsibility decreasing from left to right				
Study Design Methods Development	MC MC				
Data Collection	MC				
Data Analysis and Interpretation	MC				
Manuscript Writing Writing of Introduction Writing of Materials & Methods Writing of Discussion Writing of First Draft	MC				

Explanations (if applicable):

So far only preliminary results (Status: 28. Jan)

The doctoral researcher confirms that she/he has obtained permission from both the publishers and the co-authors for legal second publication.

The doctoral researcher and the primary supervisor confirm the correctness of the above mentioned assessment.

Manuel Ciba 31.1.2020 Aschaffenburg

Doctoral Researcher's Name | Date | Place | Signature

Prof. Andreas Bahmer 31.1.2020 Würzburg

Primary Supervisor's Name | Date | Place | Signature

Appendix D

Affidavit

I hereby confirm that my thesis entitled *Synchrony Measurement and Connectivity Estimation of Parallel Spike Trains from in vitro Neuronal Networks* is the result of my own work. I did not receive any help or support from commercial consultants. All sources and / or materials applied are listed and specified in the thesis.

Furthermore, I confirm that this thesis has not yet been submitted as part of another examination process neither in identical nor in similar form.

Place, Date Signature